INFORMATION TO USERS

This manuscript has been reproduced from the microfilm master. UMI films the text directly from the original or copy submitted. Thus, some thesis and dissertation copies are in typewriter face, while others may be from any type of computer printer.

The quality of this reproduction is dependent upon the quality of the copy submitted. Broken or indistinct print, colored or poor quality illustrations and photographs, print bleedthrough, substandard margins, and improper alignment can adversely affect reproduction.

In the unlikely event that the author did not send UMI a complete manuscript and there are missing pages, these will be noted. Also, if unauthorized copyright material had to be removed, a note will indicate the deletion.

Oversize materials (e.g., maps, drawings, charts) are reproduced by sectioning the original, beginning at the upper left-hand corner and continuing from left to right in equal sections with small overlaps.

ProQuest Information and Learning
300 North Zeeb Road, Ann Arbor, MI 48106-1346 USA
800-521-0600



Downloaded from SHAREOK. Persistent Handle URL: https://hdl.handle.net/11244/593

UNIVERSITY OF OKLAHOMA
GRADUATE COLLEGE

Many-body Dimensional Perturbation Theory for Quantum Confined Systems with a Focus on Atomic Gas Bose-Einstein Condensates

A Dissertation
SUBMITTED TO THE GRADUATE FACULTY
in partial fulfillment of the requirements for the
degree of
Doctor of Philosophy

By
Brett Allen McKinney
Norman, Oklahoma
2003

UMI Number: 3082950

UMI®

UMI Microform 3082950
Copyright 2003 by ProQuest Information and Learning Company.
All rights reserved. This microform edition is protected against unauthorized copying under Title 17, United States Code.

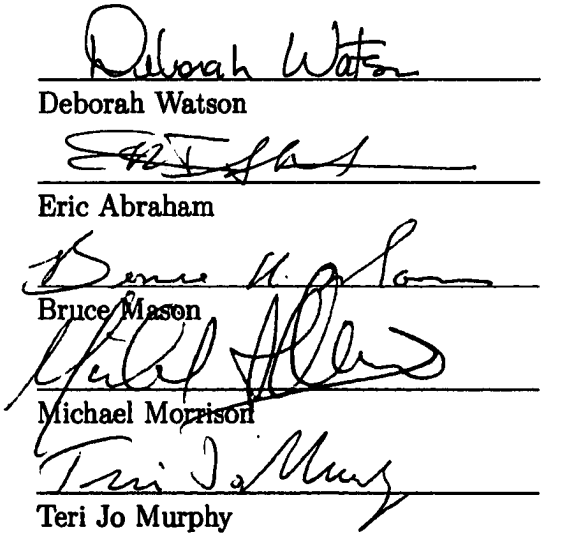
ProQuest Information and Learning Company
300 North Zeeb Road
P.O. Box 1346
Ann Arbor, MI 48106-1346

© by Brett Allen McKinney 2003
All Rights Reserved.

Many-body Dimensional Perturbation Theory for Quantum Confined Systems with a Focus on Atomic Gas Bose-Einstein Condensates

A Dissertation APPROVED FOR THE
Department of Physics and Astronomy

By



Deborah Watson

Eric Abraham

Bruce Mason

Michael Morrison

Teri Jo Murphy

Dedication

To Shauna and Jackson

Acknowledgements

Unlike a vapor Bose-Einstein condensate, a thesis is not created in a vacuum chamber. Numerous individuals have contributed either directly or indirectly to this thesis and to my scientific training. First I would like to thank my thesis advisor Deborah Watson for her guidance throughout my years as a graduate student, and for assembling and leading a research group composed of individuals who have taught me a great deal. I hope to continue a fruitful collaboration with Deborah and her group. I also appreciate her continued financial support throughout most of my graduate career, even when circumstances brought me to live in another state, during the last three years of this work. I would like to thank Olen Boydstun and John Carzoli for helpful discussions and advice early in my graduate career, and I would like to thank Martin Dunn, with whom I have worked closely on much of the many-body formalism found in this thesis. Other OU professors who have contributed to my training include Eric Abraham, Michael Morrison, Kieran Mullen, Bruce Mason, and Greg Parker.

I have also had the opportunity to meet and learn from physicists outside the OU community by presenting at conferences. At these meetings, DAMOP especially, I have found many willing mentors. Besides learning new scientific ideas, my discussions with colleagues at these meetings have shown me the way science should be carried out: in an open atmosphere of idea and information sharing in the search for scientific truth. Specifically, I would like to thank Doerte Blume (Washington State University, WA), John Bohn (JILA, CO), Michael Crescimanno (Youngstown State University, OH), and Brett Esry (Kansas State University, KS) for their glad willingness to share with me their expert knowledge and advice. And although I have never met him in person, I have had many important conversations by phone, e-mail, and fax (if that's possible) with John Loeser (Oregon State University, OR) on the first orders of many-body dimensional perturbation theory.

Finally, I would like to thank the Office of Naval Research for their financial support of this research.

Contents

Dedication iv

Acknowledgements v

List Of Tables ix

List Of Figures x

Abstract xi

1 Introduction 1
- 1.1 A tale of two particles . . . 1
- 1.2 Outline of thesis . . . 5

2 Standard methods for Bose-Einstein condensates 8
- 2.1 Basic scattering theory . . . 9
- 2.2 Ground-state Mean-field theory for bosons . . . 13
  - 2.2.1 Single-particle picture . . . 14
  - 2.2.2 Classical field picture . . . 17
- 2.3 Thomas-Fermi approximation for the GP ground state . . . 20
- 2.4 Collective excitations and the hydrodynamic limit . . . 25
  - 2.4.1 Homogeneous bose gas . . . 26
  - 2.4.2 Inhomogeneous bose gas . . . 28

3 Single degree of freedom dimensional perturbation methods 33
- 3.1 $1/D$ perturbation methods for the Gross-Pitaevskii equation . . . 34
  - 3.1.1 Effective dimensionality . . . 36
  - 3.1.2 GP equation in variable dimensionality . . . 36
  - 3.1.3 Zeroth-order density . . . 38
  - 3.1.4 Ground state in three dimensions . . . 40
  - 3.1.5 Lower dimension . . . 44
  - 3.1.6 Anisotropic trap: generalized cylindrical coordinates . . . 46
- 3.2 $1/N$ perturbation theory for a model BEC Hamiltonian . . . 48
  - 3.2.1 Formalism . . . 49
  - 3.2.2 Results . . . 54
- 3.3 $1/D$ Perturbation theory for two-electron quantum dot . . . 57

3.3.1 Formalism . . . 58
3.3.2 Perturbation expansion . . . 60
3.3.3 Results and Discussion . . . 64
3.4 Discussion . . . 66

4 Many-body dimensional perturbation theory 71
4.1 D-dimensional N-body Schrödinger equation . . . 72
4.1.1 Transformation of the Laplacian . . . 73
4.1.2 Removal of first-order derivatives . . . 74
4.2 Infinite-D analysis: Leading order energy . . . 75
4.3 Normal-mode analysis: $1/D$ first-order quantum energy correction . . . 77
4.3.1 Indical structure of F, G, and GF matrices . . . 79
4.3.2 Symmetry of the Q matrices . . . 80
4.3.3 Q matrices in terms of simple submatrices . . . 81
4.3.4 Normal mode frequencies and first-order energy . . . 82
4.4 N-electron atom . . . 85
4.4.1 Atomic infinite-D analysis . . . 87
4.4.2 Atomic normal modes . . . 88
4.5 N-electron Quantum Dot . . . 90
4.5.1 Quantum Dot infinite-D analysis . . . 92
4.5.2 Quantum Dot Normal Modes . . . 93

5 Many-body dimensional perturbation theory for Bose-Einstein condensates 96
5.1 Formalism . . . 101
5.1.1 The dimensionally scaled Schrödinger equation . . . 101
5.1.2 Leading-order energy term . . . 105
5.1.3 Normal modes and first quantum energy correction . . . 106
5.2 Motivation for low-order method . . . 113
5.3 Optimization of the interatomic parameters . . . 114
5.4 Ground-state energy . . . 115
5.4.1 Small scattering length . . . 116
5.4.2 Large and intermediate scattering length . . . 117
5.4.3 Discussion . . . 121
5.5 Excitations . . . 123

6 Summary 126

Bibliography 134

Appendices 134

A Hydrodynamic approximation for inhomogeneous bose gas 136

B Wilson FG matrix method 140

C Spectral graph theory and the symmetry of the Q matrices 142

D Gaussian reduction of Eq. (4.44) 148

E Gramian determinants 151

F Regularized Fermi pseudopotential and the low density expansion 154

G Homogeneous limit of the GP and MGP equations 157

List Of Tables

3.1 Ground state energies for Bohn-Esry-Greene model BEC hamiltonian. 56
3.2 Partial sums of $1/N$ energy series of Bohn-Esry-Greene BEC model hamiltonian. 56
3.3 Quantum dot $\gamma = 1$ $D = 2$ energies. 62
3.4 Quantum dot $\gamma = .05$ $D = 2$ energies. 63

5.1 Low-N ground-state energies for small scattering length condensate. . 116
5.2 Low-N ground-state energies for large scattering length condensate. . 118
5.3 Low-N ground-state energies for intermediate scattering length condensate. 120

List Of Figures

2.1 Scattered wave function for a Morse potential with well-depth chosen to give a positive scattering length. 10
2.2 Scattered wave function for a Morse potential with well-depth chosen to give a negative scattering length. 11
2.3 Density of two scattered particles in a square well from the asymptotic viewpoint. 17
2.4 Flattening of the GP wavefunction for increasing N and positive scattering length. 22

3.1 Chemical potential versus N for 3D isotropic ^{87}Rb condensate. 41
3.2 Ground-state wave function for 3D isotropic ^{87}Rb condensate with 10 000 atoms. 42
3.3 Ground-state wave function for 3D isotropic ^{87}Rb condensate with 10^6 atoms. 43
3.4 Condensate wave function for $D = 2$ with $l = 1$ vortex. 45
3.5 Chemical potential versus N for ^{87}Rb JILA anisotropic TOP trap. . . 48
3.6 Large-N effective potential for Bohn-Esry-Greene BEC hamiltonian for positive, negative and zero scattering length. 52
3.7 Effective potential for N near the critical number of atoms for negative scattering length. 54
3.8 Quantum dot electron-electron interaction energy for $D = 2$ and $D = 3$ for 1s, 2p, and 3d states. 66

5.1 DPT, GP and MGP calculations for the interatomic energy of a small scattering length condensate. 117
5.2 DPT, GP and MGP calculations for the interatomic energy of a large scattering length condensate. 119
5.3 DPT, GP and MGP calculations for the interatomic energy of an intermediate scattering length condensate. 121
5.4 Comparison of breathing mode frequencies for large scattering length. 125

Abstract

Systems that involve N identical, interacting particles under quantum confinement appear throughout many areas of physics, including chemical, condensed matter, and atomic physics. In this thesis, we present the methods of dimensional perturbation theory, a powerful set of tools that uses symmetry to yield simple results for studying such many-body systems. We present a detailed discussion of the dimensional continuation of the N-particle Schrödinger equation, the $D \to \infty$ equilibrium structure, and the normal-mode oscillations of this structure. We use the Wilson FG matrix method to derive general, analytical expressions for the many-body normal-mode vibrational frequencies, and we give analytical results for three N-body quantum-confined systems: the N-electron atom, N-electron quantum dot, and N-atom inhomogeneous Bose-Einstein condensate with a repulsive hard-core potential.

The focus of this thesis will be on the many-body physics of Bose-Einstein condensates (BEC). The achievement of BEC in magnetically trapped alkali-metal atoms in 1995 has generated a considerable amount of experimental and theoretical activity in recent years. In typical BEC experiments, the average distance between the bose atoms is much larger than the range of the atomic interactions, and hence, the properties of these weakly interacting condensates have been successfully described by the mean-field nonlinear Gross-Pitaevskii equation. Recently, however, no longer restricted to the atom's natural interaction parameter, experimentalists have created condensates with a "knob" (i.e., a Feshbach resonance) that allows them to adjust the interaction to whatever strength, repulsive or attractive, they wish. These strongly interacting condensates provide a new test bed for fundamental atomic and many-body physics. In this thesis we develop a theory that goes beyond the standard mean-field approximation for many-body systems.

Feshbach resonances notwithstanding, most experimentally realized atomic-vapor condensates are dilute and are best described by the mean-field Gross-Pitaevskii equation. For this reason, we use dimensional scaling methods to obtain an analytical approximation to the GP equation that is more accurate and flexible than the

commonly used ground-state Thomas-Fermi approximation. We also demonstrate the power of dimensional perturbation theory by providing a full solution of a model BEC Hamiltonian and a two-electron quantum dot Hamiltonian. A feature shared by these examples is the high degree of accuracy provided by the lowest orders of the perturbation theory. In our approach to the full many-body BEC Hamiltonian, we use the lowest orders of many-body dimensional perturbation theory to obtain semi-analytical ground-state energies and collective excitation frequencies. Our many-body calculations for BEC's compare well with the Gross-Pitaevskii results in the weakly-interacting regime, as they should, and are much improved over mean-field theory predictions in the strongly-interacting regime.

Chapter 1

Introduction

1.1 A tale of two particles

According to quantum mechanics, the universe can be divided into two types of particles – fermions and bosons – based on their fundamentally different quantum statistics. Classically, there is also a third type of statistic which both fermions and bosons obey for large temperatures, called Boltzmann statistics. By quantum statistics we do not mean the particle's quantum batting average or on base percentage. Rather, statistics here refers to the allowable arrangements of a collection of particles into energy levels. Fermions are particles with half-integer spin that obey fermi statistics, which specifies that no two *indistinguishable* fermions can be in the same state. Fermions thus have very reclusive social mores, but it is this antisocial behavior that we have to thank for the richness of chemistry and atomic physics. For example, an electron in an atom is a fermion, whose statistics prevent any two from occupying the same orbital, which gives the predictable structure that we see in the periodic table of elements. Two of the many-body systems we will discuss in this thesis involve fermions: the N-electron atom and the N-electron quantum dot.

One typically thinks of quantum theory in the context of the microscopic world of atoms and molecules, but quantum theory is also valid for macroscopic systems. This validity is oftentimes of no important consequence for ordinary macroscopic objects because one can use classical mechanics to obtain the same result more easily. Quantum mechanics is valid for basketballs, for example, but to describe its thermodynamic properties or its trajectory one would be best served to use classical physics. However, for low-temperature, macroscopic systems, where identical particles become *indistinguishable*, classical theory is no longer valid and quantum predictions can differ greatly from classical theory. An example of such a low-temperature, macroscopic,

yet quantum mechanical, system is the Bose-Einstein condensate, which results from a phase transition of a collection of identical bosons into the lowest energy quantum state. Bose-Einstein condensation (BEC) of trapped atomic gases is the focus of this thesis.

If fermions are the most antisocial members of the particle society, then bosons are the opposite extreme of temperament. They are a gregarious bunch who enjoy the company of other bosons. Not only does nothing prevent identical bosons from occupying the same state, but they actually have a tendency to join other bosons that are already in the same state. Which is not to suggest that achieving BEC is easy. See Ref. [1] for a detailed discussion of the cooling and trapping methods used to make a BEC in an atomic gas.

This macroscopic occupation of the ground state is unique to bose particles. It is evident that fermions, with their disdain for each other, cannot form a condensate (without some mechanism like Cooper pairing which tricks the fermions into forming a composite quasi-particle with integer-spin statistics). But it is not immediately obvious that distinguishable (classical) particles cannot form a condensate. One practical reason, as we will see later, is that low temperatures are necessary for BEC formation, and indistinguishability of the particles becomes most relevant at low temperature. However, there is a more fundamental argument, to follow shortly, having to do with the statistics of distinguishable particles.

Indistinguishability is at the heart of quantum mechanics. Electrons have certain properties such as mass, charge and spin. An electron can be in a spin-up or spin-down state, but every spin-up electron is identical to every other spin-up electron. If there were a way to distinguish between two spin-up electrons in an atom then one could in principle follow the trajectories of these two electrons in the atom. As it stands, however, the classical concept of trajectories for electrons in an atom is meaningless because of the indistinguishability of the electrons and the small size of atoms and electrons. The significance of small size can be seen from the Heisenberg uncertainty principle for the position and momentum, which can be written as follows,

$$\Delta x \Delta p \geq \hbar/2, \tag{1.1}$$

where Δx and Δp are the uncertainty in the position and momentum of the particle, respectively, and h is a very small number known as Planck's constant. This equation states that the more precisely you know the position of the particle, the less precisely

you can know its momentum, and vice-versa. Resolving the position of an electron in the atom would require scattering of small-wavelength light off the electron, but the smaller you make the wavelength of light the greater the momentum kick the light gives to the electron, thus, throwing the electron off its original course and making a trajectory measurement meaningless.

So, why are distinguishable (classical) particles unlikely to form a BEC? Imagine a system of N particles with a set of nondegenerate energy levels and a certain fixed amount of energy available to the system. Consider two of the many possible configurations:

1. One particle in each of the lowest N levels.

2. $N-1$ particles in the lowest level and one particle in a higher level with energy equal to that of the $N-1$ excited particles in Case 1.

For bosons, both distributions are equally likely. But for distinguishable (classical) particles, there are $N!$ arrangements corresponding to Case 1, and only N corresponding to Case 2. Thus, for distinguishable particles, arrangements like 2 with a large fraction of the particles in the lowest energy level are much less likely than other arrangements. For bosons, both distributions 1 and 2 are equally likely, which at the moment doesn't tell us much about the likelihood of a macroscopic occupation of bosons in the ground state. Low temperature holds the key to forming BEC.

Why is low temperature so important in achieving BEC? Part of the answer again has to do with indistinguishability of the bosons. In his explanation of the photoelectric effect in 1905 – one of the first applications of quantum theory – Einstein suggested that it is helpful to think of light as composed of particles instead of waves. Later, deBroglie turned this idea around, by proposing that particles with mass should likewise be thought of as waves with wavelength given by

$$\lambda_{\mathrm{dB}} = h/p, \tag{1.2}$$

where p is the particle's momentum. Consider a gas of identical atoms in a container. The temperature of this system is a measure of the average kinetic energy of the individual atoms. Further, the average kinetic energy is proportional to the mean

squared velocity $< v^2 >$ or the mean squared momentum $< p^2 >$. Hence, from Eq. (1.2) we see that the deBroglie wavelength of a particle at temperature T varies as

$$\lambda_{dB} \sim \frac{1}{\sqrt{T}}. \tag{1.3}$$

For large T, the atomic wavelengths are short enough that one can treat the atoms in the gas as distinguishable. As T is lowered, the wave-like nature of the atoms is enhanced and their deBroglie waves begin to overlap each other so that it becomes impossible to tell where one atom stops and another begins – one can no longer treat the atoms as distinguishable. As T shrinks further, the boson waves overlap to form a single macroscopic wavefunction for the entire gas. This is the wavefunction of the condensate, a quantum mechanical system that you can see with the naked eye. In addition to leading to indistinguishability, low T is important for the formation of BEC because the colder the gas, the less energy is available to thermally excite the atoms, and with no energy to occupy a higher energy state, the bosons have no choice – and nothing to prevent them, being bosons – but to all pile into the lowest state.

In 1924, based on the ideas of Bose concerning photons[2], Einstein considered a noninteracting gas of bosons with mass, and concluded that a finite fraction of the particles would occupy the lowest-energy single-particle state[3]. Far from an ideal (noninteracting) gas, however, the first occurrence of BEC was observed in strongly interacting superfiuid liquid ^{4}He in 1938. Direct measurement of the occupancy of the zero-momentum state of superfluid liquid ^{4}He is difficult because of the reduced occupancy of the zero-momentum state due to the strong interactions (approximately 10% of the atoms occupy the zero-momentum state). Besides yielding a larger condensate fraction, creating a BEC in a nearly ideal gas would prove to be of fundamental importance because it would suggest that bose statistics drives the condensation process and not interactions. Creating a gaseous BEC is not a straightforward task, however, because when you cool a gas it tends to liquify or solidify or form molecules which then solidify. It was not until 1995, with the achievement of BEC in a dilute atomic alkali gas, that BEC was observed in a nearly ideal gas as predicted 71 years earlier by Einstein. The 2001 Nobel prize in physics was awarded for this achievement.

Despite the weakness of the interactions, properties of atomic BEC, such as the energy per atom, the radius of the condensate cloud and collective excitation frequencies, show a significant dependence on the strength of the atom-atom interactions

through the s-wave scattering length. The mean-field theory (the nonlinear Gross-Pitaevskii equation) has had great success in describing these properties because in experimentally realized condensates the interatomic spacing is much larger than the range of the interatomic potential. Recently, however, experimenters have taken advantage of Feshbach resonances which allow one to tune the atom-atom interaction strength to any value by adjusting an external magnetic field. This, in turn, has allowed experimenters to create stable condensates of moderate size ($N \sim 10^4$) in a regime where the mean-field theory is no longer expected to be valid; namely, the regime of strong, repulsive interaction[4]. This thesis addresses the breakdown of the mean-field theory by applying the many-body formalism of dimensional perturbation theory.

1.2 Outline of thesis

During the last two decades, techniques to confine and manipulate atoms, ions, and electrons have led to the creation of new N-body quantum systems of both fundamental and technological interest. The condensation of atomic bose gases, the confinement of atoms using optical lattices, and the creation of quantum dots in semiconductors are all examples of novel many-body environments that can be manipulated using external potentials. These systems thus provide a unique opportunity to study many-body effects over a range of interaction strengths as external potentials are tuned. The quantum dot is a nanostructure in which electrons are confined in all three dimensions by an external potential. This "artificial atom" has shown great potential in biological and medical applications and may form the basis for a new generation of semiconductor lasers with applications in quantum computation and quantum cryptography. The atomic vapor Bose-Einstein condensate, a phase transition of a collection of externally trapped identical bosons into the lowest energy quantum state, provides a coherent source of matter waves with possible applications in atom interferometry, atom circuits, holography, precision measurements and quantum information. The confinement of atoms in single cells of optical lattices could provide the controlled interaction required to create a quantum logic gate.

These new quantum-confined N-body systems have resulted in new demands and renewed interest in the many-body techniques of quantum physics and chemistry, originally developed to study atoms and molecules. Mean-field treatments of these N-body systems such as the Hartree-Fock method in atomic physics and also the

Gross-Pitaevskii approximation for Bose-Einstein condensates are inadequate to fully describe many-body effects such as correlation and become particularly inaccurate for systems under tight confinement or strong interparticle interaction. These new systems, which can have a few hundred to millions of particles, present serious challenges for existing many-body methods, most of which were developed with small systems in mind.

In this thesis we develop a novel many-body approach known as many-body dimensional perturbation theory (DPT). In DPT, the radius of each of the N particles is allowed to have D Cartesian components and $1/D$ becomes a perturbation parameter. As $D \to \infty$ the particles become localized in the bottom of an effective potential defined by a centrifugal-like contribution from the kinetic energy and contributions from the other potential energies (i.e., the confinement and interaction potentials). In the case of attractive interparticle forces, the repulsive centrifugal-like term stabilizes the large-D configuration against collapse. The first-order quantum correction corresponds to normal-mode vibrations about the large-D effective potential minimum (see chapter 4).

We develop the methods of many-body dimensional perturbation theory for the study of large N-body systems under quantum confinement. We apply dimensional perturbation theory to many-body quantum confined systems from chemical, condensed matter, and atomic physics. We treat such systems as the N-electron atom, where the confinement is supplied by the Coulomb attraction of the nucleus, and the N-electron quantum dot, an atom-like many-body system from condensed matter physics, where the confinement of the N electrons is supplied by an external, isotropic trapping potential. Since N-electron atoms are not the primary focus of this thesis, we direct the reader to Ref. [5] and references therein for a discussion of dimensional perturbation theory of few-electron atomic systems. However, we do provide a full calculation for the two-electron quantum dot in addition to low-order results for the N-electron dot. The final application of many-body DPT is N identical hard spheres in an isotropic trap, which provides a model appropriate for describing an inhomogeneous Bose-Einstein condensate of alkali-metal atoms and which is the primary focus of this thesis.

In Chapter 2 we discuss some of the standard theoretical tools of BEC. We derive the mean-field Gross-Pitaevskii equation, and its highly useful analytical approximation to the ground state known as the Thomas-Fermi approximation. We also discuss two standard approximations to the mean-field theory of excitations of the

condensate. Also in the introduction we discuss analytical beyond-mean-field corrections to the ground-state energy and excitation frequencies. In Chapter 3 we discuss three applications of DPT to systems that can be reduced to single degree of freedom problems. As previously mentioned, one such system is the two-electron quantum dot. The other two singe degree of freedom applications of DPT in Chapter 3 are for theories describing BEC's. One of these theories results in a linear Schrödinger equation with the number of atoms as a parameter. We solve this linear equation in a manner similar to the two-electron quantum dot, except we use $1/N$ as the perturbation parameter instead of $1/D$. Since most BEC's are in the dilute regime we apply the methods of DPT to the Gross-Pitaevskii equation, which is the other BEC theory treated in this chapther. This example is a departure from previous applications of DPT to low degree of freedom systems in that the method is applied to a non-linear Schrödinger equation.

We develop the general microscopic-level many-body approach in Chapter 4, and then apply it to the N-electron atom and quantum dot. In Chapter 5 we use these methods to derive beyond-mean-field-theory results for the ground state and collective excitation spectrum of inhomogeneous atomic vapor condensates. We are most interested in a high density regime, where the gas is no longer dilute, and yet it is not so dense that the alkali atoms collapse from the metastable BEC state into their true ground state, which is a solid. We use a shape-dependent interatomic potential, and we make no prior assumptions about the separability of the condensate wave function. We present numerical results for the ground-state energies and excitation frequencies that are more accurate than mean-field predictions. Moreover, our results are semi-analytical and offer insight into the many-body physics of BEC.

The appendices contain derivations that are nonetheless important, but that we feel may take away from the flow of the main text. For the interested reader, we direct him or her to appendices for more detailed derivations and technical information.

Chapter 2

Standard methods for Bose-Einstein condensates

In this chapter we introduce some of the standard theoretical methods used to study atomic-gas Bose-Einstein condensates. With so much activity in this rapidly expanding field since the mid-1990's, not to mention the more than half-century of work before that, which focused on superfluid liquids, we can only hope to scratch the surface in this review chapter. Fortunately, however, there are some excellent review materials (e.g., Dalfovo *et al.*[6], Leggett[7], and articles from the book edited by Inguscio *et al.*[8]), which should help the interested reader.

In Sec. 2.1, we introduce some of the necessary concepts from scattering theory. Then in Sec. 2.2 we introduce the main equation of atomic BEC, the mean-field or Gross-Pitaevskii (GP) equation, which we derive using the first-quantization approach with an single-particle trial wave function. We also discuss the Bogoliubov approach and its long-wavelength interpretation of the condensate wavefunction. In Sec. 2.3 we introduce the extremely useful, simple and powerful Thomas-Fermi approximation of the GP ground state. The Thomas-Fermi approximation yields physical insight into the properties of the GP equation and becomes an exact description of the GP density for strong interaction, but, as we will see in chapter 5 when we discuss the breakdown of the mean-field theory, the GP equation itself – and hence the Thomas-Fermi approximation – becomes a poor model of the physical BEC. Finally, in Sec. 2.4, we discuss collective excitations of the condensate within the context of mean-field theory, and we derive some relationships that will be needed later in the thesis.

2.1 Basic scattering theory

Ultracold collisions play an important role in the physics of atomic BEC. The long wavelength, macroscopic phenomenon that is BEC is a manifestation of microscopic interactions. Typical condensates are dilute enough that their properties are accurately described by the s-wave scattering length and no other details of the interatomic potential. When two atoms in a gas are close to each other they feel the short-range details of the interatomic potential and the scattered wavefunction shows rapid spatial variation. However, for a dilute gas the atoms spend most of their time far away from each other and only feel the long range parts of the interatomic potential. Consequently the atomic wavefunctions are slowly varying in space, and one is justified in replacing the precise interatomic potential with an effective interaction known as the Fermi pseudopotential.

The scattered wavefunction for two identical atoms interacting via some potential $V(r)$ is given by the following Schrödinger equation in relative coordinates:

$$\left[\frac{\hbar^2}{2\mu}\nabla^2 + V(r)\right]\psi(E,r) = E\psi(E,r), \tag{2.1}$$

where $\mu = m/2$ is the reduced mass. In Figs. 2.1 and 2.2 below, we show the short-range numerical solution of this Schrödinger equation for a Morse potential for two different well-depths, D_M:

$$V_{\text{Morse}}(r) = D_M e^{-\alpha(r-r_o)}\left(e^{-\alpha(r-r_o)} - 2\right). \tag{2.2}$$

The Morse parameters, α and r_o, are associated with the width of the well and the location of the well minimum, respectively. At very short range one can see the rapid spatial variation of the scattered wavefunction due to the details of the Morse potential, which supports several bound states, but at long range (beyond that shown in the figures) the wavefunction has the form of a sine wave. These two figures illustrate the physical interpretation of the scattering length as an effective shift in the origin of the long-range wavefunction. In Fig. 2.1 the shift is positive, indicating a positive scattering length, while Fig. 2.2 shows a negative scattering length.

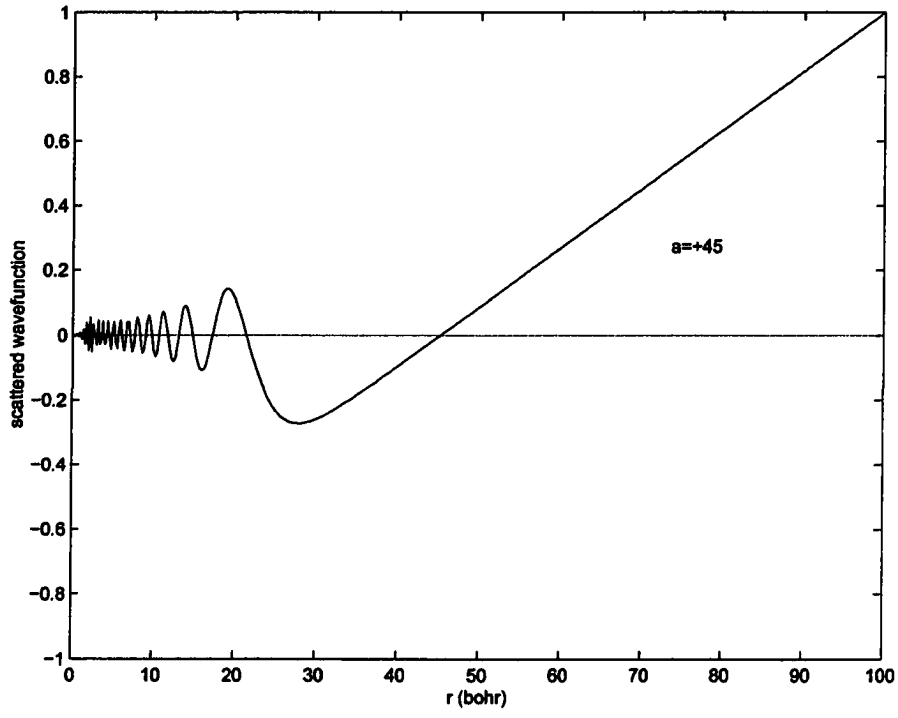


Figure 2.1: Numerical solution of Eq. (2.1) for a Morse potential in the short-range regime. The depth is chosen to give a positive scattering length, which manifests itself as positive shift in the long-range wavefunction.

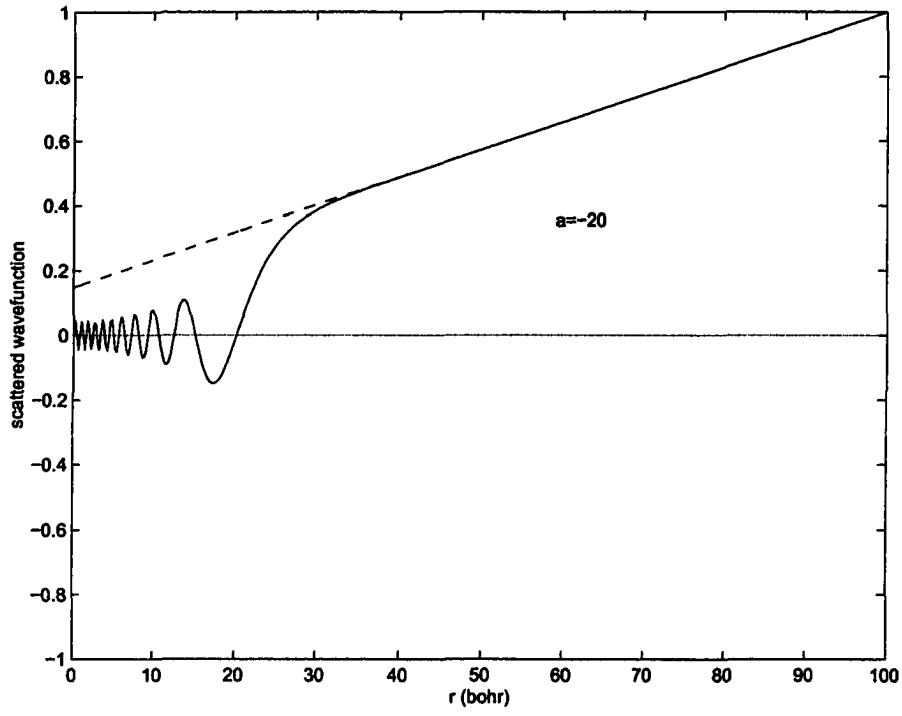


Figure 2.2: Numerical solution of Eq. (2.1) for a Morse potential in the short-range regime. The depth is chosen to give a negative scattering length, which manifests itself as a negative shift in the long-range wavefunction.

The asymptotic solution of Eq. (2.1) is of the form of an incoming plane wave, assumed to be travelling along the z-axis, plus a scattered spherical wave:

$$\psi(\mathbf{r}) = e^{ikz} + f(\theta)\frac{e^{ikr}}{r}, \tag{2.3}$$

where $k = \sqrt{2\mu E}/\hbar$ and we have assumed that the interaction is spherically symmetric so that the scattering amplitude $f(\theta)$ only depends on the scattering angle. For scattering at low energy ($k \to 0$), the scattering amplitude becomes a constant defined in terms of the scattering length: $f(\theta) = -a$. The wavefunction of Eq. (2.3) becomes

$$\psi \to 1 - a/r, \tag{2.4}$$

and again we see that the scattering length represents the r-intercept of the long-range wavefunction.

In order to transform the Schrödinger differential equation into an equivalent integral equation, we rewrite Eq. (2.1) in the following form:

$$\left[E + \frac{\hbar^2}{2\mu}\nabla^2\right] = V(r)\psi(r), \tag{2.5}$$

which is solved by the Lippman-Schwinger equation:

$$\psi(r) = e^{ikz} + \int G(r,r')V(r')\psi(r')dr'. \tag{2.6}$$

The free-particle Green's function G is given by

$$G(r,r') = -\frac{\mu}{2\pi\hbar^2}\frac{e^{ik|r-r'|}}{|r-r'|}, \tag{2.7}$$

which, for $r \gg r'$, can be approximated by

$$G(r,r') \approx -\frac{\mu}{2\pi\hbar^2}\frac{e^{ikr}}{r}\left[e^{-i\vec{k}_r\cdot\vec{r}'} + O\left(\frac{r'}{r}\right)\right], \tag{2.8}$$

where $\vec{k}_r = k\vec{r}/r$ is a vector of length k pointing in the direction of $\vec{r}$. Inserting this approximation into Eq. (2.6) and comparing the resulting equation with Eq. (2.3), one obtains an implicit expression for the scattering amplitude:

$$f(\theta) = -\frac{m}{4\pi\hbar^2}\int e^{-i\vec{k}_r\cdot\vec{r}'}V(r')\psi(r')dr'. \tag{2.9}$$

The integral in this equation can be interpreted as the T matrix, a transition matrix between the initial incoming state $\psi(r')$ and final outward travelling state $e^{-i\vec{k}_r\cdot\vec{r}'}$. Furthermore, if the effect of the interatomic potential is small, as it is should be for a dilute gas, one may replace the exact wavefunction $\psi(r')$ in the integral with the unperturbed incoming plane wave $\psi_i(r') = \exp(ikz')$. This assumption is the Born approximation, under which Eq. (2.9) can be written as

$$f^B(\theta) = -\frac{m}{4\pi\hbar^2}\int e^{-i\vec{q}\cdot\vec{r}'}V(r')dr'. \tag{2.10}$$

The vector $\vec{q} = k(\hat{e}_r - \hat{e}_z)$, where $\hat{e}_r$ and $\hat{e}_z$ are unit vectors in the direction of the radial vector and z-axis, respectively.

For low-energy (ultracold) collisions, for which $k \to 0$ and hence $q \to 0$, Eq. (2.10) becomes

$$f^B = -\frac{m}{4\pi\hbar^2}\int V(r')dr'. \tag{2.11}$$

In the low-energy limit the scattering amplitude reduces to the s-wave partial wave amplitude which can then be identified with the scattering length as $f^B = -a$ (see any scattering textbook, such as Refs. [9] and [10], for more details). This approximation can be summarized as

$$\int V(r')dr' = \frac{4\pi\hbar^2 a}{m} \tag{2.12}$$

or

$$V(r-r') = \frac{4\pi\hbar^2 a}{m}\,\delta(r-r'), \tag{2.13}$$

which, as we will see momentarily, is the underlying interaction used in the Gross-Pitaevskii equation.

2.2 Ground-state Mean-field theory for bosons

The key to deriving the $T = 0$K Gross-Pitaevskii equation for the ground state of the condensate is to understand that under dilute conditions one may replace the true interatomic potential with a delta function potential that reproduces the long-range effects of the true interatomic potential (i.e., the s-wave scattering length)[6, 7, 8]. Thus, we replace the true interatomic potential by

$$V_\delta(\mathbf{r}) = \frac{4\pi\hbar^2 a}{m}\delta(\mathbf{r}), \tag{2.14}$$

where a is the s-wave scattering length. The physical parameters in V_δ come from the Born approximation for the scattering amplitude of identical particles of mass m [Eq. (2.12)]. It is assumed that the scattering atoms are of very long wavelength and low energy. Eq. (2.14) is a good approximation when the interatomic spacing is much larger than the scattering length; the atoms spend most of their time far away from each other, and hence, they do not sample the short-range, detailed shape of the true interatomic potential.

2.2.1 Single-particle picture

In this derivation of the GP equation, we use the first-quantization formalism (i.e., where the many-body wave function is expressed in terms of the spatial coordinates) with a single-particle basis. This derivation follows closely the second-quantization Hartree theory presented in Ref. [11]. The ansatz for the ground-state wavefunction of a collection of bosons is simply

$$\Psi(\mathbf{r}_1, \ldots, \mathbf{r}_N) = \prod_{i=1}^{N} \psi(\mathbf{r}_i), \tag{2.15}$$

where ψ is some normalized (to unity), single-particle wavefunction to be determined, and N is the number of condensate atoms. The equation for ψ is found by applying the variational principle to the Hamiltonian

$$H = \sum_{i=1}^{N} H_o(\mathbf{r}_i) + \sum_{i<j}^{N} V(\mathbf{r}_i - \mathbf{r}_j), \tag{2.16}$$

where V is the interatomic potential and the single-particle Hamiltonian H_o is:

$$H_o(\mathbf{r}) = -\frac{\hbar^2}{2m} \nabla^2 + V_{\text{conf}}(\mathbf{r}), \tag{2.17}$$

where V_{conf} is the external confining potential. Given the trial wave function in Eq. (2.15), the expectation value of H or the total mean-field energy of the N-particle system in bra-ket notation is given by

$$\langle H \rangle_N = E_N^{\text{MF}} = N \frac{\langle \psi | H_o | \psi \rangle}{\langle \psi | \psi \rangle} + \frac{N(N-1)}{2} \frac{\langle \psi\psi | V | \psi\psi \rangle}{\langle \psi | \psi \rangle^2}. \tag{2.18}$$

The variation of Eq. (2.18) with respect to arbitrary ψ^* gives

$$\begin{aligned} 0 = \delta \langle H \rangle_N &= N \frac{\langle \delta\psi | H_o | \psi \rangle}{\langle \psi | \psi \rangle} + \frac{N(N-1)}{2} \frac{\langle \delta\psi\psi + \psi\delta\psi | V | \psi\psi \rangle}{\langle \psi | \psi \rangle^2} \\ &\quad - N \frac{\langle \psi | H_o | \psi \rangle}{\langle \psi | \psi \rangle^2} \langle \delta\psi | \psi \rangle - N(N-1) \frac{\langle \psi\psi | V | \psi\psi \rangle}{\langle \psi | \psi \rangle^3} \langle \delta\psi | \psi \rangle, \end{aligned} \tag{2.19}$$

which can be rearranged to give

$$\begin{aligned} 0 = \delta \langle H \rangle_N &= N \langle \delta\psi | \left[H_o + (N-1) \langle \psi | V | \psi \rangle \right] | \psi \rangle \\ &\quad - N \langle \delta\psi | \left[\langle \psi | H_o | \psi \rangle + (N-1) \langle \psi\psi | V | \psi\psi \rangle \right] | \psi \rangle, \end{aligned} \tag{2.20}$$

where we used the fact that the wave function ψ is normalized to unity. Since we have assumed arbitrary variations $\delta\psi^*$, Eq. (2.20) gives

$$\left[H_o(\mathbf{r}) + (N-1)\int d\mathbf{r}'\psi^*(\mathbf{r}')V(\mathbf{r}-\mathbf{r}')\psi(\mathbf{r}')\right]\psi(\mathbf{r}) = \mu\psi(\mathbf{r}), \tag{2.21}$$

where the eigenvalue μ is defined as

$$\mu = \frac{E_N^{\mathrm{MF}}}{N} + \frac{N-1}{2}\langle\psi\psi|V|\psi\psi\rangle, \tag{2.22}$$

which, as one can see using Eq. (2.18), is equal to the bracketed term in the second line of Eq. (2.20). A few words should be said about μ. In the first quantization approach, μ is the energy of the ground-state orbital ψ. From Eq. (2.18) one can see that $\mu = E_N^{\mathrm{MF}} - E_{N-1}^{\mathrm{MF}}$, which is approximately the energy needed to remove an atom from the condensate. This is essentially the definition of the chemical potential in the Bogoliubov approach, where μ is a Lagrange multiplier defined by the grand canonical Hamiltonian to fix the average number of atoms[12].

The final touch is to use the low-energy, dilute-gas approximation for the interatomic potential [i.e., the delta function of Eq. (2.14)] in the integral in Eq. (2.21). This gives the number-conserving Gross-Pitaevskii equation:

$$-\frac{\hbar^2}{2m}\nabla^2\psi(\mathbf{r}) + V_{\mathrm{conf}}(r)\psi(\mathbf{r}) + (N-1)U_3|\psi(\mathbf{r})|^2\psi(\mathbf{r}) = \mu\psi(\mathbf{r}), \tag{2.23}$$

with coupling constant

$$U_3 = (4\pi\hbar^2 a)/m. \tag{2.24}$$

Essentially Eq. (2.23) is a Schrödinger equation with a single-atom Hamiltonian plus a contribution from the mean field. The mean-field term can be interpreted as the potential that a representative atom feels due to the remaining $(N-1)$ atoms of density $(N-1)|\psi|^2$. When $N = 1$ or $a = 0$, the mean-field term drops out of the GP equation and one recovers the ideal gas, that is, the zero-point motion in the trap or the ground state of the trapping potential. One often sees the GP equation written with an N rather than an $(N-1)$ preceding the mean-field term, but for most experimentally realized condensates the difference is negligible. As we have seen above, the $(N-1)$ factor in front of the nonlinear mean-field term follows from number conserving Schrödinger quantum mechanics, using a single-particle initial state.

In the independent-particle approximation, each particle moves in an effective potential which represents the average effect of the interaction between the atom and the remaining $(N-1)$ atoms. The ground state of the condensate is composed of N identical single-particle orbitals ψ, and in the independent-particle approximation the motion of one atom in the ground state must be the same as the remaining $(N-1)$. The probability of finding one of these particles between x_1 and x_2 is $\int_{x_1}^{x_2} \psi^*\psi$, where $\psi^*\psi$ is a probability density. If we were to measure the position of a particle N times, each time preparing the system so that it had the same ψ, the number of times the particle would be found between x_1 and x_2 would be $N\int_{x_1}^{x_2} \psi^*\psi$, where $N\psi^*\psi$ would be the number density. Instead of measuring a single particle N times, we may equivalently measure an ensemble of N particles all at once, obtaining the same result for the number density. This collection of N particles represents the condensate in the independent-particle approximation, and hence, in the single-particle picture the condensate number density is

$$n(r) = N|\psi|^2. \tag{2.25}$$

For positive (negative) scattering length, the mean-field energy increases above (decreases below) the noninteracting ideal-gas result. This can be seen by inspection of the GP equation, but it can also be understood in terms of scattering theory by considering the scattered wavefunction of two trapped condensate atoms[13]. Recall from the discussion surrounding Figs. 2.1 and 2.2 that from the viewpoint of the asymptotic wave, the scattering length manifests itself as an effective shift of the origin of the scattered wavefunction. In this heuristic discussion, we treat the two interacting atoms in a trap as a single particle in a box. We replace the harmonic trap with a one-dimensional square well with the right wall fixed by the oscillator length $(\sqrt{\hbar/m\omega_o})$ and with the leftmost wall allowed to shift from $x = 0$ (the noninteracting case) depending on the sign of the scattering length. This is illustrated in Fig. 2.3, where the walls of the box for the noninteracting density (solid line) are vertical dotted lines. For a noninteracting gas, the length of the box is L, and the energy is proportional to $1/L$. For positive scattering length (plus-signs), the box is squeezed by an amount equal to $L - a$ and the energy increases with respect to the ideal gas energy. And for negative scattering length, the box widens by an amount equal to $L + a$, causing the energy to decrease with respect to the ideal-gas energy. For a many-atom (single-component) condensate in which the interatomic interaction yields a positive scattering length, the additional energy from the extra curvature of

the scattered wavefunction, which is imposed by the boundary condition at $r = a$, causes the condensate wavefunction to climb up the walls of the trap.

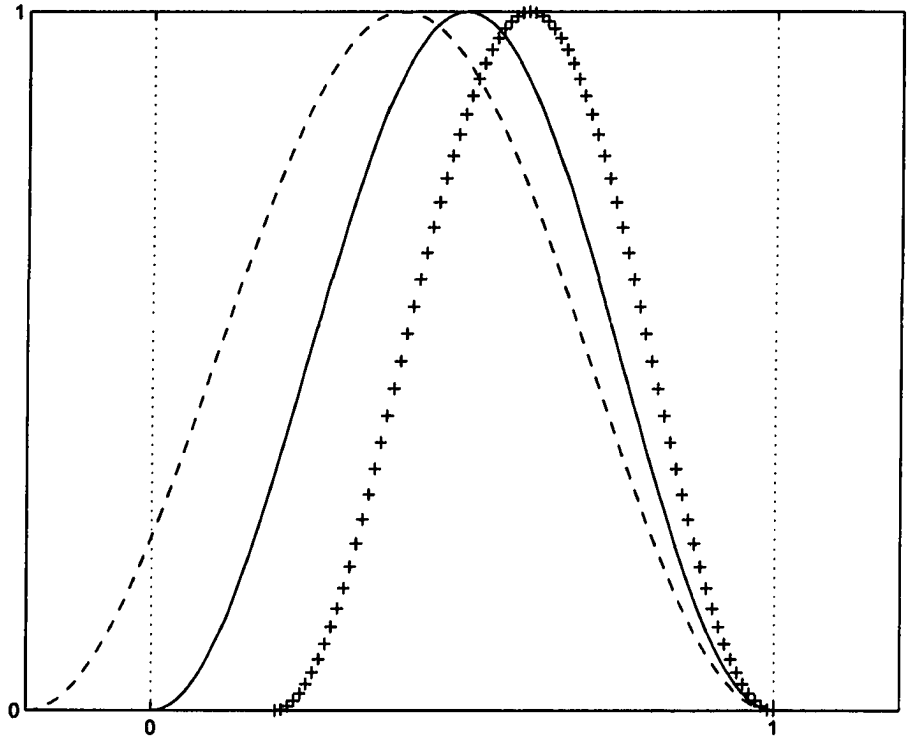


Figure 2.3: Density of a scattered particle in a square well from the asymptotic viewpoint. Vertical dotted lines represent the walls of the box for noninteracting atoms (solid line). Plus-signs signify the scattered density for positive scattering length, while minus-signs signify the negative scattering length case. The effect of a positive (negative) scattering length is to increase (decrease) the energy with respect to the ideal gas result.

2.2.2 Classical field picture

We have focused on the number conserving formalism of mean-field theory since our many-body formalism is also number conserving. The most commonly used approach for dealing with a BEC in the mean-field approximation was that proposed by Bogoliubov[14]. Since the Bogoliubov approach uses the second quantization formalism, which is not number conserving, the number of particles is conserved by

introducing the chemical potential in the grand canonical Hamiltonian. We now briefly review this theory (see articles in Ref. [8] for more details).

The many-body Hamiltonian describing N interacting bosons confined by an external potential V_{trap} is given, in second quantization, by

$$\begin{aligned}\hat{H} &= \int d\mathbf{r}\hat{\psi}^{\dagger}(\mathbf{r})\left[-\frac{\hbar^2}{2m}\nabla^2 + V_{\mathrm{trap}}(\mathbf{r})\right]\hat{\psi}(\mathbf{r}) \\ &\quad + \frac{1}{2}\int d\mathbf{r}d\mathbf{r}'\hat{\psi}^{\dagger}(\mathbf{r}')\hat{\psi}^{\dagger}(\mathbf{r})V(\mathbf{r}-\mathbf{r}')\hat{\psi}(\mathbf{r}')\hat{\psi}(\mathbf{r}),\end{aligned} \tag{2.26}$$

where $\hat{\psi}^{\dagger}(\mathbf{r})$ and $\hat{\psi}(\mathbf{r})$ are boson field operators that create and annihilate a particle at the position $\mathbf{r}$, and $V(\mathbf{r}-\mathbf{r}')$ is the two-body interatomic potential. The main idea of the Bogoliubov approach is first to separate out the condensate $\hat{a}_o\psi_o$ from the excited states $\hat{\theta}$ in the second quantization $\hat{\psi}$-operator:

$$\hat{\psi} = \hat{a}_o\psi_o + \hat{\theta}, \tag{2.27}$$

where $\hat{a}_o$ is the annihilation operator for an atom in the ground-state orbital. The c-number ψ_o is the field-function of the condensate, normalized to unity. The second part of the Bogoliubov approach is to assume that the condensate has a very large occupation of the ground-state orbital so that one may make the replacement $\hat{a}_o \approx \sqrt{N_o}$. The motivation for this replacement can be seen from the relationships for the ground-state creation and annihilation operators acting on a state labelled by a set of occupation numbers:

$$\hat{a}_o^{\dagger}|n_o, n_1, \ldots, n_N\rangle = \sqrt{n_o+1}|n_o+1, n_1, \ldots, n_N\rangle \tag{2.28}$$

$$\hat{a}_o|n_o, n_1, \ldots, n_N\rangle = \sqrt{n_o-1}|n_o-1, n_1, \ldots, n_N\rangle. \tag{2.29}$$

Assuming that the occupation of the ground state is quite large (i.e., $n_o = N_o \gg 1$), and consequently the occupation of the excited states is small, we have $N_o \pm 1 \approx N_o$. The operator $\hat{a}_o$ can be replaced by $\sqrt{N_o}$ and using this substitution one can write the following effective boson field operator:

$$\hat{\psi} = \sqrt{N_o}\psi_o + \hat{\theta}, \tag{2.30}$$

where N_o is the number of condensate atoms. In this approximation, matrix elements involving $\hat{a}_o$ are of order $\sqrt{N_o}$, while matrix elements involving excited states $\hat{\theta}$ are at

most of order unity. The c-number ψ is a long-wavelength classical field made up of condensate bosons, analogous to an electromagnetic wave, a classical field composed of photons.

The consequence of the replacement in Eq. (2.30) is that the number operator $\hat{N} = \int d\mathbf{r}\hat{\psi}^\dagger\hat{\psi}$ does not commute with the Hamiltonian $\hat{H}$, causing the number of atoms to not be conserved. To overcome this, one introduces the grand canonical Hamiltonian $\hat{K} = \hat{H} - \mu\hat{N}$, where μ is the chemical potential which is chosen to fix the average number of particles. In the standard Bogoliubov approach, one assumes that only the condensate part of the modified Hamiltonian $\hat{K}$, denoted by $\hat{K}_o$, dominates the physics at low temperature, and equating to zero the variation of $\hat{K}_o$ with respect to ψ_o one obtains the time-independent Gross-Pitaevskii equation[15, 16]:

$$-\frac{\hbar^2}{2m}\nabla^2\psi_o + V_{\text{conf}}(r)\psi_o + NU_3|\psi(\mathbf{r})|^2\psi_o = \mu\psi_o. \tag{2.31}$$

The condensate number density in the Bogoliubov approximation [Eq. (2.30)] is

$$n(r) \equiv \hat{\psi}^\dagger\hat{\psi} \approx N_o|\psi_o|^2. \tag{2.32}$$

This result helps us see that the GP equation (2.31) is a classical equation in the sense that ψ_o is not an operator, but a complex function whose modulus and gradient of the phase ϕ have a clear classical meaning:

$$\psi_o = |\psi_o|e^{i\phi}, \quad n_o(r,t) = N_o|\psi_o|^2, \quad \text{and} \quad \mathbf{v}(r,t) = \frac{\hbar}{m}\nabla\phi, \tag{2.33}$$

where n_o is the density and $\mathbf{v}$ the velocity of the classical gas of atoms. The classical meaning of the GP equation can be seen more fully in Appendix A, where we show how to write the time-dependent GP equation in the form of classical equations for the potential flow of a gas [Eqs. (A8) and (A9)]. For example, in Appendix A, we show how the quantity $\frac{\hbar}{m}\nabla\phi$ arises as the velocity field.

The single-particle approach given in the previous subsection is sometimes referred to in the literature as the Hartree-Fock approximation. The wavefunction is built up from single particle wavefunctions. For the ground-state, all of the atoms have the same wavefunction. In the Bogoliubov picture, the wavefunction has a completely different interpretation. In this picture, the wavefunction can be viewed as a long-wavelength, classical field. These two pictures complement each other and nearly coincide for the ground state in that both formalisms give the same number density

[i.e., Eqs. (2.32) and (2.25)]. In most cases the numerical predictions based on each picture are practically the same.

2.3 Thomas-Fermi approximation for the GP ground state

The ground-state Thomas-Fermi (TF) approximation is valid when the mean-field term in the GP equation dominates the kinetic and trap energies, which occurs for large $Na/a_{\rm ho}$, where N is the number of atoms and $a/a_{\rm ho}$ is the scattering length in oscillator units ($a_{\rm ho} = \sqrt{\hbar/m\omega_o}$, where ω_o is the trap frequency). The simplifying assumption of the TF approximation is to neglect the kinetic energy of the GP equation, which reduces the partial differential equation to an algebraic one. The concept of using an exactly soluble limit of a system is also the driving force behind dimensional perturbation theory. This relationship between TF and the lowest order DPT approximation of the GP is discussed further in Sec. 3.1 and Ref. [17]. The fact should be noted, and possibly has not been emphasized enough in the literature, that the TF approximation has an upper limit on the region of validity in terms of the number of atoms and scattering length. Mathematically, in the TF limit $Na/a_{\rm ho} \gg 1$, the TF density becomes a near perfect description of the mean-field GP density. However, if N and/or $a_{\rm ho}$ become too large, the mean-field theory itself, which TF describes, breaks down.

For any system of particles, the TF approximation corresponds to large N ($N >> 1$). The TF model was originally applied to the many-electron atom in the late 1920's by replacing the complicated many-body wavefunction by a density that treats the electrons as a uniform charge distribution. The TF model for atoms describes the least bound electron in a radially symmetric potential due to the mean field of the remaining electrons and the field due to the nuclear charge. This description is analogous to the description of a BEC by the number-conserving GP equation(2.23). This is a very simple model, but the TF approximation to the ground state of neutral and positively ionized atoms works unexpectedly well, but only when the number of electrons, N, is large. There are many excellent textbook reviews of the TF limit for atoms, such as Refs. [9] and [10].

The TF treatment of BEC is restricted to repulsive interactions ($a > 0$) because the TF limit (i.e., large N) cannot be reached for negative scattering length atoms

before the attractive forces cause the condensate to collapse above some critical number of condensate atoms. The TF limit ($N >> 1$) for BEC results in the quantum kinetic energy, or quantum pressure, term becoming negligibly small (compared to the trap and atom-atom energies), falling off as $N^{-\frac{4}{5}}$ [see Eqs. (2.43) and (2.44)]. The physical reason for the relative smallness of the quantum kinetic energy is that as N increases, the central density of the condensate lowers and becomes flatter assuming as we have that $a > 0$. The quantum kinetic energy coming from the uncertainty principle, $\nabla \cdot (\nabla\sqrt{n})$, where $n = N\psi^2$ is the condensate density, becomes small compared to the other energy scales except at the outer edge of the condensate beyond the classical cutoff radius R [see Eq. (2.48)] where TF breaks down. This may seem counter to classical intuition which would suggest that the kinetic energy of an oscillating particle would be smallest near the edge of the harmonic oscillator trap, but while the TF limit for the GP equation is in some sense a classical limit, the GP wavefunction is a long-wavelength classical field, and hence the classical particle picture is not relevant. This flattening of the condensate wavefunction can be seen in Fig. 2.4 below, which shows the numerical solution of the GP nonlinear Schrödinger equation for ^{87}Rb condensates (small, positive scattering length) containing different numbers of atoms.

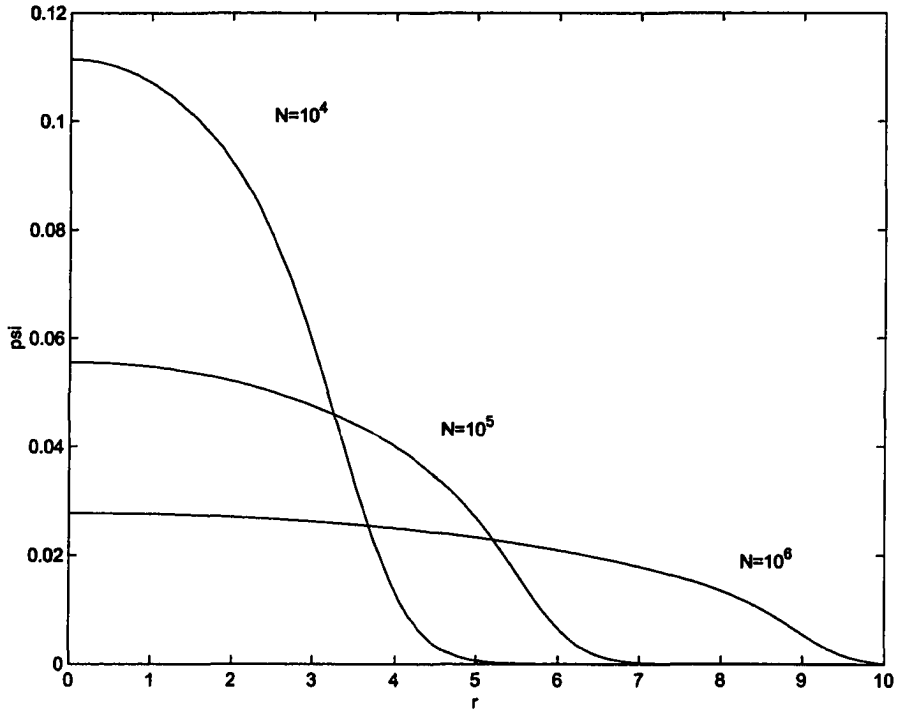


Figure 2.4: Numerical solution of the GP nonlinear Schrödinger equation for ^{87}Rb condensates (positive scattering length) containing different numbers of atoms. Flattening of the GP wavefunction occurs for increasing N and positive scattering length.

The suggestive term "Thomas-Fermi" has been applied in the BEC literature to this limit because it is a large-N limit where one would expect the system to behave statistically; however, a more appropriate modifier for this limit might be "classical" since it results in the neglect of the kinetic energy, localizing the system (see Sec. 3.1.3 and Ref. [18]). We will demonstrate the justification for the neglect of the kinetic energy term in the large-N limit by following a scaling of Eq. (2.35) originally given by Baym *et al.*[19].

We begin by considering the time-dependent Gross-Pitaevskii equation or nonlinear Schrödinger equation,

$$i\hbar\frac{\partial\Psi(\mathbf{r},t)}{\partial t} = -\frac{\hbar^2}{2m}\nabla^2\,\Psi(\mathbf{r},t) + V_{\mathrm{conf}}(\mathbf{r})\Psi(\mathbf{r},t) + NU_3|\,\Psi(\mathbf{r},t)\,|^2\Psi(\mathbf{r},t), \qquad (2.34)$$

where the three-dimensional coupling constant is $U_3 = (4\pi\hbar^2 a)/m$, a is the s-wave scattering length, V_{conf} is the external confining potential. In Eq. (2.34) we are

assuming large-N, which is why we use N instead of $N-1$ in the mean-field term. Assuming a stationary state, $\Psi(\mathbf{r},t) = e^{-\frac{i\mu t}{\hbar}}\psi(\mathbf{r})$, and inserting it into Eq. (2.34), we obtain the time-independent GP equation for $\psi(\mathbf{r})$:

$$-\frac{\hbar^2}{2m}\nabla^2\psi(\mathbf{r}) + V_{\text{conf}}(r)\psi(\mathbf{r}) + NU_3|\psi(\mathbf{r})|^2\psi(\mathbf{r}) = \mu\psi(\mathbf{r}), \tag{2.35}$$

where μ is the chemical potential, the energy needed to add an additional atom to the condensate (i.e., $\mu = \frac{\partial E}{\partial N}$), and we will assume an anisotropic trap, typical of most experimental condensates:

$$V_{\text{conf}}(\mathbf{r}) = \frac{1}{2}m(\omega_\perp^2 r_\perp^2 + \omega_z^2 z^2). \tag{2.36}$$

We next scale the radius and wavefunction as:

$$\mathbf{r} = (a_\perp\eta)\bar{\mathbf{r}} \tag{2.37}$$

$$\psi = \frac{1}{(a_\perp\eta)^{3/2}}\overline{\psi} \tag{2.38}$$

where $a_\perp = \sqrt{\hbar/m\omega_\perp}$ is the characteristic oscillator length scale and η is a dimensionless parameter characterizing the interatomic interactions. We will defer writing the explicit form of η until later in the scaling of the Schrödinger equation when its form will be logically deduced. The particular form of the wavefunction scaling in Eq. (2.38) is chosen so as to maintain a simple form for the normalization condition. With these scalings, the normalization condition remains unchanged, namely,

$$2\pi\int d\bar{z}d\bar{r}_\perp\bar{r}_\perp^2|\,\overline{\psi}(r)\,|^2 = 1. \tag{2.39}$$

Substituting Eq. (2.37) into Eq. (2.35), using the definition of U_3, and dividing through by $\frac{1}{2}\hbar\omega_\perp$ gives the following:

$$\left(-\frac{1}{\eta^2}\nabla^2 + \eta^2(\bar{r}_\perp^2 + \lambda^2\bar{z}^2) + 8\pi Naa_\perp^2|\,\overline{\psi}\,|^2\right)\overline{\psi} = \frac{2\mu}{\hbar\omega_\perp}\overline{\psi}, \tag{2.40}$$

where $\lambda = \omega_z/\omega_\perp$ is the anisotropy parameter. Now making the substitution for the wavefunction prescribed by Eq. (2.38) and dividing through by η^2 we find

$$\left(-\frac{1}{\eta^4}\nabla^2 + (\bar{r}_\perp^2 + \lambda^2\bar{z}^2) + \frac{8\pi Na}{a_\perp}\frac{1}{\eta^5}|\,\overline{\psi}\,|^2\right)\overline{\psi} = \nu\overline{\psi}, \tag{2.41}$$

where

$$\nu = \frac{2\mu}{\hbar\omega_\perp \eta^2}. \tag{2.42}$$

Accordingly, a natural definition for η is

$$\eta = \left(\frac{8\pi a}{a_\perp} N\right)^{\frac{1}{5}}, \tag{2.43}$$

which further simplifies Eq. (2.41) to

$$\left(-\frac{1}{\eta^4}\nabla^2 + \left(\bar{r}_\perp^2 + \lambda^2\bar{z}^2\right) + |\,\overline{\psi}\,|^2\right)\overline{\psi} = \nu\overline{\psi}. \tag{2.44}$$

For large Na/a_{ho}, the kinetic energy term drops off as $\eta^{-4} \sim N^{-\frac{4}{5}}$, so in the TF limit it is justified to drop the kinetic energy. The TF (large-N) limit of Eq. (2.44) gives the TF density:

$$|\,\overline{\psi}\,|^2_{\text{TF}} = \begin{cases} \nu - (\bar{r}_\perp^2 + \lambda^2\bar{z}^2), & 0 \le \bar{r}_\perp^2 + \lambda^2\bar{z}^2 < \nu \\ 0, & \bar{r}_\perp^2 + \lambda^2\bar{z}^2 \ge \nu \end{cases}. \tag{2.45}$$

The TF density defines an ellipsoid, whose transverse radius we define as R and whose conjugate radius we define as Z. Requiring that the density be continuous on the surface of the ellipsoid, we can write these radii in terms of ν:

$$\nu = R^2 \quad \nu = \lambda^2 Z^2. \tag{2.46}$$

One then uses the normalization (2.39) to calculate ν, which in turn gives the TF chemical potential, radius and density. The normalization condition gives the following:

$$1 = \int\int_{\{\bar{r}_\perp^2 + \lambda^2\bar{z}^2 \le \nu\}} \bar{r}_\perp d\bar{r}_\perp d\bar{z}\left(\nu - (\bar{r}_\perp^2 + \lambda^2\bar{z}^2)\right), \tag{2.47}$$

where the notation for the integration limits means to integrate over the interior volume of the ellipsoid. This integral is easily calculated by first integrating $d\bar{r}_\perp$ from $\bar{r}_\perp = 0$ to $\bar{r}_\perp = \sqrt{\nu - \lambda^2\bar{z}^2}$, then integrating dz from Z to $-Z$. This leaves us with a simple expression involving only Z, which we choose to write in terms of the transverse TF radius R [i.e., $Z = R/\lambda$ from Eq. (2.46)]:

$$R = \left(\frac{15\lambda}{8\pi}\right)^{1/5}, \tag{2.48}$$

which from Eqs. (2.46), (2.42), and (2.43) gives the chemical potential:

$$\bar{\mu} = \frac{1}{2}(15N\lambda a/a_\perp)^{2/5} \tag{2.49}$$

in oscillator units ($\hbar\omega_\perp$).

To get the TF ground-state energy, we integrate Eq. (2.49) (since $\mu = \frac{\partial E}{\partial N}$):

$$\frac{\bar{E}}{N} = \frac{5}{7}\bar{\mu}. \tag{2.50}$$

2.4 Collective excitations and the hydrodynamic limit

Since we are interested in quantifying the breakdown of the mean-field approximation, excitations of the condensate are of particular interest as they can be measured in the lab much more precisely than ground-state energies[20, 21]. The frequencies associated with the low-lying excitations are measured by "shaking" the condensate and watching the motion that develops. The time-dependent GP equation (2.34) corresponds to the mean-field approximation at zero temperature, and the excitation frequencies can be found from the linearized GP equation, which results from assuming small amplitude fluctuations about the (unperturbed) ground-state GP wavefunction. We assume a solution for time-dependent GP equation (2.34) of the following form:

$$\psi(r,t) = e^{-i\mu t/\hbar}\left[\psi_o(r) + u(r)e^{-i\omega t} + v^\dagger(r)e^{i\omega t}\right], \tag{2.51}$$

which is known as the Bogoliubov transformation[14, 22]. The overall phase factor $e^{-i\mu t/\hbar}$ is needed for the unperturbed state $\psi_o(r)$. The operators $v^\dagger(r)e^{i\omega t}$ and $u(r)e^{-i\omega t}$ act as creation and annihilation operators of excited quasiparticles in the second-quantization formalism, where their sum would correspond to the quantum fluctuation term $\hat{\theta}$ in Eq. (2.27). A simpler interpretation of u and v is to think of them as the shapes of the normal mode oscillations. Inserting Eq. (2.51) into Eq. (2.34) and dropping second-order terms in the small, complex amplitude functions u

and v, one obtains the coupled, linearized GP equations, or the coupled Bogoliubov equations:

$$\hbar\omega u(\mathbf{r}) = \Big[-\frac{\hbar^2}{2m}\nabla^2 + V_{\text{conf}}(\mathbf{r}) + 2n(r)U_3 - \mu\Big]u(\mathbf{r}) + n(r)U_3 v(\mathbf{r}) \tag{2.52}$$

$$-\hbar\omega v(\mathbf{r}) = \Big[-\frac{\hbar^2}{2m}\nabla^2 + V_{\text{conf}}(\mathbf{r}) + 2n(r)U_3 - \mu\Big]v(\mathbf{r}) + n(r)U_3 u(\mathbf{r}), \tag{2.53}$$

where $n(r) = N|\psi_o|^2$ is the inhomogeneous number density and $U_3 = 4\pi\hbar^2 a/m$. Since we only keep terms linear in u and v, it is not necessary to worry about the commutativity of the two operators in the second-quantization formalism, and we can treat them as c-numbers. Solving these two coupled, linearized equations (three when you realize that you must also solve the time-independent GP equation) gives the eigenfrequencies ω, and hence, the energies of the elementary excitations. These excited states do not refer to excited states of individual atoms because the atoms are interacting at low temperature, making their individual wavefunctions overlap. However, as we discuss shortly, these quasiparticle excitations can be either single-particle-*like* or phonon-*like*.

In calculations in a later chapter, we solve these coupled equations numerically, but in this section we find it useful to review certain limiting cases of the linearized GP equations. Specifically, we consider the semiclassical limit for the homogeneous bose gas and the hydrodynamic/TF limit for the inhomogeneous gas. Also in this section we discuss the first beyond-mean-field correction to the excitation frequencies from the local-density approximation.

2.4.1 Homogeneous bose gas

In this approximation the gas is treated as locally uniform[8]. The semiclassical approximation of Eqs. (2.52) and (2.53) is found by replacing the kinetic energy operator by $p^2/2m$ where $\mathbf{p} = \hbar\mathbf{k}$ is the momentum of the excitation with wavevector $\mathbf{k}$:

$$\hbar\omega u(\mathbf{r}) = \Big[\frac{p^2}{2m} + V_{\text{conf}}(\mathbf{r}) + 2n(r)U_3 - \mu\Big]u(\mathbf{r}) + n(r)U_3 v(\mathbf{r}) \tag{2.54}$$

$$-\hbar\omega v(\mathbf{r}) = \Big[\frac{p^2}{2m} + V_{\text{conf}}(\mathbf{r}) + 2n(r)U_3 - \mu\Big]v(\mathbf{r}) + n(r)U_3 u(\mathbf{r}). \tag{2.55}$$

The semiclassical approximation is valid when spatial variations of the condensate occur over distances that are large compared with the wavelengths of the excitation. Equating to zero the determinant of the coupled equations we find

$$(\hbar\omega)^2 = \Big(\frac{p^2}{2m} + V_{\rm conf}(\mathbf{r}) + n(r)U_3 - \mu\Big)\Big(\frac{p^2}{2m} + V_{\rm conf}(\mathbf{r}) + 3n(r)U_3 - \mu\Big). \qquad (2.56)$$

For a homogeneous gas one sets $V_{\rm conf}(\mathbf{r}) = 0$, and for consistency in the long-wavelength limit (i.e., when $\mathbf{p} \to \mathbf{0}$) one uses the Bogoliubov approximation for the ground-state chemical potential (i.e., $\mu = nU_3$), which ensures that the zero-momentum excitation frequency is zero. Taking the homogeneous limit and using the Bogoliubov approximation for the ground-state chemical potential, the dispersion relation for the quasi-particle spectrum for a homogeneous condensate becomes

$$(\hbar\omega)^2 = \frac{p^2}{2m}\Big(\frac{p^2}{2m} + 2nU_3\Big), \qquad (2.57)$$

where we have used the fact that the ground-state wavefunction for a uniform system is simply $\psi_o = 1/\sqrt{V}$, where V is the volume of the system, and the uniform number density is $n = N/V$.

An elementary excitation behaves as a quasi-particle moving in the volume occupied by the body with definite energy ε and momentum $\mathbf{p}$. The dispersion relation for the elementary excitations $\varepsilon(p)$ characterizes the spectrum of excited states. Again it is important to remember that the quasi-particles are fictitious bodies that conveniently describe the elementary excitations, and there is no correspondence between the quasi-particles and the true atoms of the condensate. The dispersion relation for a phonon is linear in the momentum ($\varepsilon(p) = pc$, where c is the velocity of sound in the medium, see below). Elementary excitations behave like phonons (collective motion) when the wavelength is large compared to the inter-atomic separation or, equivalently, when the momentum is small. The long wavelength of the phonon is what allows the coupling of a collective oscillation to occur. When the quasi-particle wavelength is small or the momentum large, the elementary excitation, called a roton, behaves like a free particle. The roton dispersion relation takes the form of the energy of a free particle with a shift, $\varepsilon(p) = \frac{p^2}{2m^*} + \Delta$, where m^* is the roton effective mass.

In the small (large) momentum limit of the elementary excitation spectrum, one finds that Eq. (2.57) describes phonon (roton) quasi-particles.

$$\begin{aligned} \varepsilon(p) &= pc && \text{for} && \tfrac{p}{4mnU_3} \ll 1 \\ \varepsilon(p) &= \tfrac{(p-p_{\mathrm{rm}})^2}{2m} + \Delta && \text{for} && \tfrac{p}{4mnU_3} \gg 1 \end{aligned} \tag{2.58}$$

where $c = \sqrt{nU_3/m}$ is the speed of sound, $\Delta = nU_3$ is the roton energy shift, and the relation $\sqrt{1+x} \approx 1 + x/2$ has been used in the calculation of the large momentum limit of the dispersion relation expanded about the roton minimum, p_{rm}. Another feature of the spectrum in Eq. (2.57) is a high-energy maximum called a maxon, which is in a region of such high energy that it is never thermally excited.

2.4.2 Inhomogeneous bose gas

For a homogeneous BEC (uniform density), the temperature is sufficiently low that the elementary excitation spectrum is almost completely described by phonons; rotons are of such high energy and short wavelength that they are not excited. Of course, inhomogeneous condensate gases, that is, condensates with an external trap, also form at low temperature, but the system is very dilute making the collective effects of phonons less important than in its homogenous liquid counterpart. Also the non-uniformity of the condensate density allows the single-particle-like roton part of the dispersion curve to be excited, especially near the surface of the condensate where the density is most dilute.

Recall that the type of elementary excitation depends on the relative size of the quasi-particle wavelength, which depends on the momentum via $\lambda = h/p$. To say precisely whether a quasi-particle wavelength is small or large, it must be compared to some appropriate length scale. Inside the condensate, the healing length is the appropriate length scale[6]. The healing length is the typical size of the core of a quantized vortex; it is the length scale over which the wavefunction can "heal" from zero density to the average density n. If the condensate density grows from 0 to n

within a distance ξ, then equating the quantum pressure from the uncertainty principle[1] $\sim \hbar^2/(2m\xi^2)$ and the interaction energy $\sim 4\pi\hbar^2 an/m$, one finds the following relation for the healing length:

$$\xi = (8\pi na)^{-1/2}. \tag{2.59}$$

In the region near the surface of the condensate, the appropriate comparison length scale is the surface thickness, d. The (isotropic) trap potential is $m\omega_o^2 r^2/2$, which exerts a force of $F = -m\omega_o^2 R$ on a particle on the surface, where R is the TF radius. The trap potential energy of a particle on the surface of thickness d is $V \sim -Fd = m\omega_o^2 Rd$. Balancing this energy with the zero-point kinetic energy from the uncertainty principle $\sim \hbar^2/(2md^2)$ at the surface gives[19]

$$\frac{d}{R} = 2^{-1/3}\left(\frac{a_{\rm ho}}{R}\right)^{4/3}. \tag{2.60}$$

For an inhomogeneous gas, the spectrum exhibits excitations of a collective nature (phonons) in the bulk of the condensate, and single-particle-like excitations near the surface. Collective effects become less important near the surface because the gas is considerably more dilute. The larger distance between the atoms on the surface makes it more difficult for them to act collectively. Furthermore, phonons cannot be supported on the surface because they have a very long wavelength compared to the surface thickness. Another reason that rotons (single-particle-like excitations) are not as prevalent as phonons in the bulk of the condensate is that the repulsive force of the condensate atoms actually pushes rotons out to the surface. This can be understood by considering the single-particle Hamiltonian for excitations, which is obtained by setting $v = 0$ in Eq. (2.52). Finding the single-particle excitation energies then reduces to solving the eigenvalue problem $(H_{\rm sp} - \mu)u = \hbar\omega u$, where

$$H_{\rm sp} = -\frac{\hbar^2}{2m}\nabla^2 + \frac{1}{2}m\omega_o^2 r^2 + 2NU_3|\psi_o|^2. \tag{2.61}$$

Using the TF density for $|\psi_o|^2$ one finds

$$H_{\rm sp} = -\frac{\hbar^2}{2m}\nabla^2 + \frac{1}{2}m\omega_o^2(r^2 - R^2), \tag{2.62}$$

[1]The energy due to the quantum pressure is approximately given by $E \sim (\Delta p)^2/(2m)$, where $(\Delta p^2) \sim \hbar/\xi$ comes from the uncertainty principle.

where $R = \sqrt{[2\mu/(m\omega_o^2)]}$ is the TF radius. The second term in Eq. (2.62), which corresponds to the repulsive mean-field term in Eq. (2.61) in the large-N limit, acts as a potential barrier that pushes the rotons to the surface.

In Appendix A we derive the TF approximation for the mean-field collective modes of the condensate in the hydrodynamic picture. This approximation provides a valid description of the mean-field theory for a BEC with a large number of atoms with positive scattering length. We write the time-dependent GP equation (2.34) as two coupled hydrodynamic equations in terms of the density $n(r) = N\psi^2$ and the local velocity, which is proportional to the gradient of the phase ϕ (i.e., $\mathbf{v} = \frac{\hbar}{m}\nabla\phi$). Inserting the ansatz

$$\Psi = \sqrt{n(\mathbf{r},t)}e^{i\phi(\mathbf{r},t)} \tag{2.63}$$

into Eq. (2.34) and linearizing the density (see Appendix A for details) we find that the density fluctuation δn satisfies

$$m\frac{\partial^2\delta n}{\partial t^2} = U_3\nabla\cdot(n_{\mathrm{eq}}\nabla\delta n). \tag{2.64}$$

Then in Appendix A we consider oscillations with time dependence $\delta n(r,t) = \delta n(r)\cos(\omega t+\gamma)$, where ω is the frequency of the excitation and γ is a phase shift. Equation (2.64) becomes

$$-\omega^2\delta n = \frac{U_3}{m}\left[\nabla n_{\mathrm{eq}}\cdot\nabla\delta n + n_{\mathrm{eq}}\nabla^2\delta n\right]. \tag{2.65}$$

Using the TF equilibrium density

$$n_{\mathrm{eq}} = \frac{\mu_{\mathrm{TF}} - \frac{1}{2}m\omega_o^2 r^2}{U_3}, \tag{2.66}$$

results in the following differential equation:

$$\epsilon\delta n = r\frac{d}{dr}\delta n - \frac{1}{2}\left(R^2 - r^2\right)\left(\frac{d^2}{dr^2} + \frac{2}{r}\frac{d}{dr}\right)\delta n, \tag{2.67}$$

where we have defined $\epsilon = \omega^2/\omega_o^2$. Equation (2.67) can be manipulated into a hypergeometric equation (see Appendix A). The TF excitation frequencies in terms of the trap frequency ω_o are then given by

$$\omega = \omega_o(l + 3n_r + 2n_r l + 2n_r^2)^{1/2}, \tag{2.68}$$

where n_r is the number of radial nodes and l is the angular momentum of the excitation. The density fluctuation is given by

$$\delta n(r,t) = Cr^l F(-n, l+n+3/2, l+3/2, r^2/R^2) Y_{l,m}(\theta,\phi)\cos(\omega t+\gamma), \qquad (2.69)$$

where C is a normalization constant.

Despite the significant departure from the non-interacting case ($\omega = \omega_{\rm ho}(2n_r+l)$), the mean-field frequency does not depend on the scattering length or the number of atoms in the TF limit. This curious lack of dependence on the interaction strength $Na/a_{\rm ho}$ can be seen as follows. The time-dependent equation after linearization in the TF limit (2.64) can be interpreted as a wave equation:

$$\frac{\partial^2 \delta n}{\partial t^2} = \nabla\cdot(c^2(r)\nabla\delta n), \qquad (2.70)$$

where $c(r)$ is the speed of sound in the condensate. Comparing this equation with Eq. (2.64), we see that the TF speed of sound is $c = \sqrt{U_3 n_{\rm eq}/m}$. The frequency of an excitation is given by $\omega \sim c/\lambda$, where λ is the wavelength of the excitation. In the phonon regime, λ is on the order of the size of the condensate, which is approximately given by the TF radius $R = \sqrt{\hbar\omega_o/m}(15Na/a_{\rm ho})^{1/5}$. Using the TF speed of sound at the center of the condensate, which has the same $Na/a_{\rm ho}$-dependence as λ, we find that the dependence on the interaction of the excitation frequency cancels in the quotient c/λ, and ω is then on the order or ω_o. For the inhomogeneous gas, as $Na/a_{\rm ho}$ increases, the quantum pressure causes the size of the condensate and hence the phonon wavelength to increase, but the speed of sound increases proportionally. This cancellation does not occur in the homogeneous gas because, while the speed of sound does increase with $Na/a_{\rm ho}$, the wavelength of the phonon is fixed by the size of the container. The above argument is similar to that given in Ref. [6].

Stringari and Pitaevskii find the following beyond-mean-field fractional shift of the monopole frequency ($n_r = 1$, $l = 0$) in the hydrodynamic limit[23]:

$$\frac{\delta\omega_M}{\omega_M} = \frac{63}{256\sqrt{2}}(15Na^6)^{1/5}, \qquad (2.71)$$

where ω_M is the mean-field monopole frequency in the hydrodynamic limit [$n_r = 1$, $l = 0$ in Eq. 2.68], ω is the hydrodynamic-limit beyond-mean-field frequency, and

$\omega = \omega_M + \delta\omega_M$. Essentially, Stringari and Piteavskii use the low density expansion for a homogeneous gas [Eq. (F10)] for the chemical potential:

$$\mu = U_3 n \left(1 + \frac{32}{3\sqrt{\pi}}\sqrt{a^3 n(0)}\right), \tag{2.72}$$

to derive a generalized hydrodynamic equation:

$$m\omega^2 \delta n + \nabla(U_3 n_{eq} \nabla \delta n) = 0, \tag{2.73}$$

which they solve perturbatively. In their calculation for the monopole frequency-shift above, they used $\omega = \sqrt{5}\omega_o$ and $\delta n \sim (1 - 5r^2/R^2)$ as the unperturbed frequency Eq. (2.68) and density fluctuation Eq. (2.69), respectively. In a later chapter, we compare this beyond-mean-field result with our many-body DPT predictions for the monopole frequency, also known as the breathing mode frequency.

Chapter 3

Single degree of freedom dimensional perturbation methods

In preparation for the many-body formalism to follow in the next chapter, we discuss dimensional perturbation theory for confined systems that can be reduced to a single degree of freedom. In the first system, using the leading order of DPT, we derive a simple approximation that is more accurate and flexible than the Thomas-Fermi (TF) ground-state approximation of the Gross-Pitaevskii equation[17]. We use a perturbation parameter that depends on the effective dimensionality of the condensate and on the angular momentum quantum number. Our approximation is well-suited for calculating properties of Bose-Einstein condensates in three dimensions and in low effective dimensionality, such as vortex states in a highly anisotropic trap. This approximation is unique among previous applications of DPT in that it involves a nonlinear Schrödinger equation.

In the second example, we present a perturbation solution of a model Bose-Einstein Hamiltonian derived by Bohn, Esry and Greene. In our solution we use $1/N$ as the perturbation parameter, where N is the number of particles in the condensate[24]. Ground state energies are reported for parameters approximating the J.I.L.A. ^{87}Rb experiments. We predict the critical number of atoms with negative scattering lengths that can be trapped using the effective trap frequency of the first-order equation. The $N \to \infty$ perturbation limit, which retains an additional single term beyond the conventional Thomas-Fermi limit, gives ground state energies that agree to three digits with converged results, thus providing a much improved limit for large N.

Finally, dimensional perturbation theory is applied to the two-electron D-dimensional quantum dot, obtaining accurate values for the ground and excited state energies[25].

The expansion parameter is $1/\kappa$, where $\kappa = D + 2|l|$, D is the effective spatial dimensionality of the quantum dot environment and l is the relative-motion angular momentum quantum number. In this method, we include correlation at each order, including zeroth order. Analytic approximations for ground and excited state energies are obtained from the zeroth- and first-order terms of the perturbation expansion; thus, constituting a semiclassical approach to the quantum dot from a perturbation formalism. Using this analytical form of the energy, parameterized by D, the effects of the effective quantum dot dimensionality on the energy spectra may be investigated. Systematic corrections are made to the semiclassical approximation by adding higher-order perturbation terms. The method described is extended in the next chapter to obtain an analytical approximation to the ground state energy of the many-electron D-dimensional quantum dot Hamiltonian by truncating the $1/D$ expansion to low order.

3.1 $1/D$ perturbation methods for the Gross-Pitaevskii equation

The most commonly used approach to describe a dilute gas of atoms in a BEC at $T = 0$ is mean-field theory, which takes the form of the time-independent GP equation of Eq. (2.35). The $N \to \infty$ Thomas-Fermi (TF) approximation has been proven to be a highly successful analytical approximation of the GP equation [19, 26]. The strength of the $N \to \infty$ TF approximation is its simplicity: neglecting the kinetic energy results in a simple approximation of the ground-state condensate density that is effective in analyzing properties of large-N condensates. For condensates with a moderate number of atoms and condensates with attractive interactions, the TF approximation breaks down. The kinetic energy is important in each case, especially in the latter, where the kinetic energy is necessary to prevent collapse. The effects of attractive interactions have been studied using approximation techniques such as variational trial wave functions [27, 28, 29]. Other approximations that have been employed to extend the TF regime of validity include the $\hbar \to 0$ TF approximation [18], a method that uses two-point Padé approximants between the weakly- and strongly-interacting limits of the ground-state [30], and a variational method for anisotropic condensates [31].

With the study of BEC in highly anisotropic traps as a motivation, we use a perturbation formalism that permits the effective dimensionality, D, to vary. Because it readily allows one to approximate quantities in any dimension, such a formalism is ideally suited for condensates in the anisotropic traps used in many laboratories where the condensate can be effectively one-, two- or three-dimensional. The perturbation parameter is $\delta = 1/\kappa$, where κ depends on the effective dimensionality of the condensate and on the angular momentum quantum number. The $\delta \to 0$ limit becomes an exactly soluble problem, the solution of which is used by the various dimensional-scaling methods as the starting point for the solution of the full three-dimensional problem [32, 33, 34]. The $\delta \to 0$ approximation to the condensate density, which retains part of the kinetic energy, is quite accurate for both a large and moderate number of atoms in the BEC ground state, and the dimensional scaling formalism, which treats the dimensionality as a parameter, is advantageous when studying condensates of low effective dimensionality due to extreme trap anisotropy. The centrifugal-like term in the $\delta \to 0$ density also makes it a good physical starting point for treating vortex states.

In the case of positive scattering length, the repulsive interaction causes the density to become flat, and the kinetic energy of the condensate becomes negligible in the $N \to \infty$ limit. This limit of the GP equation is referred to as the Thomas-Fermi ($N \to \infty$ TF) approximation. See Sec. 2.3 where we discussed the TF approximation for an anisotropic trap. The $N \to \infty$ TF density for the ground state in a three-dimensional isotropic trap is [19, 26]

$$n_{\rm TF}(r) = |\psi|^2 = \frac{1}{NU_3}(\mu_{\rm TF} - \frac{1}{2}m\omega^2 r^2) \tag{3.1}$$

for $\mu_{\rm TF} \geq \frac{1}{2}m\omega^2 r^2$ and $n_{\rm TF} = 0$ elsewhere. Eq. (3.1) provides an excellent description of the condensate ground-state density in the bulk interior. This approximation breaks down near the surface of the gas where the density is not flat; the wave function must vanish smoothly, making the kinetic energy appreciable in the boundary layer. Boundary layer theory techniques have been employed to obtain corrections to the $N \to \infty$ TF approximation at the condensate surface where the gradient of the density is no longer small [35, 36, 37]. The leading order correction to the ground state chemical potential due to the boundary layer at the surface is of order $R^{-4}\ln(R)$.

3.1.1 Effective dimensionality

We use a perturbation formalism where the effective dimensionality, D, of the condensate is allowed to vary. The effective-dimensionality of the condensate depends on the relative size of the condensate in each of the three spatial dimensions. Most experimentally realized traps are axially symmetric with some having a high degree of anisotropy [38, 39]. In the case of axial symmetry, the trapping potential takes the form, $V_{\mathrm{trap}}(r) = \frac{1}{2}m\omega_\perp^2 r_\perp^2 + \frac{1}{2}m\omega_z^2 z^2 = \frac{1}{2}m\omega_\perp^2(r_\perp^2 + \lambda^2 z^2)$, where $\lambda = \omega_z/\omega_\perp$ is a measure of the degree of anisotropy. The system reduces to a three-dimensional isotropic condensate for $\lambda = 1$. In the small- (large-) λ limits, the system reduces to an effective one- (two-)dimensional isotropic condensate[1].

As an illustration, consider $\lambda \gg 1$ where the motion of the atoms in the z-direction becomes frozen and their motion is described by a gaussian of small width. To determine the 2D effective coupling constant, we assume the wave function in Eq. (2.35) is separable: $\psi(\mathbf{r}) = \psi_2(r_\perp)\chi(z)$, where $\chi(z)$ is assumed to be a gaussian, and operating with $\int dz\chi^*$, one finds a new effective 2D GP equation:

$$\left(-\frac{\hbar^2}{2m}\nabla_2^2 + \frac{1}{2}m\omega_2^2 r^2 + N_2 U_3|\psi_2|^2\right)\psi_2 = \mu_2\psi_2, \tag{3.2}$$

which has the same form as Eq. (2.35), but r is the 2D radius, $\omega_2 = \omega_\perp$, $\mu_2 = \mu - \hbar\omega_z/2$, $N_2 = N\int dz|\chi|^4$. Requiring that ψ_2 and χ be normalized to unity, $\int dz|\chi|^4$ has units of 1/length; thus, we interpret N_2 as the number of atoms in the 2D condensate per unit length along the z-axis. In our subsequent scalings, we will adopt a notation for the number of atoms that is similar to that of Jackson *et al.* [40]. For $\lambda \ll 1$, one may assume the motion in the radial-direction in the x-y plane is described by a gaussian of small width, $\chi(r_\perp)$, and, following the same procedure, one obtains a 1D equation analogous to Eq. (3.2), where N_1 would represent the number of atoms in the 1D condensate per unit area in the xy-plane.

3.1.2 GP equation in variable dimensionality

We begin by explicitly generalizing the nonlinear Schrödinger equation (NLSE), Eq. (2.35), to D-dimensions where r becomes the radius of a D-dimensional sphere with

[1]It is conceivable that an isotropic hamiltonian in a fractional-dimensional space could be used to describe experimental condensates for intervening values of λ, but we will focus our attention on integer dimensions.

$D-1$ remaining angles. The Laplacian is generalized to D-dimensions (Bohn, Esry and Greene[41, 24] treat the Laplacian in a similar fashion, in which they use hyperspherical coordinates to define a mean condensate radius.), and the potential terms retain their three-dimensional form; the coupling constant is generalized in the final scaling. We obtain the Schrödinger equation:

$$\left\{-\frac{\hbar^2}{2m}\left[\frac{1}{r^{D-1}}\frac{\partial}{\partial r}\left(r^{D-1}\frac{\partial}{\partial r}\right)+\frac{L_{D-1}^2}{r^2}\right]+\frac{1}{2}m\omega^2r^2+NU_3|\psi(\mathbf{r})|^2\right\}\psi(\mathbf{r})=\mu\psi(\mathbf{r}), \quad (3.3)$$

where L_{D-1}^2 is a generalized angular momentum operator depending on $D-1$ angles with eigenvalues $-l(D+l-2)$ [42]; the angular momentum quantum number, l, is non-negative. Substituting these eigenvalues and introducing the radial Jacobian factor in a transformation of the wave function, $\phi(r)=r^{(D-1)/2}\psi(r)$, to eliminate the first derivative terms, we find

$$\left\{-\frac{\hbar^2}{2m}\left[\frac{\partial^2}{\partial r^2}-\frac{(D-1)(D-3)}{4r^2}-\frac{l(D+l-2)}{r^2}\right]+\frac{1}{2}m\omega^2r^2+NU_3|\psi(\mathbf{r})|^2\right\}\phi(\mathbf{r})=\mu\phi(\mathbf{r}). \quad (3.4)$$

Finally, we make two sets of scalings to arrive at the NLSE in dimensionally scaled oscillator units. The first scaling is a purely dimensional scaling: $r=\kappa^2\tilde{r}$, $\tilde{\omega}=\kappa^3\omega$, $\tilde{\mu}=\kappa^2\mu$, and $\tilde{\psi}=\kappa^D\psi$, where $\kappa=D+2l$. The final scaling is to scaled oscillator units (denoted by bars): $\tilde{r}=\tilde{a}_{\mathrm{ho}}\bar{r}$, $\tilde{\mu}=\hbar\tilde{\omega}\bar{\mu}$, and $\tilde{\psi}=\tilde{a}_{\mathrm{ho}}^{D/2}\bar{\psi}$, where $\tilde{a}_{\mathrm{ho}}=\sqrt{\hbar/m\tilde{\omega}}$. Combining these two scalings, we arrive at

$$\left\{-\frac{1}{2}\delta^2\frac{\partial^2}{\partial\bar{r}^2}+\frac{1-4\delta+3\delta^2}{8\bar{r}^2}+\frac{1}{2}\bar{r}^2+\bar{g}_{D_p}|\bar{\psi}(\bar{\mathbf{r}})|^2\right\}\bar{\phi}(\bar{\mathbf{r}})=\bar{\mu}\bar{\phi}(\bar{\mathbf{r}}), \quad (3.5)$$

where everything is now in dimensionally scaled oscillator units. The perturbation parameter is $\delta=1/\kappa$ and D_p refers to the effective dimension we are interested in studying. For the effective dimensions of primary interest in this study, the dimensionally scaled coupling constants are, for 3D, $\bar{g}_3=g_3/\kappa^{5/2}$, where $g_3=4\pi N_3a/a_{\mathrm{ho}}$ and N_3 is the number of condensate atoms; and for 2D, $\bar{g}_2=g_2/\kappa^2$, where $g_2=4\pi N_2a$ and N_2 represents the number of atoms in the 2D condensate per unit length along the z-axis. The definition of N_2 makes g_2 dimensionless. For general D,

$$\bar{g}_{D_p}=\frac{4\pi N_{D_p}a}{\kappa^{\frac{D_p+2}{2}}a_{\mathrm{ho}}^{D_p-2}}, \quad (3.6)$$

making Eq. (3.5) valid for describing condensates in any effective dimension. In the next section, we describe a simple and accurate zeroth-order approximation to Eq. (3.5).

3.1.3 Zeroth-order density

It has been pointed out by Schuck and Viñas [18] that the true TF limit ($\hbar \to 0$ as originally applied to the case of Fermi statistics [43, 44]) is not equivalent to $N \to \infty$, and they show that the $\hbar \to 0$ TF limit for bosons does not neglect the kinetic energy for the ground state. The $N \to \infty$ TF approximation to the ground state is too harsh on the kinetic energy for a moderate number of atoms. A less harsh and nearly as simple approximation is the zeroth-order ($\delta \to 0$) approximation of Eq. (3.5). Unlike the ground-state $N \to \infty$ TF approximation, which neglects the entire kinetic energy, our zeroth-order approximation of the Jacobian-transformed generalized GP equation of Eq. (3.5) neglects the derivative part of the kinetic energy but retains a centrifugal-like term. For vortex states, one understands this term as being a centrifugal-like barrier due to quantized circulation, which pushes atoms away from the axis of rotation. This centrifugal-like barrier arises from the condensate phase of the wavefunction: $|\nabla S|^2$ ($\psi = \sqrt{n}e^{iS}$, where n is the condensate density and S is the spatially dependent condensate phase; then the velocity of the condensate atoms is given by $\mathbf{v} = \frac{\hbar}{m}\nabla S$). For the ground state, this centrifugal-like term in the zeroth-order density has an alternate, quantum mechanical interpretation, which helps explain its good agreement with numerical calculations. We discuss this interpretation in Section 3.1.4.

The $\delta \to 0$ limit of Eq. (3.5) results in the following zeroth-order density in scaled oscillator units:

$$n(\bar{r}) = |\bar{\psi}|^2 = \frac{1}{\bar{g}_D}(\bar{\mu} - \frac{1}{8\bar{r}^2} - \frac{1}{2}\bar{r}^2), \tag{3.7}$$

for $\bar{R}_o(\bar{\mu}) \leq \bar{r} \leq \bar{R}_{\max}(\bar{\mu})$ and $n = 0$ elsewhere. The normalization condition[2] becomes

$$\Omega(D) \int_{\bar{R}_o(\bar{\mu})}^{\bar{R}_{\max}(\bar{\mu})} d\bar{r}\bar{r}^{D-1}|\bar{\psi}|^2 = 1, \tag{3.8}$$

where $\Omega(D) = 2\pi^{D/2}/\Gamma(D/2)$. The $\delta \to 0$ limit can be thought of as a large-D or large-l limit.

Eq. (3.7) is valid where the density is non-negative. In addition to the $N \to \infty$ TF-like classical cutoff radius near the surface, $\bar{R}_{\max}$, the centrifugal-like term requires that another cutoff be defined, $\bar{R}_o$, slightly removed from the origin, to satisfy the requirement that the density be non-negative. In terms of the chemical potential, the cutoff radii in scaled oscillator units are defined as

$$\bar{R}_o^2(\bar{\mu}) = \bar{\mu} - \sqrt{\bar{\mu}^2 - \tfrac{1}{4}}$$
$$\text{and}$$
$$\bar{R}_{\max}^2(\bar{\mu}) = \bar{\mu} + \sqrt{\bar{\mu}^2 - \tfrac{1}{4}}. \tag{3.9}$$

In regular oscillator units (a_{ho}),

$$R_o^2(\mu) = \mu - \sqrt{\mu^2 - \tfrac{\kappa^2}{4}}$$
$$\text{and}$$
$$R_{\max}^2(\mu) = \mu + \sqrt{\mu^2 - \tfrac{\kappa^2}{4}}. \tag{3.10}$$

Notice for the ground state in the strongly interacting regime that $\mu \gg 1$ and the cutoff radii for the ground state becomes $N \to \infty$ TF-like: $R_o \approx 0$ and $\mu \approx R_{\max}^2/2$; thus, the strongly interacting limit, or, equivalently, the $N \to \infty$ limit of our zeroth-order approximation collapses to the $N \to \infty$ TF approximation, as expected. (For finite N, as will be shown later, our zeroth-order approximation gives better agreement with the numerical solution of the GP equation than the $N \to \infty$ TF approximation.) Using the integration limits defined in Eq. (3.9), along with the condensate

[2]As the GP equation is nonlinear, one cannot treat excited-l states (vortices) for $D > 2$ radially symmetric traps in the usual manner of separating the wave function into radial and angular parts. Presently, however, vortices in 3D radially symmetric traps are not realized. Vortex states in a 2D isotropic trap do not pose a problem to theory because the spherical harmonic wave function acts as a phase factor. In 1D, the spherical harmonic wave function is a constant and, since there are no angles, one can think of $l = 0$ and $l = 1$ as even and odd parity states.

density defined in Eq. (3.7), the normalization condition (Eq. 3.8) gives an equation for the zeroth-order chemical potential that is easily solved in any dimension. (See Section 3.1.5 where this procedure is illustrated for two dimensions.)

Once the chemical potential is calculated, it is then used in Eq. (3.7) to complete the description of the zeroth-order wave function. One can then calculate the energy from

$$\begin{aligned} E/N &= \int d^D\mathbf{r}\Big[\frac{\hbar^2}{2m}|\nabla\psi|^2 + \frac{1}{2}m\omega^2 r^2\psi^2 + \frac{g_D}{2}\psi^4\Big] \\ &= E_{\mathrm{kin}}/N + E_{\mathrm{ho}}/N + E_{\mathrm{int}}/N, \end{aligned} \tag{3.11}$$

or in the zeroth-order approximation and scaled oscillator units,

$$\begin{aligned} \bar{E}/N &\approx \Omega(D)\int_{\bar{R}_o(\bar{\mu})}^{\bar{R}_{\mathrm{max}}(\bar{\mu})} \bar{r}^{D-1}d\bar{r}\Big[\frac{1}{8\bar{r}^2}\bar{\psi}^2 + \frac{1}{2}\bar{r}^2\bar{\psi}^2 + \frac{\bar{g}_D}{2}\bar{\psi}^4\Big] \\ &\approx \bar{E}_{\mathrm{kin}}/N + \bar{E}_{\mathrm{ho}}/N + \bar{E}_{\mathrm{int}}/N. \end{aligned} \tag{3.12}$$

3.1.4 Ground state in three dimensions

The numerical effect of the centrifugal-like term in the zeroth-order approximation on the ground state of a stationary condensate is clear from Fig. 3.1, where we compare the numerical solution of the GP chemical potential with our zeroth-order approximation and the $N \to \infty$ TF approximation for up to 10 000 ^{87}Rb atoms in a spherical trap. Our zeroth-order approximation is more accurate than the $N \to \infty$ TF approximation for all N, most notably for a moderate number of atoms. The accuracy of the zeroth-order approximation is comparable to boundary layer corrections: the zeroth-order approximation is slightly more accurate for small coupling constant, while boundary layer theory is slightly more accurate for larger coupling constant, but the difference between all three approximations becomes small for very large coupling constant.

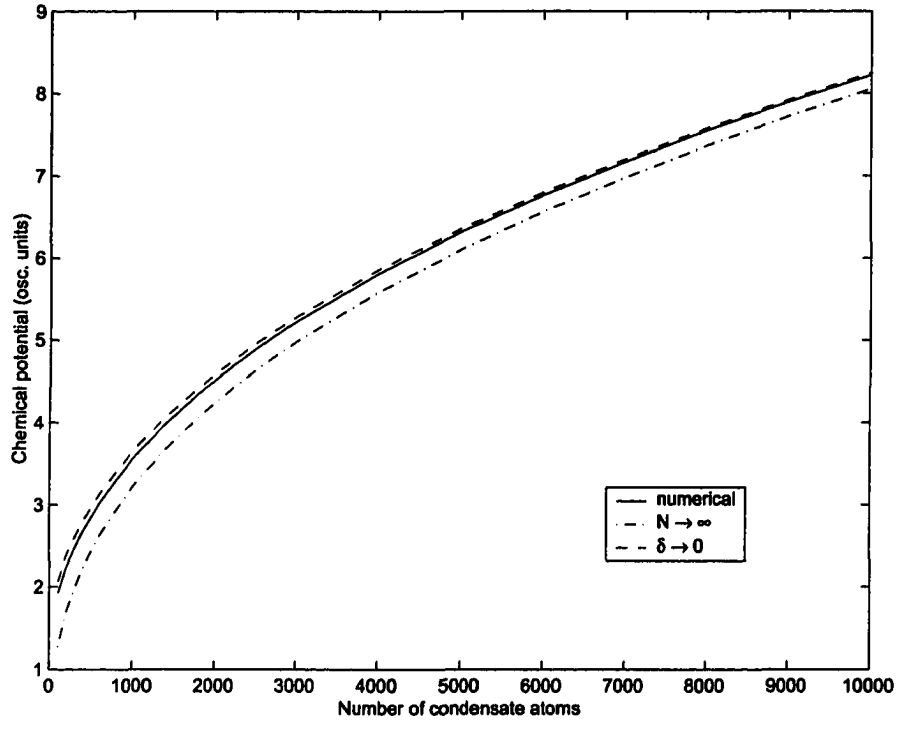


Figure 3.1: Chemical potential in oscillator units vs. number of condensate atoms for a ^{87}Rb condensate in a 3D isotropic trap, where $a = 100$ bohr and $\nu = 200$ Hz. The zeroth-order ($\delta \to 0$) approximation of dimensional perturbation theory presented here (dashed) is in better agreement with the numerical solution of the GP equation (solid) than the $N \to \infty$ Thomas-Fermi approximation (dash-dot).

The correct physical interpretation of this centrifugal-like term, as originally noted by Chatterjee[45], is that it is the component of the kinetic energy needed to satisfy the minimum uncertainty principle. The zeroth-order density includes a centrifugal-like term from the kinetic energy, which pushes the wave function away from the origin in the ground state as if there were a non-zero quantum of angular momentum; however, the $1/r^2$ contribution to the ground state density of a nonrotating cloud clearly is not due to any rotational motion of the cloud. This effect, which becomes less pronounced as N increases, is demonstrated in Figs. 3.2 and 3.3, which show the numerically calculated GP ground-state non-Jacobian weighted wave function (ψ) along with our zeroth-order approximation and the $N \to \infty$ TF approximation.

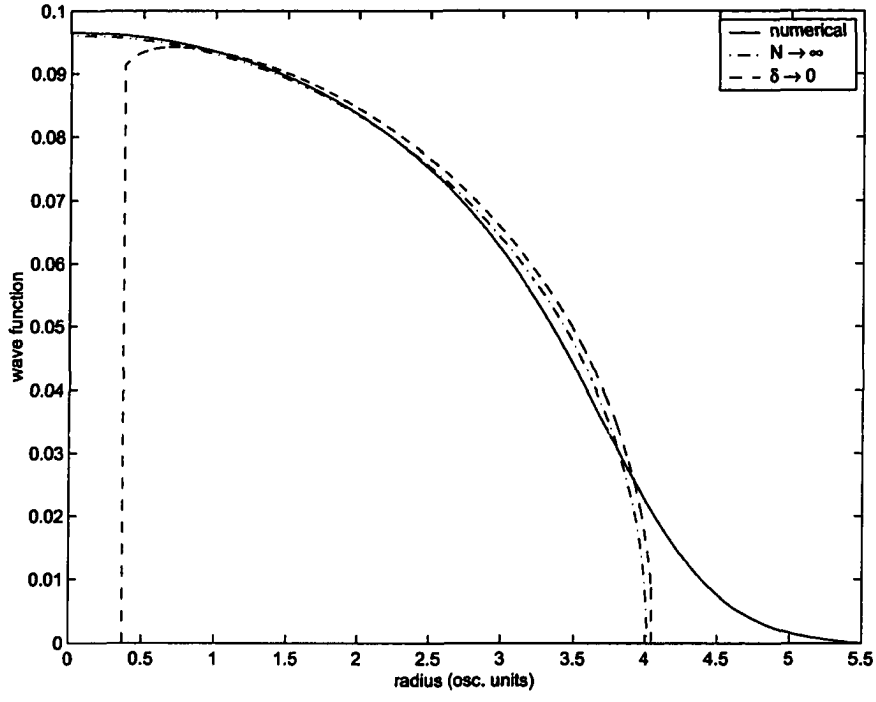


Figure 3.2: Ground state wave functions (ψ – non-Jacobian weighted) for a ^{87}Rb condensate of 10 000 atoms in a 3D isotropic trap, where $a = 100$ bohr and $\nu = 200$ Hz. These parameters correspond to $g_3 \approx 872.04$. Plotted are the numerical solution of the GP equation (solid), the $N \to \infty$ Thomas-Fermi approximation (dash-dot) and our zeroth-order ($\delta \to 0$) approximation (dashed). Our zeroth-order approximation contains an unphysical core near the origin, but the added kinetic energy, which causes the core to appear, is also responsible for the increased accuracy seen in Fig. 3.1.

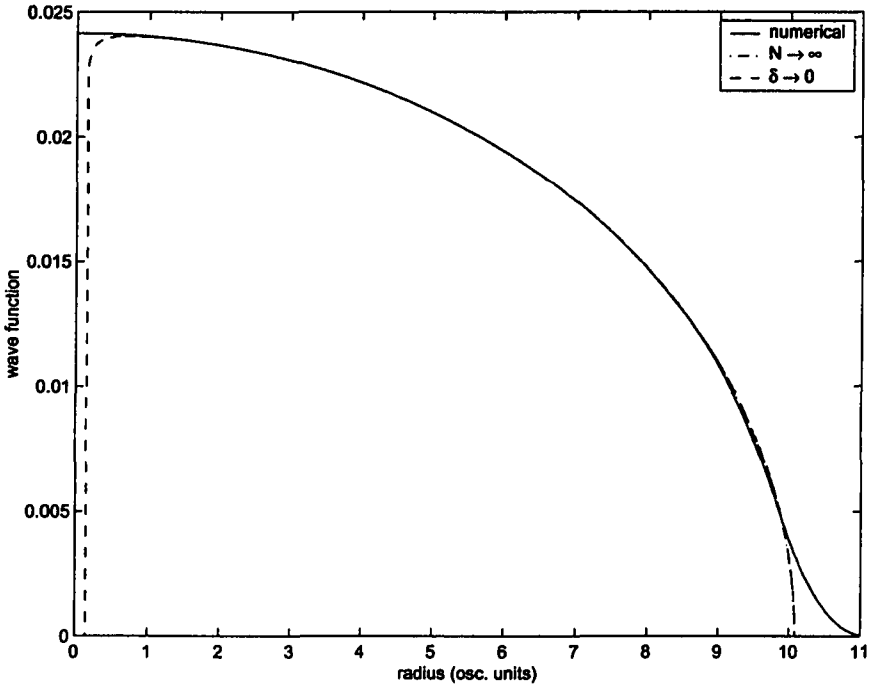


Figure 3.3: Same as Fig. 3.2 but with 10^6 atoms, corresponding to $g_3 \approx 87,204$. As the number of atoms increases, the unphysical core in our zeroth-order wave function shrinks. Near the origin, the $N \to \infty$ TF and numerically calculated wave functions overlap, while the $N \to \infty$ TF and our zeroth-order wave function overlap in the boundary region. For sufficiently large N, the three wave functions become indistinguishable.

The centrifugal-like term in the lowest order of dimensional perturbation theory ($\delta \to 0$) can be understood as arising from the requirement that the system's uncertainty product be a minimum[45]. Another way to see how a centrifugal-like term may arise in the ground state – this time within the $N \to \infty$ TF approximation – is by applying the Langer modification[10] of WKB theory to the $N \to \infty$ TF density. For vortices, one may not neglect the entire kinetic energy in the $N \to \infty$ limit. A slightly more general $N \to \infty$ TF density than Eq. (3.1) that includes vortices is

$$n_{\rm TF}(r) = |\psi|^2 = \frac{1}{NU_3}(\mu_{\rm TF} - \frac{\hbar^2\Lambda^2}{2mr^2} - \frac{1}{2}m\omega^2 r^2). \tag{3.13}$$

For a spherical trap, $\Lambda^2 = l(l+1)$, which reduces to the usual ground state $N \to \infty$ TF density for $l = 0$, but using the Langer modification, where the correct asymptotic

phase of the WKB wave function is obtained by the replacement $l(l+1) \rightarrow (l+1/2)^2$ in the centrifugal-like potential, a centrifugal-like barrier remains in the ground-state:

$$n_{\rm TF}(r) \rightarrow |\psi|^2 = \frac{1}{NU_3}(\mu_{\rm TF} - \frac{\hbar^2}{8mr^2} - \frac{1}{2}m\omega^2 r^2). \tag{3.14}$$

The dependence of our perturbation parameter on the angular momentum quantum number suggests that the zeroth-order density will be a good physical starting point for vortex states, which we explore in the next section for $D = 2$. The remaining centrifugal-like term in our zeroth-order approximation is a lowest-order correction to the kinetic energy, which, for a moderate number of atoms, greatly improves the ground state approximation ($l = 0$) over the $N \rightarrow \infty$ TF approximation. For a very large number of atoms, the contribution from the kinetic energy becomes very small, as can be seen by comparing the wave functions in Figs. 3.2 and 3.3, for $N = 10^4$ and $N = 10^6$ ^{87}Rb atoms, respectively. As the number of atoms increases, our unphysical core becomes smaller than the healing length, eventually vanishing: our zeroth-order and the $N \rightarrow \infty$ TF wave functions become indistinguishable from the numerical solution for large N.

3.1.5 Lower dimension

The $\delta \rightarrow 0$ density (Eq. 3.7) is well suited for describing condensates in the presence of a vortex, where the centrifugal-like term models the vortex core (see Fig. 3.4). In this section, we present explicit expressions for the $D = 2$ ground-state and vortex states. In the angular-dimensional scaling of the GP equation, one has considerable freedom in the choice of the scaling parameter, $\delta = 1/\kappa$. In the previous section, we used $\kappa = D + 2l$ or, for the ground state, $\kappa = D$. The choice $\kappa = D + 2l - 2$ exactly reduces our expressions below for the chemical potential and energy to a two-dimensional $N \rightarrow \infty$ TF approximation that includes the leading contribution to the kinetic energy due to fluid motion of the condensate[46]. Slightly improved agreement of the zeroth-order energy with the numerical solution of the 2D GP equation for a wide range of values of the mean-field coupling constant can be obtained by choosing $\kappa = D + 2l - 1$, which changes the numerator in the centrifugal-like term of Eq. (3.5) to $1 - \delta^2$. Zeroth order predictions show a small amount of variability with the choice of κ, but the results of higher order perturbation theory should not depend on the particular choice of κ.

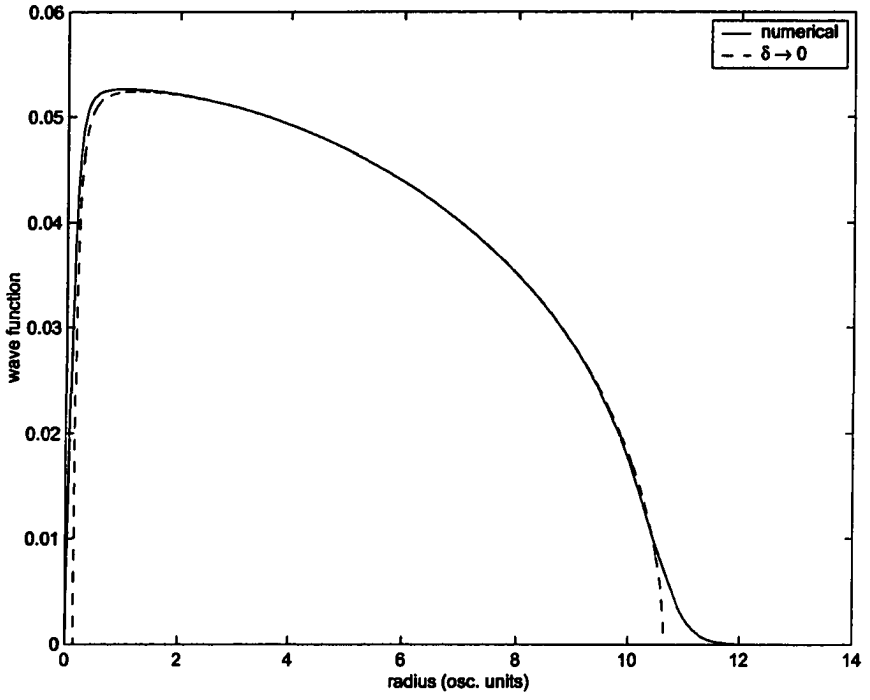


Figure 3.4: Comparison of the condensate wave function (ψ – non-Jacobian weighted) with an $l = 1$ vortex in a 2D isotropic trap with $g_2 = 10\,000$. The solid line is the numerical solution of the GP equation and the dashed line is our zeroth-order ($\delta \longrightarrow 0$) wave function, whose centrifugal-like term models the vortex core.

Using Eqs.(3.7,3.8,3.9) for $D = 2$, one finds that the scaled chemical potential satisfies

$$\frac{\bar{g}_2}{2\pi} = \frac{\bar{\mu}}{2}\sqrt{\bar{\mu}^2 - \frac{1}{4}} + \frac{1}{16}\ln\left(\frac{\bar{\mu} - \sqrt{\bar{\mu}^2 - \frac{1}{4}}}{\bar{\mu} + \sqrt{\bar{\mu}^2 - \frac{1}{4}}}\right). \tag{3.15}$$

Recalling the earlier conversion relations leading to Eq. (3.5), the chemical potential, in regular oscillator units, satisfies

$$\frac{g_2}{2\pi} = \frac{\mu}{2}\sqrt{\mu^2 - \frac{\kappa^2}{4}} + \frac{\kappa^2}{16}\ln\left(\frac{\mu - \sqrt{\mu^2 - \frac{\kappa^2}{4}}}{\mu + \sqrt{\mu^2 - \frac{\kappa^2}{4}}}\right). \tag{3.16}$$

Solving Eq. (3.15) for the scaled zeroth-order chemical potential, $\bar{\mu}$, and using the resulting wave function, Eq. (3.7) and Eq. (3.12) give a simple analytical approximation for the 2D energy,

$$E = \frac{2\pi}{3g_2}\left(\mu^2 - \frac{\kappa^2}{4}\right)^{3/2}, \tag{3.17}$$

where we have already converted to regular oscillator units. Eq. (3.16) and Eq. (3.17) for the chemical potential and energy per atom, respectively, are analagous to the results of the $N \to \infty$ TF approximation for vortices given in Ref. [46], which includes a kinetic energy term associated with the fluid motion that is encoded in the wave function's phase. This similarity is due to the zeroth-order $\delta \to 0$ limit being a large angular momentum limit or, in the language of hydrodynamics, a large quantum of circulation limit. The zeroth-order approximation for $D = 2$ results in a shifted TF-like energy spectrum, whose ground state approximation is, just as for $D = 3$, more accurate than the $N \to \infty$ TF approximation for any coupling constant, most noticeably for smaller coupling. For the energy of a single charge vortex located at the center of the trap, the above expressions are more accurate than the unregulated $N \to \infty$ TF approximation in Ref. [46] for a moderately sized coupling constant, and slightly less accurate for very large coupling. For our zeroth-order approximation and the $N \to \infty$ TF approximation, respectively, the relative errors in the first vortex state energy are 0.56% and −0.88% for $g_2 = 1\,000$; and 0.015% and −0.012% for $g_2 = 100,000$.

3.1.6 Anisotropic trap: generalized cylindrical coordinates

In the previous sections we dealt with traps that are isotropic in some effective dimensionality for special limits of the anisotropy parameter λ. For such isotropic traps, we analyzed the condensate from the vantage point of a D-dimensional space with spherical symmetry. We now consider a D-dimensional space with cylindrical symmetry, which is a more suitable vantage for axially symmetric traps with an arbitrary anisotropy parameter, λ. Such axially symmetric traps are the most prevalent in current gaseous BEC experiments.

We begin by writing the GP equation in generalized cylindrical coordinates as

$$\left\{-\frac{\hbar^2}{2m}\Big[\frac{1}{r_\perp^{D-2}}\frac{\partial}{\partial r_\perp}\Big(r_\perp^{D-2}\frac{\partial}{\partial r_\perp}\Big) + \frac{L_{D-2}^2}{r_\perp^2} + \frac{\partial^2}{\partial z^2}\Big]\right.$$
$$\left. + \frac{1}{2}m{\omega_\perp}^2(r_\perp^2 + \lambda^2 z^2) + NU_3|\psi(\mathbf{r})|^2\right\}\psi(\mathbf{r}) = \mu\psi(\mathbf{r}), \tag{3.18}$$

where $\lambda = \omega_z/\omega_\perp$ is the anisotropy parameter and $r_\perp$ is the radius of a $D-1$ dimensional sphere with $D-2$ remaining angles. Just as we did in Sect. 3.1.2 for the isotropic case, we introduce the eigenvalue of L_{D-2}^2, $-l(D-l-3)$, and the Jacobian

transformation of the wave function, $\phi = r^{(D-2)/2}\psi$, arriving at the dimensionally scaled GP equation,

$$\left\{-\frac{1}{2}\delta^2\frac{\partial^2}{\partial\bar{r}_\perp^2}+\frac{1-6\delta+8\delta^2}{8\bar{r}_\perp^2}+\frac{\partial^2}{\partial\bar{z}^2}+\frac{1}{2}(\bar{r}_\perp^2+\lambda^2 z^2)\right.$$
$$\left.+\bar{g}_3|\bar{\psi}(\bar{r}_\perp,\bar{z})|^2\right\}\bar{\phi}(\bar{r}_\perp,\bar{z})=\bar{\mu}\bar{\phi}(\bar{r}_\perp,\bar{z}), \tag{3.19}$$

where $r_\perp = \kappa^{1/2}a_\perp\bar{r}_\perp$, $z = \kappa^{1/2}a_\perp\bar{z}$, $\mu = \kappa\hbar\omega_\perp\bar{\mu}$ and $\psi = (\kappa/a_\perp)^{D/2}\bar{\psi}$, and where $a_\perp = \sqrt{\hbar/m\omega_\perp}$, $\kappa = D+2l$ and $\delta = 1/\kappa$. We are primarily interested in the $D=3$ scaled coupling constant, which is

$$\bar{g}_3 = \frac{4\pi Na}{\kappa^{5/2}a_\perp}. \tag{3.20}$$

The normalization becomes

$$\Omega(D-1)\int\bar{r}_\perp^{D-2}d\bar{r}_\perp\int d\bar{z}|\bar{\psi}|^2 = 1. \tag{3.21}$$

Using the $\delta\to 0$ density,

$$|\bar{\psi}|^2 \to \frac{1}{\bar{g}_D}\Big(\bar{\mu}-\frac{1}{8\bar{r}_\perp^2}-\frac{1}{2}(\bar{r}_\perp^2+\lambda^2\bar{z}^2)\Big), \tag{3.22}$$

in the normalization condition and using the units, $\bar{r}_\perp = \sqrt{2\bar{\mu}}\hat{r}_\perp$ and $\bar{z} = \sqrt{2\bar{\mu}}\hat{z}$, the chemical potential for $D=3$ satisfies

$$1 = \frac{\pi(2\bar{\mu})^{5/2}}{\bar{g}_3}\int_{\hat{r}_\perp^-}^{\hat{r}_\perp^+}\hat{r}_\perp d\hat{r}_\perp\int_{\hat{z}^-}^{\hat{z}^+}d\hat{z}(1-\hat{r}_\perp^2-\frac{\alpha^2}{\hat{r}_\perp^2}-\lambda^2\hat{z}^2), \tag{3.23}$$

where $\alpha = 1/4\bar{\mu}$. For large N, α becomes a very good perturbation parameter, but even for moderate N it is quite good, and the integral in scaled units to second order in α is

$$1 \approx \frac{\pi(2\bar{\mu})^{5/2}}{\bar{g}_3}\frac{4}{3\lambda}\Big[\frac{1}{5}-\frac{3\alpha^2}{2}\Big(\ln\frac{2}{\alpha}-\frac{2}{3}\Big)\Big], \tag{3.24}$$

or

$$N \approx \frac{(2\mu)^{5/2}}{3a\lambda}\Big[\frac{1}{5}-\frac{3\kappa^2}{32\mu^2}\Big(\ln\frac{8\mu}{\kappa}-\frac{2}{3}\Big)\Big] \tag{3.25}$$

in regular oscillator units. A similar perturbative integration is performed in Ref. [47] for a TF approximation for vortices in an anisotropic condensate.

Recall the TF ground state chemical potential for an axially symmetric trap[19],

$$\mu_{\rm TF} = \frac{1}{2}\left(\frac{15Na\lambda}{a_\perp}\right)^{2/5}, \tag{3.26}$$

which we compare with our Eq. 3.25 results in Figure 3.5 for a condensate with JILA TOP trap parameters[20].

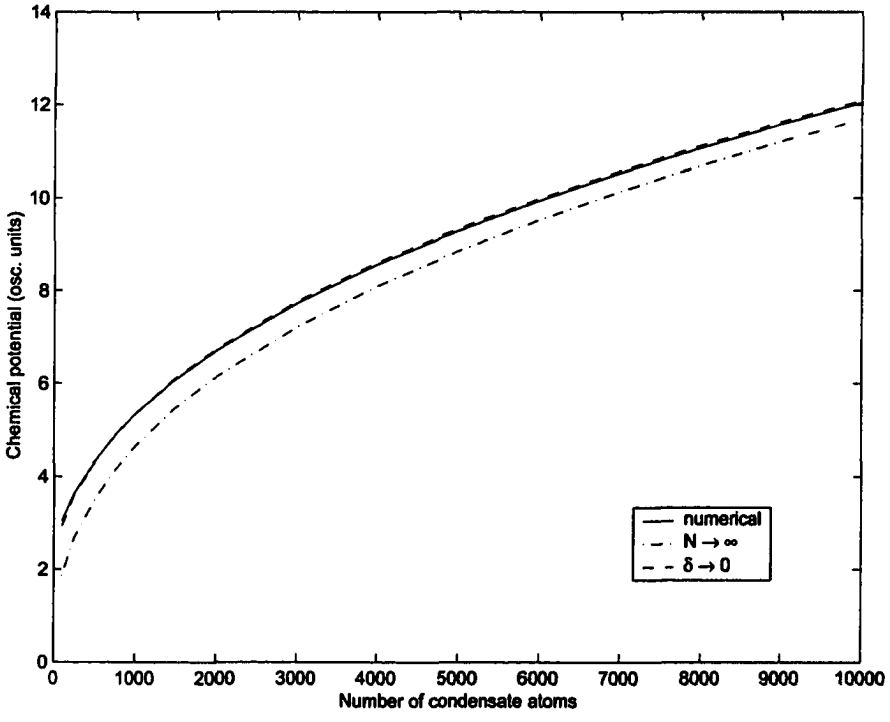


Figure 3.5: Chemical potential in oscillator units vs. number of condensate atoms for a ^{87}Rb condensate with parameters corresponding to the JILA TOP trap[20]; we let $a = 110$ bohr, $\nu_\perp = 133$ Hz and $\lambda = \sqrt{8}$. The zeroth-order approximation of dimensional perturbation theory presented here (dashed) is in better agreement with the numerical solution of the GP equation (solid) than the $N \to \infty$ Thomas-Fermi approximation (dash-dot).

3.2 $1/N$ perturbation theory for a model BEC Hamiltonian

Using ordinary Schrödinger quantum mechanics, Bohn, Esry and Greene[48] have derived effective potentials for dilute Bose-Einstein condensates. The many-atom

problem is reduced to a linear Schrödinger equation by identifying a single coordinate, R, the mean condensate radius. Bohn *et al.* use hyperspherical coordinates to define R, expand in hyperspherical harmonics, and then retain only a single term in this expansion. They refer to this as the "K-harmonic" approximation following terminology from nuclear theory. The resulting one dimensional linear Schrödinger equation gives quite good results for ground state energies in a trap roughly approximating the JILA ^{87}Rb experiments[20], faring slightly better than other variational approaches. Their effective potential is also able to predict reasonably well the critical number of bosons with negative scattering lengths that can be condensed, as well as other characteristics of the condensate such as low lying excitation frequencies, peak densities and decay rates from two- and three-body processes.

We chose this model Hamiltonian to test a perturbation formalism which uses $1/N$ as the perturbation parameter, where N is the number of particles in the condensate. This formalism is analogous to the dimensional perturbation methods used successfully in many areas of physics[32, 33, 49, 50, 51, 52, 53, 54]. In particular we use a matrix method developed for atomic systems to solve the perturbation equation[55]. We find that this perturbation approach takes advantage of the simplicity of the Thomas-Fermi limit which is valid for N large, but improves on this limit significantly for the zeroth order starting point by including a single additional term beyond Thomas-Fermi.

3.2.1 Formalism

The derivation of Bohn *et al.* begins with the full N-body Hamiltonian:

$$H = -\frac{\hbar^2}{2m}\sum_{i=1}^{N}\nabla_i^2 + \sum_{i=1}^{N}\frac{1}{2}m\omega^2 r_i^2 + \sum_{i<j}^{N}U_{\rm int}(\vec{r_i}-\vec{r_j}), \tag{3.27}$$

where $U_{\rm int}$ is the two-body atomic interaction potential. All three-body and higher interactions are ignored under the assumption of a dilute gas. The mean condensate radius of the atoms from the trap center is:

$$R = \Big(\frac{1}{\sum_{i=1}^{N} m_i}\sum_{i=1}^{N} m_i r_i^2\Big)^{\frac{1}{2}} = \Big(\frac{1}{N}\sum_{i=1}^{N} r_i^2\Big)^{\frac{1}{2}}, \tag{3.28}$$

where we assume all the particles in the condensate are identical. The remaining $3N-1$ coordinates are then given in terms of hyperangles collectively denoted by

Ω[56]. Using the transformation $(\vec{r_1},....\vec{r_N}) \rightarrow (R,\Omega)$ and assuming $U_{\rm int}(\vec{r_1}-\vec{r_2}) = (4\pi\hbar^2 a/m)\,\delta(\vec{r_1}-\vec{r_2})$, where a is the s-wave scattering length, yields a transformed Schrödinger equation:

$$\left\{-\frac{\hbar^2}{2M}\left[\frac{\partial^2}{\partial R^2}-\frac{(3N-1)(3N-3)}{4R^2}-\frac{\Lambda^2}{R^2}\right]+\frac{1}{2}M\omega^2R^2 \right. \\ \left. +\sum_{i<j}^{N}\frac{4\pi\hbar^2 a}{m}\delta(\vec{r_i}-\vec{r_j})-E\right\}R^{(3N-1)/2}\psi(R,\Omega)=0. \tag{3.29}$$

where Λ^2 is a "grand angular momentum operator" [42]. Expanding in hyperspherical harmonics and retaining a single term, results in the final equation:

$$\left\{-\frac{\hbar^2}{2M}\frac{\partial^2}{\partial R^2}++V_{\rm eff}^{\rm Bohn}(R)-E\right\}F(R)=0, \tag{3.30}$$

where:

$$V_{\rm eff}^{\rm Bohn}=\frac{\hbar^2}{2M}\frac{(3N-1)(3N-3)}{4R^2}+\frac{1}{2}M\omega^2R^2+\zeta\sqrt{\frac{1}{2\pi}}\frac{\hbar^2 aN^2(N-1)}{MR^3}, \tag{3.31}$$

$$\zeta=\frac{\Gamma(3N/2)}{\Gamma((3N-3)/2)N^{\frac{3}{2}}}. \tag{3.32}$$

is the effective potential. Bohn and coworkers solve this equation numerically using a B-spline approach.

In our solution of this equation we use a perturbation approach where $1/N$ is the perturbation parameter. We transform the equation using scalings that give a stable $N\rightarrow\infty$ limit:

$$R=N^2\hat{R},\ \ \omega=N^{-4}\hat{\omega},\ \ a=N\hat{a},\ \ E=N^{-3}\epsilon,$$

and then change to scaled oscillator units: $\hat{R}=\sqrt{\frac{\hbar}{m\hat{\omega}}}\bar{R}$, $\hat{\epsilon}=\hbar\hat{\omega}\bar{\epsilon}$, which yields

$$\left\{-\frac{1}{2}\delta^2\frac{\partial^2}{\partial\bar{R}^2}+\left[\frac{(9-12\delta+3\delta^2)}{8\bar{R}^2}\right]+\frac{1}{2}\bar{\omega}^2\bar{R}^2+\frac{\zeta\hat{a}}{\sqrt{2\pi}}\sqrt{\frac{m\hat{\omega}}{\hbar}}\frac{(1-\delta)}{\bar{R}^3}-\bar{\epsilon}\right\}\hat{\Phi}(\bar{R})=0, \tag{3.33}$$

where $\delta=1/N$ and $\bar{\omega}=1$ in scaled oscillator units. To obtain a zeroth-order starting point we let $N\rightarrow\infty$ i.e. $\delta\rightarrow 0$. In this limit the derivative term and part of the centrifugal-like potential drop out and the problem reduces to finding the minimum of the effective potential, $V_{\rm eff}^{\infty}$;

$$\left[V_{\mathrm{eff}}^{\infty}(\bar{R}_m) - \bar{\epsilon}\right]\hat{\Phi}(\bar{R}_m) = 0, \tag{3.34}$$

$$V_{\mathrm{eff}}^{\infty}(\bar{R}) = \frac{9}{8\bar{R}^2} + \frac{1}{2}\bar{\omega}^2\bar{R}^2 + \frac{\lambda}{\bar{R}^3}, \tag{3.35}$$

$$\lambda = \frac{\zeta\hat{a}}{\sqrt{2\pi}}\sqrt{\frac{m\hat{\omega}}{\hbar}} = \frac{N\zeta a}{\sqrt{2\pi}}\sqrt{\frac{m\omega}{\hbar}}. \tag{3.36}$$

Note that this effective potential retains an additional term, $9/(8\bar{R}^2)$, compared to the Thomas-Fermi limit of Eq. (3.30). This additional term comes from the centrifugal-like part of the effective potential which originates in the kinetic energy. The Thomas-Fermi limit of Eq. (3.30) drops the entire kinetic energy including the centrifugal-like potential. Note also that all the terms in Bohn's effective potential are included at least in part. The importance of including a term from the centrifugal-like potential is obvious from Figure 3.6 where we compare our $N \to \infty$ effective potential, $V_{\mathrm{eff}}^{\infty}$, for $a < 0$ and $a > 0$ to the Thomas-Fermi limit of Bohn's potential using the same values of a. In contrast to the Thomas-Fermi potential, our $V_{\mathrm{eff}}^{\infty}$ retains the correct features for both positive and negative scattering lengths. For $a > 0$, $V_{\mathrm{eff}}^{\infty}$ gains a repulsive contribution from the interaction term increasing the strength of the effective trap, compared to the Thomas-Fermi limit which is too deep. For $a < 0$, the competition between the positive centrifugal-like term, $9/8\bar{R}^2$ and the negative term, $\lambda/\bar{R}^3$, which contains the negative scattering length, creates a potential barrier for small $\bar{R}$ and a metastable well in our $V_{\mathrm{eff}}^{\infty}$, while for the Thomas-Fermi potential, no metastable region exists.

Eq. (3.35) can be solved for the $\bar{R} = \bar{R}_m$ which yields the minimum energy $\bar{\epsilon}_{\infty} = V_{\mathrm{eff}}^{\infty}(\bar{R}_m)$. The perturbation series is then generated by defining a scaled displacement coordinate, r, by $\bar{R} = \bar{R}_m + \delta^{\frac{1}{2}}r$ and expanding:

$$\hat{\Phi}(r) = \sum_{j=0}^{\infty}\hat{\phi}_j(r)\delta^{j/2}, \qquad \bar{\epsilon} = \bar{\epsilon}_{\infty} + \delta\sum_{j=0}^{\infty}\epsilon_{2j}\delta^j. \tag{3.37}$$

The first-order equation in delta is harmonic:

$$\left\{-\frac{1}{2}\frac{\partial^2}{\partial r^2} + \frac{1}{2}\omega_{\mathrm{eff}}^2 r^2 + v_0\right\}\hat{\phi}_0(r) = \epsilon_0\hat{\phi}_0(r), \tag{3.38}$$

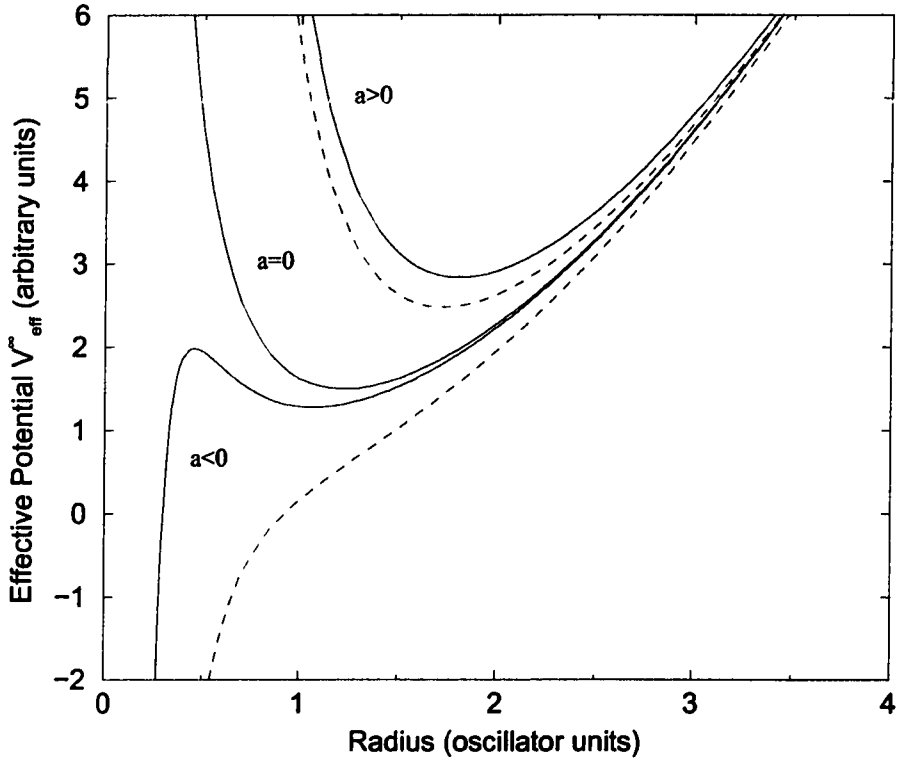


Figure 3.6: Comparison of V^{∞}_{eff} for different values of the scattering length, a. The solid lines are our $N \rightarrow \infty$ effective potential, V^{∞}_{eff}, for $a > 0, a = 0$ and $a < 0$. The short dashed lines are the Thomas-Fermi limit of the Bohn potential for $a > 0$ and $a < 0$

$$\epsilon_0 = \left(\nu + \frac{1}{2}\right)\omega_{eff} + v_0, \tag{3.39}$$

$$\hat{\phi}_0(r) = (\omega_{eff})^{1/4} h_\nu(\omega_{eff}^{1/2} r), \tag{3.40}$$

where:

$$v_0 = -\frac{3}{2\bar{R}_m^2} - \frac{\lambda}{\bar{R}_m^3}, \tag{3.41}$$

$$\omega_{eff}{}^2 = \frac{27}{4\bar{R}_m^4} + \frac{12\lambda}{\bar{R}_m^5} + \bar{\omega}^2, \tag{3.42}$$

and h_ν is a harmonic oscillator solution. This equation defines the harmonic basis functions that are used to solve the higher order equations. Note that the harmonic frequency, ω_{eff}, Eq. (3.42), automatically adapts as the trap frequency and/or scattering length changes, essentially folding these interactions into an effective trap. Thus this first-order equation provides basis functions that are sensitive to the interplay between the trap frequency, ω and the scattering length, a. For $a < 0$, $\omega_{eff}{}^2$ shows the gradual "softening" of the effective trap, $\frac{1}{2}\omega_{eff}{}^2 r^2$, due to the attractive potential, $\lambda/\bar{R}^3$, which increases as N increases. (See Eqs. (3.35) and (3.36)). As the metastable well slowly disappears, the minimum and maximum of V_{eff}^{∞} coincide in an inflection point where $\partial^2 V_{eff}^{\infty}/\partial\bar{R}^2 = 0$. This occurs at $R_c = (1/5)^{\frac{1}{4}}(3/2)^{\frac{1}{2}}$, and corresponds to $\omega_{eff}^2 = 0$ (since $\omega_{eff}^2 = \partial^2 V_{eff}^{\infty}/\partial\bar{R}^2$), i.e. no effective trap exists. The resulting critical number, N_c, of negative scattering length atoms that can be trapped is found to be:

$$N_c = 0.671\sqrt{\frac{\hbar}{m\omega}}\frac{1}{|a|} \tag{3.43}$$

which is the same N_c obtained by Bohn *et al.* from his effective potential. (This is not unexpected since Bohn *et al.* assume that $N \gg 1$ in their alternative derivation of N_c. (see Ref. [48] Eq. (4.4).)) This result is also in excellent agreement with the results obtained from several variational treatments[27, 29, 57, 58]. Figure 3.7 shows the change in our V_{eff}^{∞} as the number of particles changes from slightly below N_c to slightly above this value. (For this graph we use trap parameters that approximate the ^{7}Li experiments at Rice[59].)

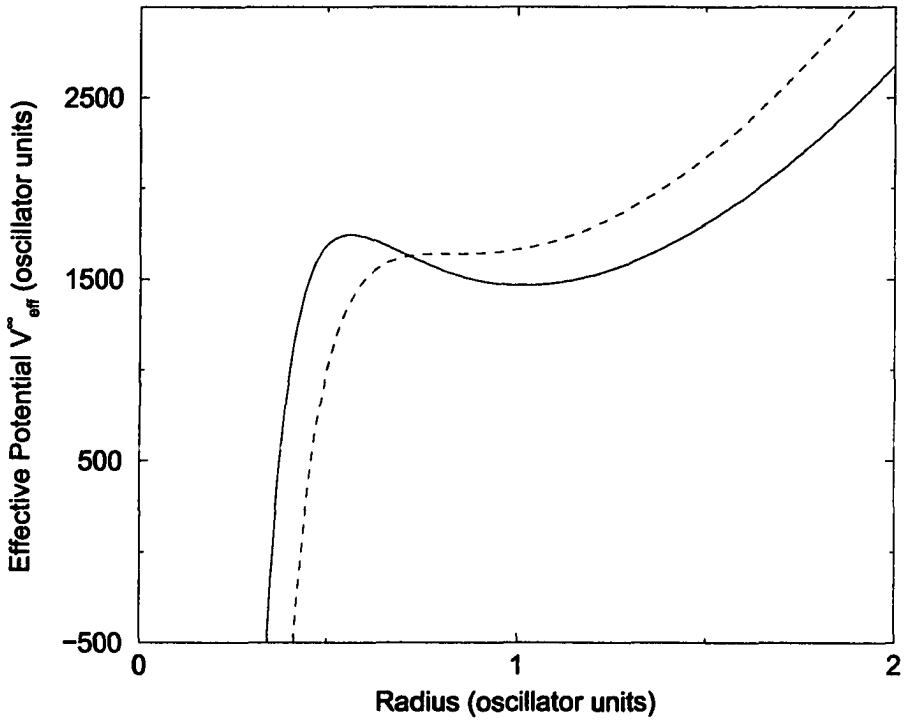


Figure 3.7: Plots of our $N \rightarrow \infty$ effective potential, V^{∞}_{eff}, for $a = -27.3$ bohr and $\nu = 144.6$ Hz. The solid curve represents the case where the number of particles, N, is just less than the critical number, N_c. The dashed curve shows the case where $N > N_c$ resulting in no metastable region.

Higher order terms bring in coupling between the higher order terms in the centrifugal-like potential and the atomic interaction term. The external harmonic trap is included entirely in the first-order harmonic equation. The infinite set of differential equations for the $\hat{\phi}_j(r)$ and the ϵ_{2j} are computed using a linear algebraic method that expands the $\hat{\phi}_j(r)$ in terms of the harmonic oscillator functions h_ν and represents the displacement coordinate r as a matrix in this basis. A recursion relation yields the wave function and energy coefficients[55].

3.2.2 Results

Our results for this one dimensional problem using values of $a = 100$ bohr and $\nu = 200$ Hz, roughly approximating the JILA ^{87}Rb experiments[20], are extremely encouraging. Our converged results, of course, compare quite well to the results

of Bohn *et al.*, agreeing to 5 digits. (See Table 3.1.) Table 3.1 also compares our zeroth-order results to converged results. The agreement is striking. Our zeroth-order results agree to 3 or 4 digits with the converged results. (100.02% of the converged value). The Thomas-Fermi results, which are obtained from the effective Hamiltonian of Bohn *et al.* (See Eq. (3.30)) by dropping the full kinetic energy including the centrifugal-like potential, and finding the minimum of the remaining potential, are 45% of the converged results at $N = 500$, improving to 97% agreement at $N = 10\,000$. (Bohn *et al.* compare their results to the results from the Gross Pitaevskii equation as well as to the Thomas-Fermi limit of the Gross Pitaevskii equation. See Ref [48], Fig. 3.7)) Our zeroth-order equation retains just a single additional term beyond the Thomas-Fermi limit of the Schrödinger equation used by Bohn *et al.*, a term from the centrifugal-like potential. This is an impressive improvement over Thomas-Fermi since the zeroth-order perturbation term is obtained from a trivial calculation. The first order term brings in the interplay between the trap and the interatomic interaction term and adds two more decimal places of accuracy. Table 3.2 shows the extremely rapid convergence to five or six digits by first order and ten or more digits by sixth order for three condensates. This is obtained by a simple summing of the series rather than Padé summation reflecting the excellence of the zeroth-order starting point. We obtain similar agreement with the excitation energies of Bohn *et al.*(See Ref. [1], Fig. 3) By first order our results agree to 4 or more digits with the converged results of Bohn *et al.*[60].

Table 3.1: Results for ground state energies in oscillator units, tabulated in the form $E/N - \frac{3}{2}\hbar\omega$ for a condensate with $a = 100$ bohr and $\nu = 200$ Hz. We compare our zeroth-order and our converged results (10th order) to the results of Bohn *et al.* We also compare the Thomas-Fermi limit of the effective Hamiltonian of Bohn *et al.* to our zeroth-order results.

N	TF of Eq. (4)	Zero order	Converged	Bohn *et al.*
500	0.37509	0.83749	0.83732	0.83732
1000	0.97643	1.33807	1.33784	1.33783
2000	1.76914	2.04852	2.04828	2.04827
3000	2.34534	2.58465	2.58443	2.58441
4000	2.81462	3.02877	3.02857	3.02855
5000	3.21766	3.41402	3.41382	3.41380
6000	3.57472	3.75759	3.75741	3.75738
7000	3.89759	4.06975	4.06958	4.06955
8000	4.19382	4.35719	4.35702	4.35700
9000	4.46857	4.62454	4.62439	4.62436
10000	4.72555	4.87518	4.87503	4.87500

Table 3.2: Partial sums for the ground state energy using $a = 100$ bohr and $\nu = 200$ Hz for condensates with 500 particles, 5000 particles, and 10000 particles in oscillator units, tabulated in the form $E/N - \frac{3}{2}\hbar\omega$.

order	$N = 500$	$N = 5\,000$	$N = 10\,000$
0	0.837 487 821 79	3.414 016 707 69	4.875 183 724 38
1	0.837 324 621 72	3.413 825 082 25	4.875 032 178 85
2	0.837 323 748 09	3.413 824 807 49	4.875 032 077 37
3	0.837 323 665 36	3.413 824 805 36	4.875 032 076 83
4	0.837 323 663 03	3.413 824 805 33	4.875 032 076 83
5	0.837 323 662 93	3.413 824 805 33	4.875 032 076 83
6	0.837 323 662 93	3.413 824 805 33	4.875 032 076 83

Our $V_{\mathrm{eff}}^{\infty}$ potential is quite similar in form to several other effective potentials[27, 29, 57, 58] in the literature, which have been obtained using variational approaches.

Our method, which is based on a rigorous perturbation analysis of the Hamiltonian with a perturbation parameter of $1/N$, offers the possibility of systematic improvement by including higher-order terms.

3.3 $1/D$ Perturbation theory for two-electron quantum dot

In recent years, various theoretical approaches have been employed to calculate the approximate energy spectra of quantum dot systems, systems in which correlation and exchange effects have been found to play a significant role. In the early development of quantum dot theory, the approaches used were "exact" diagonalization[61, 62] and Hartree-Fock [61, 62, 63, 64]. More recent approaches include semiclassical[65, 66] and perturbation methods[30, 67] proposed with the goals of including correlation and maintaining accuracy for many-electron dots while simultaneously reducing computational expense.

A variation of the dimensional perturbation method to be described in this section has been applied to two-dimensional semiconductor systems like magnetoexitons[68] and hydrogenic donor states in a magnetic field[69]. This approach is known as the shifted $1/N$ expansion where N is the number of spatial dimensions. In this method, the energy is expanded in inverse powers of $N - a$ where the shift parameter, a, is determined by requiring that the first-order energy correction vanish.

The effective dimensionality of the quantum dot environment depends on the relative size of the confinement length scales in each of the three spatial dimensions. The effective dimensionality may be one, two or three; or for some quantum dots, the experimental energy spectra may be better described by the energy obtained via a model Hamiltonian in a space with some non-integer effective dimensionality to account for anisotropy in the quantum dot interactions. The concept of fractional dimensionality has been applied to semiconductor systems like exitons in anisotropic or confined quantum well structures in order to account for the effective medium and the anisotropy of the interactions[70, 71, 72]. An advantage of dimensional perturbation theory is that we obtain analytical energy approximations in terms of the parameter D.

Dimensional perturbation theory[32, 33] has been successfully applied to atomic systems in which correlation is significant. In this chapter, we present a perturbation

approach to the two-electron quantum dot with expansion parameter, $\frac{1}{D+2|l|}$, where D is the effective dimensionality of the quantum dot environment and l is the angular momentum quantum number for the relative motion of the electrons. The anisotropy of the quantum dot interactions is modeled by a Hamiltonian in an isotropic D-dimensional space where D is a measure of the degree of anisotropy and may be integer or non-integer. In the $D = 2$ and $D = 3$ limits of this generalized Hamiltonian, we regain the usual isotropic Hamiltonians in plane polar and spherical coordinates, respectively.

The zeroth- plus first-order terms of the energy series provide an accurate analytical approximation to the energy. In the zeroth-order calculation, we take the infinite-D limit of the Hamiltonian which results in an effective potential. The zeroth-order problem is then reduced to a simple minimization calculation of the effective potential that turns out to be similar in form to WKB and other semiclassical approximations of the $D = 2$, two-electron quantum dot[65, 66]. This similarity is not fortuitous because the infinite-D limit is itself a classical limit.

When a higher degree of accuracy than that provided by the analytical approximation is desired, our method allows for systematic improvement by including higher-order terms; the partial sums of the resulting energy series are calculated using straight summation. We compare our results with exact numerical results obtained by directly integrating the Schrödinger equation using a Numerov method for $D = 2$ and $D = 3$. In Sec. V, we briefly discuss extensions of this perturbation method including the extension to the many-electron D-dimensional quantum dot.

3.3.1 Formalism

To illustrate the dimensional perturbation method, we consider a two-electron dot within the effective mass approximation where the two electrons, each with effective mass m^*, move in a medium with dielectric constant ϵ. Before considering the more general quantum dot with effective dimensionality $0 < D \leq 3$, we will work with the more restricted $D = 3$ case with a spherical harmonic confining potential with frequency ω_o. In three dimensions, this system is described by the Hamiltonian:

$$H = -\frac{\hbar^2}{2m^*}({\nabla_1}^2 + {\nabla_2}^2) + \frac{1}{2}m^*\omega_o^2({r_1}^2 + {r_2}^2) + \frac{e^2}{\epsilon|\mathbf{r}_1 - \mathbf{r}_2|}. \tag{3.44}$$

We define:

$$a^* = \frac{\epsilon\hbar^2}{m^* e^2} \tag{3.45}$$

$$l_o = \sqrt{\frac{\hbar}{m^*\omega_o}} \tag{3.46}$$

where a^* is the effective Bohr radius and l_o is the characteristic size of the dot. Letting $\mathbf{r}_i \rightarrow a^*\mathbf{r}_i$ yields the Hamiltonian:

$$H = -\nabla_1^2 - \nabla_2^2 + \frac{1}{4}\gamma^2(r_1^2 + r_2^2) + \frac{2}{|\mathbf{r}_1 - \mathbf{r}_2|} \tag{3.47}$$

where the energy is in units of effective Rydbergs R^* and $\gamma = 2(\frac{a^*}{l_o})^2$. The parameter γ describes the relative magnitude of the confinement energy and Coulombic energy scales. Later we investigate quantum size effects on our accuracy by varying $\gamma^{-\frac{1}{2}}$.

The Hamiltonian of Eq. (4) can be separated into center-of-mass and relative-motion pieces as

$$H = H_{\text{c.m.}} + H_{\text{rel}} \tag{3.48}$$

with

$$H_{\text{c.m.}} = -\frac{1}{2}\nabla_{\text{c.m.}}^2 + \frac{1}{2}\gamma^2 R^2 \tag{3.49}$$

and

$$H_{\text{rel}} = -2\nabla_{\text{rel}}^2 + \frac{1}{8}\gamma^2 r^2 + \frac{2}{r} \tag{3.50}$$

where $\mathbf{R} = \frac{1}{2}(\mathbf{r}_1 + \mathbf{r}_2)$, $\nabla_{\text{c.m.}} = \nabla_1 + \nabla_2$, $\mathbf{r} = \mathbf{r}_1 - \mathbf{r}_2$ and $\nabla_{\text{rel}} = \frac{1}{2}(\nabla_1 - \nabla_2)$. This essentially reduces the problem to two one-particle equations. In the rest of this section and the following, our main focus will be on calculating the relative-motion energy, E_{rel}, by applying a perturbation approach to the Hamiltonian of Eq. (7) in arbitrary dimension.

Next we explicitly generalize the Schrödinger equation to D-dimensions where r becomes the radius of a D-dimensional sphere with $D-1$ remaining angles. Using the procedure where the Laplacian is generalized to D-dimensions, but the potential terms retain their three-dimensional form, we obtain the following Schrödinger equation:

$$\left\{-2\Big[\frac{1}{r^{D-1}}\frac{\partial}{\partial r}\Big(r^{D-1}\frac{\partial}{\partial r}\Big) + \frac{L_{D-1}^2}{r^2}\Big] + \frac{1}{8}\gamma^2 r^2 + \frac{2}{r}\right\}\Psi(r) = E_{\text{rel}}\Psi(r), \tag{3.51}$$

where L^2_{D-1} is a generalized angular momentum operator depending on $D-1$ angles with eigenvalues $-|l|(D+|l|-2)$[42]. Substituting these eigenvalues and introducing the radial Jacobian factor in a transformation of the wave function, $\Phi(r) = r^{(D-1)/2}\Psi(r)$ to eliminate the first derivative terms, we find:

$$\left\{-2\Big[\frac{\partial^2}{\partial r^2}+\frac{(D-1)(D-3)}{4r^2}-\frac{|l|(D+|l|-2)}{r^2}\Big]+\frac{1}{8}\gamma^2r^2+\frac{2}{r}\right\}\Phi(r) = E_{\rm rel}\Phi(r). \quad (3.52)$$

We now define an expansion parameter, κ, as

$$\kappa = D + 2|l|, \quad (3.53)$$

and introducing the dimensionally-scaled variables

$$r = \kappa^2\tilde{r}, \quad \tilde{\gamma} = \kappa^3\gamma, \quad \epsilon_{\rm rel} = \kappa^2 E_{\rm rel} \quad (3.54)$$

we obtain a dimensionally-scaled Schrödinger equation that has a finite energy as $D \to \infty$:

$$\left\{-2\delta^2\Big(\frac{\partial^2}{\partial\tilde{r}^2}\Big)+\frac{1-4\delta+3\delta^2}{2\tilde{r}^2}+\frac{1}{8}\tilde{\gamma}^2\tilde{r}^2+\frac{2}{\tilde{r}}\right\}\Phi(\tilde{r}) = \epsilon_{\rm rel}\Phi(\tilde{r}) \quad (3.55)$$

where $\delta = 1/\kappa$ is treated as a continuous parameter. Hence, D may be non-integer as well as integer by this dimensional continuation. One may find similar dimensional scalings for atomic systems in Refs. [73] and [74].

One may perform a similar dimensional scaling of the center-of-mass Hamiltonian, Eq. (6). The eigenenergies can be obtained exactly and are found to be

$$E_{\rm c.m.}(N, L, D) = (2N + |L| + \frac{D}{2})\gamma \quad (3.56)$$

where N and L are the radial and orbital quantum numbers for the center-of-mass motion and D is the effective dimensionality of the quantum dot. The total energy is $E = E_{\rm c.m.} + E_{\rm rel}$

3.3.2 Perturbation expansion

To obtain the zeroth-order energy approximation for the relative-motion energy, we begin by taking the infinite-dimension limit, $D \to \infty$ (i.e. $\delta \to 0$) of Eq. (12). In this

limit, the derivative terms of the kinetic energy drop out of the Hamiltonian reducing the calculation of the zeroth-order energy, ϵ_∞, to finding the minimum of an effective potential, V_{eff}:

$$\epsilon_\infty = V_{\mathit{eff}}(\tilde{r}_m). \tag{3.57}$$

V_{eff} takes the form:

$$V_{\mathit{eff}}(\tilde{r}) = \frac{1}{2\tilde{r}^2} + \frac{1}{8}\tilde{\gamma}^2\tilde{r}^2 + \frac{2}{\tilde{r}}, \tag{3.58}$$

and $\tilde{r}_m$ is the smallest positive root of the quartic polynomial:

$$\tilde{\gamma}^2\tilde{r}_m^4 - 8\tilde{r}_m - 4 = 0. \tag{3.59}$$

The zeroth-order energy is already in good agreement with exact values for $\gamma = 1$ and $\gamma = .05$ for states with $n = 0$ (see Tables 3.3 and 3.4). Our effective potential has the same form as those found in other semiclassical approximations of two-electron dots for $D = 2$. Klama *et al.*[65] propose a simple model within the WKB context called the harmonic approximation which results in an analytical approximation to the energy. They achieve this by replacing the WKB potential in the Schrödinger equation with its Taylor expansion about its minimum up to harmonic order. This results in a linear oscillator spectrum. Also within the WKB context, García-Castelán *et al.*[66] obtain analytical results by approximating the true potential curve by matching two half parabolas at the minimum of the WKB effective potential.

Table 3.3: Comparison of the results of our analytical zeroth-order, first-order and numerically calculated sixth-order approximations to the exact energies for $\gamma = 1$ and $D = 2$. The energy state is specified in the first column by the quantum numbers $(n, l; N, L)$. Total energy is in units of effective Rydbergs.

$(n, l; N, L)$	exact	zero order	first order	sixth order
(0,0;0,0)	3.3242	2.8998	3.1575	3.3188
(0,1;0,0)	3.8279	3.6784	3.7929	3.8279
(0,0;0,1)	4.3242	3.8998	4.1575	4.3188
(0,2;0,0)	4.6437	4.5641	4.6306	4.6436
(0,1;0,1)	4.8279	4.6784	4.7929	4.8278
(1,0;0,0)	5.1568	2.8998	5.0150	5.1456
(0,0;1,0)	5.3242	4.8998	5.1575	5.3188
(0,3;0,0)	5.5432	5.4924	5.5369	5.5432
(0,2;0,1)	5.6436	5.5641	5.6306	5.6436
(1,1;0,0)	5.7439	3.6784	5.7224	5.7439
(0,1;1,0)	5.8279	5.6784	5.7929	5.8278
(1,0;0,1)	6.1568	3.8998	6.0150	6.1456
(0,0;1,1)	6.3242	5.8998	6.1575	6.3188
(0,4;0,0)	6.4782	6.4423	6.4746	6.4782
(1,2;0,0)	6.5957	4.5641	6.5882	6.5957
(0,2;1,0)	6.6436	6.5641	6.6306	6.6436

Table 3.4: Comparison of the results of our analytical zeroth-order, first-order and numerically calculated sixth-order approximations to the exact energies for $\gamma = .05$ and $D = 2$. The energy state is specified in the first column by the quantum numbers $(n, l; N, L)$. Total energy is in units of effective Rydbergs.

$(n,l;N,L)$	exact	zero order	first order	sixth order
(0,0;0,0)	0.2963	0.2624	0.2896	0.2963
(0,1;0,0)	0.3062	0.2856	0.3028	0.3062
(0,0;0,1)	0.3463	0.3124	0.3396	0.3463
(0,2;0,0)	0.3311	0.3177	0.3293	0.3311
(0,1;0,1)	0.3562	0.3356	0.3528	0.3562
(1,0;0,0)	0.3853	0.2624	0.3778	0.3853
(0,0;1,0)	0.3963	0.3624	0.3896	0.3963
(0,3;0,0)	0.3644	0.3550	0.3633	0.3644
(0,2;0,1)	0.3811	0.3677	0.3793	0.3811
(1,1;0,0)	0.3968	0.2856	0.3939	0.3968
(0,1;1,0)	0.4062	0.3856	0.4028	0.4062
(1,0;0,1)	0.4353	0.3124	0.4278	0.4353
(0,0;1,1)	0.4463	0.4124	0.4396	0.4463
(0,4;0,0)	0.4025	0.3955	0.4018	0.4025
(1,2;0,0)	0.4240	0.3177	0.4227	0.4240
(0,2;1,0)	0.4311	0.4177	0.4293	0.4311

In contrast, we systematically improve upon our semiclassical, zeroth-order approximation by adding the next higher-order term of the energy series. The perturbation series is generated by defining a scaled displacement coordinate, x, by $\tilde{r} = \tilde{r}_m + \delta^{1/2}x$ and expanding the wave function and energy as:

$$\Phi(x) = \sum_{j=0}^{\infty} \phi_j(x)\delta^{j/2}, \tag{3.60}$$

$$\epsilon_{\mathtt{rel}} = \epsilon_\infty + \delta \sum_{j=0}^{\infty} \epsilon_{2j}\delta^j. \tag{3.61}$$

The first-order equation in δ is harmonic:

$$\left\{-2\frac{\partial^2}{\partial x^2}+\frac{1}{2}\omega_{\mathit{eff}}^2 x^2+v_{oo}\right\}\phi_o(x)=\epsilon_o\phi_o(x), \tag{3.62}$$

$$\epsilon_o=(n+\frac{1}{2})2\omega_{\mathit{eff}}+v_{oo}, \tag{3.63}$$

$$\phi_o(x)=\left(\frac{\omega_{\mathit{eff}}}{2}\right)^{\frac{1}{4}}h_n\left(\left(\frac{\omega_{\mathit{eff}}}{2}\right)x\right), \tag{3.64}$$

where

$$v_{oo}=-\frac{2}{\tilde{r}_m^2}, \tag{3.65}$$

$$\omega_{\mathit{eff}}^2=V''_{\mathit{eff}}(\tilde{r}_m)=\frac{3}{\tilde{r}_m^4}+\frac{1}{4}\tilde{\gamma}^2+\frac{4}{\tilde{r}_m^3}, \tag{3.66}$$

and the h_n are harmonic oscillator eigenfunctions. This first-order correction represents normal mode vibrations about the classical minimum. The analytical, semiclassical approximation of the energy to first order can then be compactly written as

$$E_{\mathrm{rel}}(n,l,D)\approx\delta^2\epsilon_\infty+\delta^3\left((n+\frac{1}{2})2\omega_{\mathit{eff}}+v_{oo}\right) \tag{3.67}$$

where n is the harmonic quantum number for the relative motion and we have used the relations in Eq. (11) to convert the energy units to unscaled effective Rydbergs. E_{rel} is parameterized explicitly by n and implicitly by l and D. Eq. (24) may then be evaluated at the physically relevant spatial dimension that best describes a particular quantum dot namely, $0<D\leq 3$.

The infinite set of differential equations for the $\phi_j(x)$ and the ϵ_{2j} are computed using a linear algebraic method that expands the $\phi_j(x)$ in terms of the harmonic oscillator functions, h_n, and represents the displacement coordinate, x, as a matrix in the harmonic oscillator basis. A recursion relation yields the wave function and energy coefficients[55].

3.3.3 Results and Discussion

In the special case of $D=2$, we compare our analytical zeroth-order, first-order and numerically calculated sixth-order approximations for ground and excited state energies to exact values obtained by numerical integration of the Schrödinger equation. In Table 3.3, we show this comparison for $\gamma=1$, which is an intermediate regime where neither the confinement energy nor the Coulombic energy scale dominates the

other. Table 3.4 makes the same comparison for $\gamma = .05$, which is a regime where the repulsive interaction energy becomes more dominant and the dot becomes larger. For all three approximations in each table, we add the exact center-of-mass energy, Eq. (13), to the relative-motion energy to obtain the total energy approximation. For $\gamma = 1$, the analytical results of dimensional perturbation theory to first order are in good agreement with exact calculations with relative error less than 5% for states with $|l| = 0$ and less than 1% for states with $|l| > 0$. For $\gamma = .05$, the analytical results to first order agree with exact calculations with relative error less than 2.3% for states with $|l| = 0$ and less than 1.1% for states with $|l| > 0$. By sixth order, all energies are converged to at least 7 digits for $\gamma = .05$ while some of the energies are slightly less accurate for $\gamma = 1$.

Effects of the harmonic quantum number, n, are not brought into the calculation until first order by Eq. (23). Tables 3.3 and 3.4 illustrate this fact by the marked improvement of the first-order over the zeroth-order approximation for states with $n > 0$. For states with $n = 0$, the zeroth-order results are already in good agreement with exact values, making higher-order terms only minor corrections. Tables 3.3 and 3.4 also show that the accuracy of the zeroth-order perturbation starting point improves as the magnitude of the relative-motion angular momentum quantum number, $|l|$, increases. This is understood by noting that increasing $|l|$ decreases the size of the perturbation parameter, δ. For the same reason, we expect the accuracy to improve as the effective dimensionality increases.

In order to demonstrate the flexibility of this method with respect to the quantum dot dimensionality, we compare electron-electron interaction energies, $E_{e-e}(n, l, D)$, for $D = 2$ and $D = 3$. The eigenenergies for the relative motion without the electron-electron interaction may be obtained exactly:

$$E_o(n, l, D) = (2n + \mid l \mid + \frac{D}{2})\gamma. \tag{3.68}$$

The electron-electron interaction energies may then be obtained simply by subtracting out this relative-motion energy without the electron-electron interaction from the full relative-motion energy, $E_{rel}(n, l, D)$:

$$E_{e-e}(n, l, D) = E_{rel}(n, l, D) - E_o(n, l, D). \tag{3.69}$$

In Fig. 3.8, we show the behavior for the 1s, 2p and 3d states in two and three dimensions as γ increases. We use notation conventions from atomic physics where

the principal quantum numbers are given by $(n+ |l| +1)$ and the azimuthal quantum numbers, $|l|= 0, 1, 2, 3, ...$, are designated by s, p, d, f,... Fig. 3.8 is in excellent agreement with the energy ordering predicted by other calculations done separately for $D = 2$ and $D = 3$[75], and shows that the electron-electron interaction energy is proportional to $\gamma^{\frac{1}{2}}$.

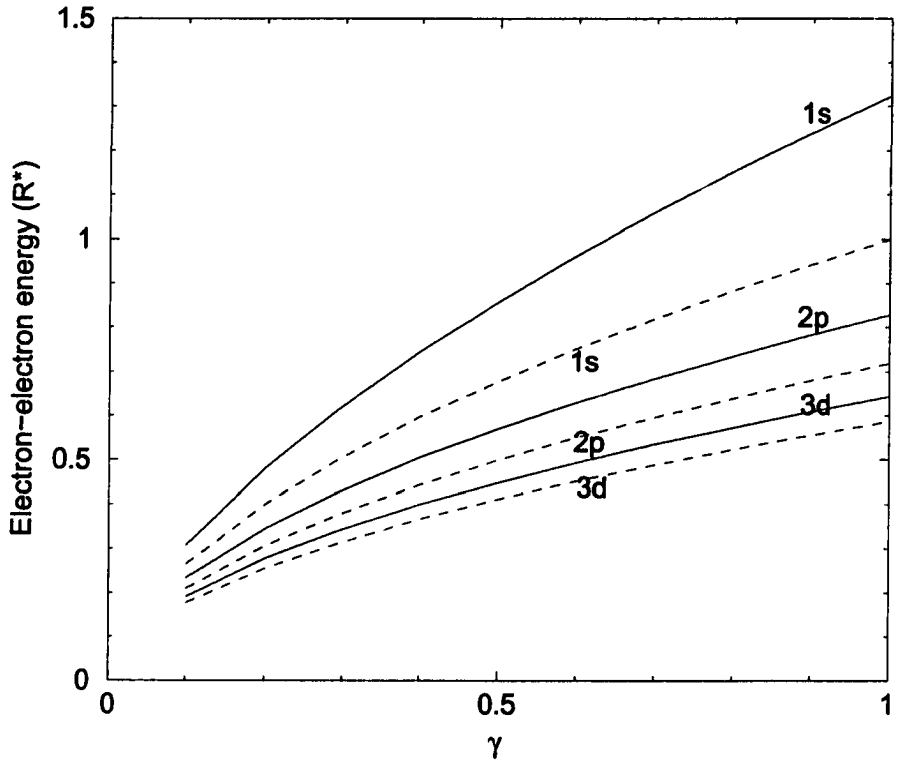


Figure 3.8: Comparison of $E_{e-e}(n, l, D)$ vs γ for $D = 2$ and $D = 3$ for states 1s, 2p and 3d. The solid lines indicate $D = 2$ and dashed lines indicate $D = 3$.

3.4 Discussion

In Sec. 3.1 we allowed the effective dimensionality of a BEC to be a variable quantity, and we used the parameter $\delta = 1/\kappa$ to scale the GP equation in arbitrary dimension, where κ depends on the effective dimensionality of the condensate and on the angular momentum quantum number. We have shown that our zeroth-order ($\delta \rightarrow 0$) limit of the Gross-Pitaevskii equation provides a less severe approximation of the kinetic energy than the $N \rightarrow \infty$ Thomas-Fermi approximation for the ground state, which

neglects the entire kinetic energy. The zeroth-order ($\delta \to 0$) limit is a simple approximation that, in order to satisfy the minimum uncertainty principle, retains a kinetic energy contribution, rather than neglecting the entire KE, making it more accurate and flexible than the ground-state $N \to \infty$ TF approximation. As shown in Fig. 3.1, our zeroth-order approximation is more accurate than the $N \to \infty$ TF approximation for the chemical potential. The accuracy of the zeroth-order approximation is comparable to the lowest order correction due to the boundary layer at the condensate surface. Improved accuracy for the ground state is most noticeable for a moderate number of atoms, the case in which the kinetic energy is most significant. For a sufficiently large number of atoms with positive scattering length, the kinetic energy becomes small for the ground state chemical potential, and the three approximations converge to the numerical solution of the GP equation.

The core near the origin and the presence of the angular momentum quantum number, l, in the scaling parameter, $\delta = 1/\kappa$, make the zeroth-order ($\delta \to 0$) density an especially good starting point for studying properties of vortices. The ground-state $N \to \infty$ TF approximation is unable to accommodate such states, but it can be extended to include vortices by introducing the gradient of the phase from the Laplacian [46, 57, 47, 76]. We expect higher order, finite-δ corrections to further refine the shape of our zeroth-order density for the ground state and vortex states.

We have shown that the dimensional scaling formalism is conducive to analysis of condensates of any dimension. We outlined how simple yet accurate approximations can be achieved for any effective D, and we demonstrated the improved numerical results for $D = 3$. In addition to 3D BEC, the dimensional scaling formalism provides a useful analytical tool in the study of BEC in lower effective dimensionality. We also extended this method to D-dimensional cylindrical coordinates, where the anisotropy parameter was included explicitly for treatment of axially symmetric traps with arbitrary anisotropy.

For the linear model Bose-Einstein Hamiltonian of Bohn, Esry and Greene, we used the methods of DPT in Sec. 3.2 with $1/N$ as the perturbation parameter. The zeroth-order term is similar to the TF approximation in the large-N limit, but improves on the usual TF approximation by retaining a term from the centrifugal-like potential which stabilizes the $N \to \infty$ limit. The first-order equation is harmonic with a frequency that reflects not only the trap frequency but also the interatomic interaction.

The harmonic oscillator basis set (obtained from the first-order equation) is expanded about the point R_m which is the minimum of the $N \to \infty$ effective potential, $V_{\mathrm{eff}}^{\infty}$. This value of R_m is thus sensitive to the balance between the trap potential and the interatomic potential(see Eq. (3.35)). For example, for the case of no interaction between the particles ($a = 0$), $\bar{R}_M = \sqrt{3/2}$ (in oscillator units), which is the value of the uncertainty, ΔR, for the ground state of a harmonic oscillator. $V_{\mathrm{eff}}^{\infty}$ at this minimum is $\frac{3}{2}\hbar\omega$ corresponding to an ideal Bose condensate. For $a > 0$, $\bar{R}_m > \sqrt{3/2}$, due to the repulsive interaction of the particles with a positive scattering length while for $a < 0$, $\bar{R}_M < \sqrt{3/2}$, due to the attractive interaction of the particles with a negative scattering length. Thus, the basis set is not only chosen with a frequency that is responsive to both the trap frequency and the scattering length, but this basis set is also expanded about a point, R_m, which adjusts to changes in these two parameters.

The zeroth-order energy, E_0, is quite close to the converged result reflecting the excellent starting point provided by the $N \to \infty$ effective potential which retains terms from all parts of the full effective potential.

Although it involves particles with fundamentally different statistics (fermi vs. bose) and involves only two particles, the two-electron quantum dot in Sec. 3.3 demonstrates the advantages of DPT and sets the stage for the many-body formalism. We obtained an analytical approximation, parameterized by D, for the ground and excited state energies of a two-electron quantum dot with an effective dimensionality D, which is a measure of the degree of anisotropy in the quantum dot interactions or confinement. Our zeroth-order approximation results in an effective potential reminiscent of semiclassical WKB approaches[65, 66]. This is to be expected because the parameter, κ, acts as an effective mass so that the electrons become infinitely heavy as D or $|l|$ approaches infinity. This in turn causes the derivative terms of the kinetic energy to become zero and the infinitely heavy electrons to remain stationary at the bottom of the effective potential. The effective potential evaluated at its minimum provides a good zeroth-order analytical starting point for the perturbation expansion because the minimum, r_m, is sensitive to the interplay between the confining energy and the repulsive electron interaction energy scales via γ. We then systematically improve upon this classical approximation by adding the semiclassical first-order harmonic correction, which is analogous to vibrations of a Wigner molecule.

Dimensional perturbation theory is applicable to the entire range of γ, unlike perturbation methods that use the confinement strength or the Coulomb strength as the perturbation parameter or methods that use a basis set that takes advantage of

a high- or low-limit of γ. For all values of γ, the analytical semiclassical results of DPT perform extremely well for $|l|> 0$ excitations because in our scaling the kinetic energy scales as the inverse square of the angular momentum. For $|l|= 0$ states, analytical semiclassical results are extremely accurate for typical dots in the mesoscopic regime ($\gamma < 1$) because the kinetic energy scales linearly with γ[77]. Not surprisingly, the domain of validity of γ for different values of l is the same as that of the WKB approximation, which can be determined in terms of either the de Broglie wavelength or the classical momentum[66]. The domain of validity of the semiclassical perturbation expansion for $l = 0$ may be extended to very large γ by applying sophisticated summation methods such as Padé approximants to the asymptotic series; however, even for quantum dot systems where the kinetic and potential energy scales are comparable ($\gamma \approx 1$) the analytical semiclassical results continue to work surprisingly well suggesting that DPT is a particularly robust method for treating quantum dot systems. These results also suggest that DPT would be well suited for application to a quantum dot in an external magnetic field.

Another advantage of this semiclassical method is the ready extension to systems with many degrees of freedom allowing one, for example, to obtain an analytical approximation to the ground and excited states of the N-electron quantum dot or N-atom Bose-Einstein condensate. One way to approach this problem is similar to the large-dimension limit described above for the $N = 2$ electron dot. The idea, which is described fully in the next chapter, is as follows. We begin by writing out the full N-electron quantum dot Hamiltonian in generalized-D form; and dimensionally scale it as we have done for the two-electron dot. In the classical infinite-D limit, the derivative terms of the kinetic energy become zero and we assume a symmetric geometry for the electrons in the effective potential minimum. We would then be able to obtain an analytical zeroth-order approximation of this new effective potential by assuming the electrons are equivalent. This classical result could then be improved upon by appending the semiclassical harmonic correction term which represents normal mode vibrations about the symmetric equivalent geometry. The normal modes may be obtained by applying the FG matrix method to the N-electron Hamiltonian[78].

A semiclassical technique that uses correlated "pocket state" basis functions and the WKB approximation has been used to study the low lying excitation spectrum for quantum dots with two or more electrons[79]. Although the method is different, many of the ideas are similar to the arbitrary-N perturbation method described

above. The total potential is a double well, and each basis function of the finite dimensional "pocket state" basis is strongly localized at a potential minimum becoming smaller further from the minimum. The WKB method is used to compare the magnitudes of off-diagonal Hamiltonian matrix elements, which describe correlated tunneling between different arrangements of the N electrons. For sufficiently low electron densities (or small γ in the notation of this chapter), only one tunneling integral dominates exponentially. As the quantum dot electrons become more Wigner molecule-like, this method becomes more accurate.

The large-D limit is analogous to the prequantum valence models of Lewis and Langmuir. In the large-D limit of the N-electron quantum dot, the electrons become frozen in a Lewis structure. The first-order harmonic oscillations are Langmuir vibrations about the Lewis structure, or, in condensed matter terminology, vibrations about the Wigner structure. This semiclassical perturbation method would be amenable to the calculation of correlation energies, and the prospects for a treatment of the many-electron quantum dot are promising based on successful applications to many-electron atomic systems[80]. Along with the general formalism, in the next chapter we give analytical results for the N-electron atom and N-electron quantum dot. Then in Chapter 5 we apply these same methods to the trapped N-atom Bose-Einstein condensate.

Chapter 4

Many-body dimensional perturbation theory

In this chapter the methods of many-body dimensional perturbation theory are developed for the study of large N-body systems under quantum confinement. We apply dimensional perturbation theory to many-body quantum confined systems from chemical, condensed matter, and atomic physics. The first application originated in Ref.[80], in which Loeser introduced low-order many-body dimensional perturbation methods to the N-electron atom. In this instrumental paper, Loeser obtains low-order, analytical results for the ground-state energy of neutral atoms for $Z = 1$ to 127 that compare well to Hartree-Fock energies with a correlation correction. We then discuss the formalism and general theory behind Loeser's results for the N-electron atom, in which the quantum confinement of the N electrons is supplied by the Coulomb attraction of the nucleus. We follow this atomic physics system with the quantum dot, an atom-like many-body system from condensed matter physics, where the confinement of the N electrons is supplied by an external, isotropic trapping potential.

In the next chapter, we consider N identical hard spheres in an isotropic trap. Although our results are more general, this model is appropriate for describing a Bose-Einstein condensate of an inhomogeneous alkali metal gas. Atomic BEC, like the quantum dot, acts as a bridge between the areas of atomic and condensed matter physics and is the emphasis of this thesis.

In many-body dimensional perturbation theory, the N particle radii are allowed to have D Cartesian components and $1/D$ becomes a perturbation parameter. An overview of the formalism to be described in this chapter is as follows. The Schrödinger equation is written in terms of a similarity transformed wave function that removes first-order derivatives from the Laplacian and introduces a centrifugal-like potential containing all of the explicit dimension dependence of the Laplacian. The explicit

dimension-dependence of the centrifugal-like potential is quadratic, and in order to regularize the $D \to \infty$ limit of the Hamiltonian (the leading-order term in the $1/D$ expansion) we choose a scaling of the length and energy that is also quadratic in D. Then as $D \to \infty$ the second-order derivative parts of the kinetic energy vanish and the particles become localized in the bottom of an effective potential defined by a centrifugal-like contribution from the kinetic energy and contributions from the other potential energies (i.e., the confinement and interaction potentials). In the case of attractive interparticle forces, the repulsive centrifugal-like term stabilizes the large-D configuration against collapse. The first-order quantum correction corresponds to normal-mode vibrations about the large-D effective potential minimum. We find the normal-mode frequencies using the FG matrix technique of molecular physics[78]. Higher orders can be calculated using a matrix method developed specifically for dimensional perturbation theory[55].

4.1 D-dimensional N-body Schrödinger equation

For an N-body system of particles confined by a spherically symmetric potential and interacting via a common two-body potential g_{ij}, the Schrödinger equation in D-dimensional Cartesian coordinates is

$$H\Psi = \left[\sum_{i=1}^{N} h_i + \sum_{i=1}^{N-1}\sum_{j=i+1}^{N} g_{ij}\right]\Psi = E\Psi, \tag{4.1}$$

where

$$h_i = -\frac{\hbar^2}{2m_i}\sum_{\nu=1}^{D}\frac{\partial^2}{\partial x_{i\nu}^2} + V_{\text{conf}}\left(\sqrt{\textstyle\sum_{\nu=1}^{D} x_{i\nu}^2}\right), \tag{4.2}$$

$$\text{and} \quad g_{ij} = V_{\text{int}}\left(\sqrt{\textstyle\sum_{\nu=1}^{D}(x_{i\nu} - x_{j\nu})^2}\right) \tag{4.3}$$

are the single-particle Hamiltonian and the two-body interaction potential, respectively, and V_{conf} is the confining potential. The operator H is the D-dimensional Hamiltonian, and $x_{i\nu}$ is the ν^{th} Cartesian component of the i^{th} particle. For the N-electron atom, V_{conf} is the Coulomb attraction holding the electrons to the nucleus, while for the N-electron quantum dot and N-atom hard-sphere (BEC) problem we will model the confinement as a harmonic trapping potential. The two-body interaction potential V_{int} is Coulombic in the first two systems and hard sphere in the third.

4.1.1 Transformation of the Laplacian

Restricting our attention to spherically symmetric ($L = 0$) states of the many-body system, we transform the coordinates of all particles, each with D Cartesian components $x_i = (x_{i1}, x_{i2}, \ldots, x_{iD})$ $(1 \le i \le N)$, to internal coordinates. A convenient internal coordinate system for confined systems is

$$r_i = \sqrt{\sum_{\nu=1}^{D} x_{i\nu}^2} \quad (1 \le i \le N) \quad \text{and} \quad \gamma_{ij} = \cos(\theta_{ij}) = \left(\sum_{\nu=1}^{D} x_{i\nu} x_{j\nu}\right) / r_i r_j \quad (1 \le i < j \le N), \tag{4.4}$$

which are the D-dimensional scalar radii r_i of the N particles from the center of the confining potential and the cosines γ_{ij} of the $N(N-1)/2$ angles between the radial vectors. Now for a function Ψ dependent on two functions $r(x)$ and $\gamma(x)$, which represent the internal coordinates, one can write

$$\frac{d^2\Psi(r(x),\gamma(x))}{dx^2} = \frac{d^2r}{dx^2}\frac{d\Psi}{dr} + \frac{d^2\gamma}{dx^2}\frac{d\Psi}{d\gamma} + \left(\frac{dr}{dx}\right)^2 \frac{d^2\Psi}{dr^2} + \left(\frac{d\gamma}{dx}\right)^2 \frac{d^2\Psi}{d\gamma^2} + 2\frac{d\gamma}{dx}\frac{dr}{dx}\frac{d^2\Psi}{dr d\gamma}. \tag{4.5}$$

Generalizing this, when operating on the state $\Psi(r_i(x_{i\nu}), \gamma_{i,1}(x_{i\nu}) \ldots \gamma_{i,k}(x_{i\nu}) \ldots \gamma_{i,N}(x_{i\nu}))$ (where $k \neq i$ and $\nu = 1, \ldots, D$)), ∇_i^2 can be written in terms of the internal coordinates of Eq. (4.4) as

$$\begin{aligned}
\nabla_i^2\Psi \equiv \sum_{\nu=1}^{D} \frac{\partial^2}{\partial x_{i\nu}^2}\Psi \;=\; & \sum_{\nu=1}^{D}\left(\frac{\partial^2 r_i}{\partial {x_{i\nu}}^2}\right)\frac{\partial}{\partial r_i}\Psi + \sum_{\nu=1}^{D}\sum_{j\neq i}\left(\frac{\partial^2\gamma_{ij}}{\partial {x_{i\nu}}^2}\right)\frac{\partial}{\partial\gamma_{ij}}\Psi + \\
& \sum_{\nu=1}^{D}\left(\frac{\partial r_i}{\partial x_{i\nu}}\right)^2\frac{\partial^2}{\partial {r_i}^2}\Psi + \sum_{\nu=1}^{D}\sum_{j\neq i}\sum_{k\neq i}\left(\frac{\partial\gamma_{ij}}{\partial x_{i\nu}}\right)\left(\frac{\partial\gamma_{ik}}{\partial x_{i\nu}}\right)\frac{\partial^2}{\partial\gamma_{ij}\partial\gamma_{ik}}\Psi + \\
& 2\sum_{\nu=1}^{D}\sum_{j\neq i}\left(\frac{\partial r_i}{\partial x_{i\nu}}\right)\left(\frac{\partial\gamma_{ij}}{\partial x_{i\nu}}\right)\frac{\partial^2}{\partial r_i\partial\gamma_{ij}}\Psi.
\end{aligned} \tag{4.6}$$

The relevant derivatives of the internal coordinates are

$$\frac{\partial r_i}{\partial x_{i\nu}} = \frac{x_{i\nu}}{r_i} \qquad \frac{\partial\gamma_{ij}}{\partial x_{i\nu}} = \frac{1}{r_i}\left(\frac{x_{j\nu}}{r_j} - \frac{x_{i\nu}}{r_i}\gamma_{ij}\right) \tag{4.7}$$

$$\frac{\partial^2 r_i}{\partial {x_{i\nu}}^2} = \frac{1}{r_i}\left(1 - \frac{x_{i\nu}^2}{r_i^2}\right) \qquad \frac{\partial^2\gamma_{ij}}{\partial {x_{i\nu}}^2} = \frac{1}{r_i^2}\left(3\frac{x_{i\nu}^2}{r_i^2}\gamma_{ij} - 2\frac{x_{i\nu}}{r_i}\frac{x_{j\nu}}{r_j} - \gamma_{ij}\right), \tag{4.8}$$

which lead to the effective S-wave Laplacian in internal coordinates:

$$\sum_i \nabla_i^2\Psi \;=\; \sum_i \frac{D-1}{r_i}\frac{\partial}{\partial r_i}\Psi - \sum_i \frac{D-1}{r_i^2}\sum_{j\neq i}\gamma_{ij}\frac{\partial}{\partial\gamma_{ij}}\Psi +$$

$$\sum_i \frac{\partial^2}{\partial {r_i}^2}\Psi + \sum_i \sum_{j\neq i} \sum_{k\neq i} \frac{\gamma_{jk} - \gamma_{ij}\gamma_{ik}}{r_i^2} \frac{\partial^2}{\partial\gamma_{ij}\partial\gamma_{ik}}\Psi. \tag{4.9}$$

4.1.2 Removal of first-order derivatives

Next we wish to find a transformation of the Hamiltonian that removes the first-order derivatives from the Laplacian (Eq. 4.9) so that the kinetic energy operator is reduced to a sum of terms of two kinds, namely, a second-order derivative term and a repulsive centrifugal-like term. When this is done the zeroth and first orders of the dimensional $(1/D)$ expansion of the Hamiltonian become exactly soluble for any value of N. In the $D \to \infty$ limit, the second derivative terms drop out, resulting in a static problem at zeroth order, while first order correction corresponds to simple harmonic normal-mode oscillations about the infinite-dimensional structure.

In Ref. [81], Avery *et al.* considered the problem of performing a similarity transformation of the wave function Ψ and operators $\hat{O}$:

$$\Phi = \chi^{-1}\Psi \quad \text{and} \quad \tilde{O} = \chi^{-1}\hat{O}\chi, \tag{4.10}$$

where the transforming function, with adjustable parameters α and β, is of the form:

$$\chi = (r_1 r_2 \ldots r_N)^{-\alpha}\Gamma^{-\beta/2}. \tag{4.11}$$

Here Γ is the Gramian determinant, the determinant of the matrix whose elements are γ_{ij} (see Appendix E). One of the cases considered by Avery *et al.* in Ref. [81] for α and β ($\alpha_1 = (D-1)/2$ and $\beta_1 = (D-N-1)/2$) causes the weight function for matrix elements, $W = J\chi^2$, to equal unity, where J is the Jacobian of the transformation to internal coordinates:

$$J = (r_1 r_2 \ldots r_N)^{D-1}\Gamma^{(D-N-1)/2}. \tag{4.12}$$

As will be discussed in a future publication[82], this scenario has the advantage of making matrix elements easier to calculate using DPT, and makes the physical interpretation of the large-dimension normal-mode structure more transparent. However, the results in this chapter are easier to derive if we use $\alpha = \beta = (D-1)/2$, which removes the first-order derivatives from the Laplacian while giving the same results as α_1 and β_1 through first order in $1/D$. Carrying out the transformation of the

Hamiltonian and wave function of Eq. (4.1) via Eq. (4.10) with $\alpha = \beta = (D-1)/2$ in Eq. (4.11), the Schrödinger equation becomes[80]:

$$(T+V)\Phi = E\Phi \tag{4.13}$$

$$T = \sum_{i=1}^{N}\left(-\frac{\hbar^2}{2m_i}\frac{\partial^2}{\partial r_i^2} - \sum_{j\neq i}\sum_{k\neq i}\frac{\hbar^2(\gamma_{jk}-\gamma_{ij}\gamma_{ik})}{2m_i r_i^2}\frac{\partial^2}{\partial\gamma_{ij}\partial\gamma_{ik}} + \right.$$
$$\left. + \frac{\hbar^2(D-1)(D-2N-1)}{8m_i r_i^2}\frac{\Gamma^{(i)}}{\Gamma}\right) \tag{4.14}$$

$$V = \sum_{i=1}^{N} V_{\text{conf}}(r_i) + \sum_{i=1}^{N-1}\sum_{j=i+1}^{N} V_{\text{int}}(r_{ij}). \tag{4.15}$$

The Gramian matrix whose determinant is $\Gamma^{(i)}$ is the i^{th} principal minor formed by deleting from Γ the row and column corresponding to the i^{th} particle, and $r_{ij} = \sqrt{r_i^2 + r_j^2 - 2r_i r_j \gamma_{ij}}$ is the interparticle separation. The similarity-transformed Hamiltonian for the energy eigenstate Φ is $\chi^{-1}H\chi$, where $H = (T+V)$.

We remark that for the hard-sphere system in Ch. 5, we find it expedient to choose a dimensional continuation of V_{int} that contains explicit dimension dependence, which is not expressed in the equation above. However, the general discussion to follow in Secs. 4.2 - 4.3 holds for the hard-sphere with only slight modification to the first-order energy approximation. This is discussed further in Ch. 5. We will also assume identical particles in each system so that all the particle masses m_i are equal.

4.2 Infinite-D analysis: Leading order energy

To begin the perturbation analysis we regularize the large-dimension limit of the Schrödinger equation by defining dimensionally scaled variables:

$$\bar{r}_i = r_i/\kappa(D), \quad \bar{E} = \kappa(D)E, \quad \text{and} \quad \bar{H} = \kappa(D)H \tag{4.16}$$

with dimension-dependent scale factor $\kappa(D)$. From Eq. (4.14) one can see that the kinetic energy T scales in the same way as $1/r^2$, so the scaled version of Eq. (4.13) becomes

$$\bar{H}\Phi = \left(\frac{1}{\kappa(D)}\bar{T} + \bar{V}\right)\Phi = \bar{E}\Phi, \tag{4.17}$$

where barred quantities simply indicate that the variables are now in scaled units. Because of the quadratic D dependence in the centrifugal-like term in T of Eq. (4.14), we conclude that the scale factor $\kappa(D)$ must also be quadratic in D, otherwise the $D \rightarrow \infty$ limit of the Hamiltonian would not be finite. The factor of $\kappa(D)$ in the denominator of the scaled kinetic energy acts as an effective mass that increases with D, causing the derivative terms to become suppressed while leaving behind a centrifugal-like term in an effective potential,

$$V_{\mathit{eff}} = \sum_{i=1}^{N} \left(\frac{\hbar^2}{8 m_i \bar{r}_i^2} \frac{\Gamma^{(i)}}{\Gamma} + \bar{V}_{\mathrm{conf}}(\bar{r}_i) \right) + \sum_{i=1}^{N-1} \sum_{j=i+1}^{N} \bar{V}_{\mathrm{int}}(\bar{r}_{ij}), \tag{4.18}$$

in which the particles become frozen at large D. In the $D \rightarrow \infty$ limit, the excited states have collapsed onto the ground state, which is found at the minimum of V_{eff}.

We assume a totally symmetric minimum characterized by the equality of all particle radii and angle cosines when $D \rightarrow \infty$, i.e.,

$$\bar{r}_i = \bar{r}_\infty \ \ (1 \leq i \leq N), \quad \gamma_{ij} = \gamma_\infty \ \ (1 \leq i < j \leq N). \tag{4.19}$$

Since each particle radius and angle cosine is equivalent, we can take derivatives with respect to an arbitrary $\bar{r}_i$ and γ_{ij} in the minimization procedure. Then evaluating all $\bar{r}_i$ and γ_{ij} at the infinite-D radius and angle cosine, $\bar{r}_\infty$ and γ_∞, respectively, we find that $\bar{r}_\infty$ and γ_∞ satisfy

$$\left. \frac{\partial V_{\mathit{eff}}}{\partial \bar{r}_i} \right|_\infty = 0 \tag{4.20}$$

$$\left. \frac{\partial V_{\mathit{eff}}}{\partial \gamma_{ij}} \right|_\infty = 0, \tag{4.21}$$

where the ∞ subscript means to evaluate all $\bar{r}_i$ at $\bar{r}_\infty$ and all γ_{ij} at γ_∞. In scaled units the zeroth-order ($D \rightarrow \infty$) approximation for the energy becomes

$$\bar{E}_\infty = V_{\mathit{eff}}\big|_\infty = V_{\mathit{eff}}(\bar{r}_\infty, \gamma_\infty). \tag{4.22}$$

In this leading order approximation, the centrifugal-like term that appears in V_{eff}, even for the ground state, is a zero-point energy contribution required by the minimum uncertainty principle[45].

4.3 Normal-mode analysis: $1/D$ first-order quantum energy correction

At zeroth-order, the particles can be viewed as frozen in a completely symmetric high-D configuration or simplex. It is somewhat analogous to the Lewis structure in atomic physics terminology. Likewise, the first-order $1/D$ correction can be viewed as small oscillations of this structure, analogous to Langmuir oscillations. Solving Eqs. (4.20) and (4.21) for $\bar{r}_\infty$ and γ_∞ gives the infinite-D structure and zeroth-order energy and provides the starting point for the $1/D$ expansion. To obtain the $1/D$ quantum correction to the energy for large but finite values of D, we expand about the minimum of the $D \to \infty$ effective potential. We first define a position vector consisting of all $P \equiv N(N+1)/2$ internal coordinates whose transpose is

$$\bar{y}^T = (\bar{r}_1, \bar{r}_2, \ldots, \bar{r}_N, \gamma_{12}, \gamma_{13}, \ldots, \gamma_{N-1,N}). \tag{4.23}$$

We then make the following substitutions for all radii and angle cosines:

$$\bar{r}_i = \bar{r}_\infty + \delta^{1/2}\bar{r}'_i \tag{4.24}$$

$$\gamma_{ij} = \gamma_\infty + \delta^{1/2}\gamma'_{ij}, \tag{4.25}$$

where $\delta = 1/D$ is the expansion parameter, and we define a displacement vector consisting of the internal displacement coordinates (primed in Eqs. (4.24) and (4.25)):

$$\bar{y}'^T = (\bar{r}'_1, \bar{r}'_2, \ldots, \bar{r}'_N, \gamma'_{12}, \gamma'_{13}, \ldots, \gamma'_{N-1,N}). \tag{4.26}$$

We may then obtain a power series in $\delta^{1/2}$ of the effective potential about the $D \to \infty$ symmetric minimum:

$$\begin{aligned} V_{\mathit{eff}} = V_{\mathit{eff}}\big|_\infty \;&+\; \delta^{1/2}\sum_{\mu=1}^{P}\left[\frac{\partial V_{\mathit{eff}}}{\partial \bar{y}'_\mu}\right]_\infty \bar{y}'_\mu + \\ &+\; \frac{1}{2}\delta\sum_{\mu=1}^{P}\sum_{\nu=1}^{P}\bar{y}'_\mu\left[\frac{\partial^2 V_{\mathit{eff}}}{\partial \bar{y}'_\mu \partial \bar{y}'_\nu}\right]_\infty \bar{y}'_\nu + O\left(\delta^{3/2}\right), \end{aligned} \tag{4.27}$$

where

$$P \equiv \frac{N(N+1)}{2} \tag{4.28}$$

is the number of radial and angular coordinates. The first term in the power series (Eq. 4.27) is simply the zeroth-order energy (Eq. 4.22). The second term is zero since we are expanding about the minimum of the effective potential; the system is said to be in equilibrium since the forces acting on the system vanish [Eqs. (4.20) and (4.21)]. The third term defines the elements of the Hessian matrix[83] **F** of Eq. (4.30) below. The derivative terms in the kinetic energy are taken into account by a similar series expansion beginning with a first-order term that is bilinear in $\partial/\partial\bar{y}'$, i.e.,

$$\mathcal{T} = -\frac{1}{2}\delta \sum_{\mu=1}^{P}\sum_{\nu=1}^{P} G_{\mu\nu}\partial_{\bar{y}'_\mu}\partial_{\bar{y}'_\nu} + O\left(\delta^{3/2}\right), \tag{4.29}$$

where $\mathcal{T}$ is the derivative portion of the kinetic energy T (see Eq. (4.14)). Thus, obtaining the first-order energy correction is reduced to a harmonic problem, which is solved by obtaining the normal modes of the system.

We use the Wilson FG matrix method[78] to obtain the normal-mode vibrations and, thereby, the first-order energy correction. It follows from Eqs. (4.27) and (4.29) that **G** and **F**, both constant matrices, are defined in the first-order $\delta = 1/D$ Hamiltonian as follows:

$$\widehat{H}_1 = -\frac{1}{2}\partial_{\bar{y}'}{}^T\mathbf{G}\partial_{\bar{y}'} + \frac{1}{2}\bar{y}'^T\mathbf{F}\bar{y}', \tag{4.30}$$

where T here refers to the traspose operation. After the Schrödinger equation (4.13) has been dimensionally scaled, the second-order derivative terms are of order δ, and by comparing these terms with the first part of $\widehat{H}_1$, the elements of the kinetic-energy matrix **G** are easily determined. The elements of the Hessian matrix[83], $F_{\mu\nu} = [\partial^2 V_{\mathit{eff}}/\partial\bar{y}'_\mu\bar{y}'_\nu]_\infty$, on the other hand, require a bit more effort to obtain, as we will see in detail in later sections.

We include a derivation of the FG matrix method in Appendix B, but we state here the main result of the method, which consists of finding the roots of the following characteristic polynomial in λ:

$$\det(\lambda\mathbf{I} - \mathbf{GF}) = 0. \tag{4.31}$$

Depending on the number of particles, the number of roots λ, which number from 1 to $P \equiv N(N+1)/2$, is potentially quite large. However, as we will see shortly, there is a high degree of degeneracy in the roots λ due to the total symmetry of the infinite-D Lewis structure. In fact, there are only five distinct roots: λ_σ, $1 \le \sigma \le 5$.

And as we conclude in Eq. (4.60) the energy through first-order can be written in terms of the distinct normal-mode vibrational frequencies, which are related to the roots λ_σ of **GF** by the following (see Eq. B5):

$$\lambda_\sigma = \bar{\omega}_\sigma^2. \tag{4.32}$$

In the next subsections, we show explicitly how to find analytical expressions for the roots of **GF**.

4.3.1 Indical structure of F, G, and GF matrices

The **F**, **G**, and **GF** matrices, which we generically denote by **Q**, are $P \times P$ matrices with the same indical structure as $\bar{y}\bar{y}^T$:

$$\bar{y}\bar{y}^T = \left(\begin{array}{cccc|cccc} \bar{r}_1\bar{r}_1 & \bar{r}_1\bar{r}_2 & \cdots & \bar{r}_1\bar{r}_N & \bar{r}_1\gamma_{12} & \bar{r}_1\gamma_{13} & \cdots & \bar{r}_1\gamma_{N-1N} \\ \bar{r}_2\bar{r}_1 & \bar{r}_2\bar{r}_2 & \cdots & & \bar{r}_2\gamma_{12} & \bar{r}_2\gamma_{13} & \cdots & \bar{r}_2\gamma_{N-1N} \\ \vdots & \vdots & \ddots & \vdots & \vdots & \vdots & \ddots & \vdots \\ \bar{r}_N\bar{r}_1 & \cdots & & \bar{r}_N\bar{r}_N & \bar{r}_N\gamma_{12} & & \cdots & \bar{r}_N\gamma_{N-1N} \\ \hline \gamma_{12}\bar{r}_1 & \gamma_{12}\bar{r}_2 & \cdots & \gamma_{12}\bar{r}_N & \gamma_{12}\gamma_{12} & \gamma_{12}\gamma_{13} & \cdots & \gamma_{12}\gamma_{N-1N} \\ \gamma_{13}\bar{r}_1 & \gamma_{13}\bar{r}_2 & \cdots & \gamma_{12}\bar{r}_1 & \gamma_{13}\gamma_{12} & \gamma_{13}\gamma_{13} & \cdots & \gamma_{13}\gamma_{N-1N} \\ \vdots & \vdots & \ddots & \vdots & \vdots & \vdots & \ddots & \vdots \\ \gamma_{N-1N}\bar{r}_1 & & \cdots & \gamma_{N-1N}\bar{r}_N & \gamma_{N-1N}\gamma_{12} & \gamma_{N-1N}\gamma_{13} & \cdots & \gamma_{N-1N}\gamma_{N-1N} \end{array}\right). \tag{4.33}$$

The indical structure of this matrix suggests a convenient set of indices for describing the elements of the **Q** matrices. The upper left quadrant of Eq. (4.33) is an $(N \times N)$ matrix with elements associated with $(\bar{r}_i, \bar{r}_j)$; hence we use the subscript (i, j) to refer to these elements. The upper right quadrant is an $(N \times N(N-1)/2)$ matrix with elements associated with $(\bar{r}_i, \gamma_{jk})$; hence, we use the subscript (i, jk) to refer

to these elements. Finally, the lower left quadrant is an $(N(N-1)/2 \times N)$ matrix with elements associated with $(\gamma_{ij}, \bar{r}_k)$; hence, we use the subscript (ij,k) to refer to these elements. The lower right quadrant is an $(N(N-1)/2 \times N(N-1)/2)$ matrix with elements associated with $(\gamma_{ij}, \gamma_{kl})$; hence, we use the subscript (ij,kl) to refer to these elements.

4.3.2 Symmetry of the Q matrices

As the number of particles N increases, diagonalizing the $P \times P$ **GF** matrix becomes, prima facie, a daunting task ($P = N(N+1)/2$). However, one of the advantages of dimensional perturbation theory is the simplifications that occur in the large-dimension limit, a limit in which one is often able to find analytical expressions for the normal-mode frequencies of oscillation about the symmetric configuration. In particular, since we are dealing with identical particles in a totally symmetric configuration (the Lewis structure) in which all the particles are equivalent, the **Q** matrices display a high degree of symmetry with many identical elements. Specifically,

$$
\begin{aligned}
Q_{i,i} &= Q_{i',i'} \equiv Q_a \\
Q_{i,j} &= Q_{i',j'} \equiv Q_b \quad (i \neq j) \text{ and } (i' \neq j') \\
Q_{ij,i} &= Q_{i'j',i'} \equiv Q_c \quad (i \neq j) \text{ and } (i' \neq j') \\
Q_{jk,i} &= Q_{j'k',i'} \equiv Q_d \quad (i \neq j \neq k) \text{ and } (i' \neq j' \neq k') \\
Q_{i,ij} &= Q_{i',i'j'} \equiv Q_e \quad (i \neq j) \text{ and } (i' \neq j') \\
Q_{i,jk} &= Q_{i',j'k'} \equiv Q_f \quad (i \neq j \neq k) \text{ and } (i' \neq j' \neq k') \\
Q_{ij,ij} &= Q_{i'j',i'j'} \equiv Q_g \quad (i \neq j) \text{ and } (i' \neq j') \\
Q_{ij,jk} &= Q_{i'j',j'k'} \equiv Q_h \quad (i \neq j \neq k) \text{ and } (i' \neq j' \neq k') \\
Q_{ij,kl} &= Q_{i'j',k'l'} \equiv Q_\iota \quad (i \neq j \neq k \neq l) \text{ and } (i' \neq j' \neq k' \neq l').
\end{aligned}
\tag{4.34}
$$

Note the indices in the relationships above run over all particles $(1, 2, \ldots, N)$ with the exceptions noted in the far right column. For example, $Q_{i,j} = Q_{i',j'} \equiv Q_b$, where $(i \neq j)$ and $(i' \neq j')$, means that all off-diagonal elements of the upper left block (the pure radial block) of $\mathbf{Q}$ are equal to the same constant Q_b. Similarly, $Q_{ij,kl} = Q_{i'j',k'l'} \equiv Q_\iota$, where $(i \neq j \neq k \neq l)$ and $(i' \neq j' \neq k' \neq l')$, means that any elements of $\mathbf{Q}$ in the lower right block (the pure angular block) that do not have a repeated index are all equal to the same constant Q_ι. We should remark here that $\mathbf{G}$ and $\mathbf{F}$ are also symmetric matrices ($\mathbf{G}^T = \mathbf{G}$ and $\mathbf{F}^T = \mathbf{F}$); however, while $\mathbf{GF}$ does display the high degree of symmetry of Eq. (4.34), it is not a symmetric matrix.

4.3.3 Q matrices in terms of simple submatrices

The symmetry of the $\mathbf{Q}$ matrices ($\mathbf{F}$, $\mathbf{G}$, and $\mathbf{GF}$) described in Eq. (4.34) allows us to write these matrices in terms of six simple submatrices. We first define the number of γ_{ij} coordinates to be

$$M \equiv N(N-1)/2, \tag{4.35}$$

and let $\mathbf{I}_N$ be an $N \times N$ identity matrix, $\mathbf{I}_M$ an $M \times M$ identity matrix, $\mathbf{J}_N$ an $N \times N$ matrix of ones and $\mathbf{J}_M$ an $M \times M$ matrix of ones. Further, we let $\mathbf{R}$ be an $N \times M$ matrix[1] such that $R_{i,jk} = \delta_{ij} + \delta_{ik}$, $\mathbf{J}_{NM}$ be an $N \times M$ matrix of ones, and $\mathbf{J}_{NM}^T = \mathbf{J}_{MN}$.

We then write the $\mathbf{Q}$ matrices as

$$\mathbf{Q} = \begin{pmatrix} \mathbf{Q}_1 & \mathbf{Q}_2 \\ \mathbf{Q}_3 & \mathbf{Q}_4 \end{pmatrix}, \tag{4.36}$$

where the block $\mathbf{Q}_1$ has dimension $(N \times N)$, block $\mathbf{Q}_2$ has dimension $(N \times M)$, block $\mathbf{Q}_3$ has dimension $(M \times N)$, and quadrant $\mathbf{Q}_4$ has dimension $(M \times M)$. Now, as we show in Appendix C, Eq. (4.34) allows us to write the following:

$$\mathbf{Q}_1 = (Q_a - Q_b)\mathbf{I}_N + Q_b\mathbf{J}_N \tag{4.37}$$

$$\mathbf{Q}_2 = (Q_e - Q_f)\mathbf{R} + Q_f\mathbf{J}_{NM} \tag{4.38}$$

$$\mathbf{Q}_3 = (Q_c - Q_d)\mathbf{R}^T + Q_d\mathbf{J}_{NM}^T \tag{4.39}$$

[1] In graph theoretic terminology $\mathbf{R}$ is called a vertex-edge matrix (see Appendix C).

$$\mathbf{Q}_4 = (Q_g - 2Q_h + Q_\iota)\mathbf{I}_M + (Q_h - Q_\iota)\mathbf{R}^T\mathbf{R} + Q_\iota \mathbf{J}_M. \tag{4.40}$$

In particular, letting $\mathbf{Q} = \mathbf{GF}$, Eq. (4.36) becomes

$$\mathbf{GF} = \begin{pmatrix} (a-b)\mathbf{I}_N + b\mathbf{J}_N & (e-f)\mathbf{R} + f\mathbf{J}_{NM} \\ (c-d)\mathbf{R}^T + d\mathbf{J}_{MN} & (g-2h+\iota)\mathbf{I}_M + (h-\iota)\mathbf{R}^T\mathbf{R} + \iota\mathbf{J}_M \end{pmatrix}, \tag{4.41}$$

where we have used the following abbreviations:

$$\begin{aligned}
a &\equiv (GF)_a = G_a F_a \\
b &\equiv (GF)_b = G_a F_b \\
c &\equiv (GF)_c = G_g F_e + (N-2)G_h F_e + (N-2)G_g F_f \\
d &\equiv (GF)_d = G_g F_f + 2G_h F_e + 2(N-3)G_h F_f \\
e &\equiv (GF)_e = G_a F_e \\
f &\equiv (GF)_f = G_a F_f \\
g &\equiv (GF)_g = G_g F_g + 2(N-2)G_h F_f \\
h &\equiv (GF)_h = G_g F_h + G_h F_e + (N-2)G_h F_h + (N-3)G_h F_\iota \\
\iota &\equiv (GF)_\iota = G_g F_\iota + 4G_h F_h + 2(N-4)G_h F_\iota.
\end{aligned} \tag{4.42}$$

The righthand sides of Eq (4.42), the **GF** matrices expressed in terms of the **F** and G matrix elements, are derived in Appendix C.

4.3.4 Normal mode frequencies and first-order energy

Having obtained the **GF** matrix of Eqs. (4.41) and (4.42), we may then, according to Eq. (4.31), find the eigenvalues λ of **GF** by solving

$$\det(\mathbf{E}) = 0, \tag{4.43}$$

where we have defined $\mathbf{E}$ as

$$\mathbf{E} \equiv \begin{pmatrix} \lambda \mathbf{I}_N & \mathbf{0} \\ \mathbf{0} & \lambda \mathbf{I}_M \end{pmatrix} - \mathbf{GF}. \tag{4.44}$$

To find an analytical expression for det($\mathbf{E}$) we multiply $\mathbf{E}$ by three matrices: $\mathbf{X}$, $\mathbf{Y}$ and $\mathbf{Z}$, such that

$$\mathbf{XYEZ} = \begin{pmatrix} \frac{t}{v}\mathbf{I}_N + \frac{u}{v}\mathbf{J}_N & \mathbf{0} \\ \cdots & v\mathbf{I}_M \end{pmatrix}, \tag{4.45}$$

where $\det(\mathbf{X}) = \det(\mathbf{Y}) = \det(\mathbf{Z}) = 1$ so that $\det(\mathbf{E}) = \det(\mathbf{XYEZ})$. In Appendix D we construct the matrices $\mathbf{X}$, $\mathbf{Y}$ and $\mathbf{Z}$ needed to transform $\mathbf{E}$ of Eq. (4.44) to $\mathbf{XYEZ}$ of Eq. (4.45). We find

$$v \equiv \lambda - g + 2h - \iota \tag{4.46}$$

$$t \equiv (\lambda - a + b)v + (N-2)(\iota - h)(\lambda - a + b) + (N-2)(d-c)(e-f) \tag{4.47}$$

$$u \equiv -kv - (h-\iota)(\lambda - a + b) + (d-c)(e-f) + \frac{N-1}{2} \times [f(2(d-c) - Nd) - \iota(\lambda - a - (N-1)b) + 4b(h-\iota) - 2d(e-f)] \tag{4.48}$$

The determinant of $\mathbf{XYEZ}$, which does not depend on the submatrix in the lower left quadrant, is found from Appendix C (see Eq. (C30)) to be

$$\det(\mathbf{E}) = \det(\mathbf{XYEZ}) = t^{N-1}(t + Nu)v^{M-N}. \tag{4.49}$$

There are five distinct roots, which naturally arise from the terms in Eq. (4.49) with t, u, and v given by Eqs. (4.46), (4.47) and (4.48). From Eq. (4.49), $\det(\mathbf{E}) = 0$ factors into three terms, resulting in three equations for the five distinct roots:

$$t^{N-1} = 0 \tag{4.50}$$

$$(t + Nu) = 0 \tag{4.51}$$

$$v^{M-N} = v^{N(N-3)/2} = 0, \tag{4.52}$$

From Eqs. (4.46) and (4.47), one can see that t is quadratic in λ. Hence, from Eq. (4.50) there are two roots with multiplicity $N-1$ given by

$$t = 0. \tag{4.53}$$

Similarly, the $(t + Nu)$ term in Eq. (4.49) is quadratic in λ and, hence, there are two roots with multiplicity 1. Finally, v is linear in λ; hence, there is one root with multiplicity $N(N-3)/2$ from Eq. (4.52) given by

$$v = 0. \tag{4.54}$$

From Eqs. (4.54) and (4.46), the root of multiplicity $N(N-3)/2$ is

$$\lambda_2 = g - 2h + \iota. \tag{4.55}$$

From Eqs. (4.53) and (4.47), the two roots with multiplicity $(N-1)$ are

$$\lambda_{1\pm} = \eta_1 \pm \sqrt{\eta_1{}^2 - \Delta_1}, \tag{4.56}$$

where

$$\begin{aligned} \eta_1 &= \tfrac{1}{2}\left[a - b + g + (N-4)h - (N-3)\iota\right] \\ \Delta_1 &= (N-2)(c-d)(e-f) + (a-b)\left[g + (N-4)h - (N-3)\iota\right]. \end{aligned} \tag{4.57}$$

From the $t + Nu$ term in Eq. (4.49) along with Eqs. (4.47) and (4.48), the two roots with unit multiplicity are

$$\lambda_{0\pm} = \eta_0 \pm \sqrt{\eta_0{}^2 - \Delta_0}, \tag{4.58}$$

where

$$\begin{aligned} \eta_0 &= \frac{1}{2}\left[a - (N-1)b + g + 2(N-2)h + \frac{(N-2)(N-3)}{2}\iota\right] \\ \Delta_0 &= (a-(N-1)b)\left[g + 2(N-2)h - \frac{(N-2)(N-3)}{2}\iota\right] + \\ &\quad -\frac{N-2}{2}(2c + (N-2)d)(2e + (N-2)f). \end{aligned} \tag{4.59}$$

The five λ's or distinct roots belong to three different irreducible representations of the symmetric group S_N of order N[80, 84]. The multiplicity-$N(N-3)/2$ root is designated by **2**. The two multiplicity-$(N-1)$ roots, which are a mixture of asymmetric stretching and bending motions, are designated by $\mathbf{1}^-$ and $\mathbf{1}^+$, respectively. Finally, the two multiplicity-1 roots, which are a mixture of symmetric stretching and bending motions, are designated by $\mathbf{0}^-$ and $\mathbf{0}^+$, respectively.

The distinct roots λ_σ, where $1 \leq \sigma \leq 5$, are equal to the square of the normal-mode vibrational frequencies (i.e., Eq. (4.32)), and the energy through first-order in $\delta = 1/D$ is then

$$\begin{aligned} \bar{E} &= \bar{E}_\infty + \delta \bar{E}_o + O(\delta^2) \\ &= V_{\mathrm{eff}}(\bar{r}_\infty, \gamma_\infty) + \delta \left[\sum_\sigma \sum_{n_\sigma} (n_\sigma + \frac{1}{2}) d_{\sigma,n_\sigma} \bar{\omega}_\sigma + v_o \right] + O(\delta^2), \end{aligned} \tag{4.60}$$

where the n_σ are the vibrational quantum numbers of the normal modes of the same frequency $\bar{\omega}_\sigma$, and d_{σ,n_σ} is the occupancy of the manifold of normal modes with vibrational quantum number n_σ and normal mode frequency $\bar{\omega}_\sigma$. The total occupancy of the normal modes with frequency $\bar{\omega}_\sigma$ is equal to the multiplicity of the root λ_σ (see the discussion after Eq. (4.52)). This equation differs slightly from the version found in Ref. [80], where d_μ is the multiplicity of the μ^{th} root. In Eq. (4.60), d_{σ,n_σ} counts the number of particles with n_σ quanta in the normal mode of frequency ω_σ. One can also view d_{σ,n_σ} as the number of normal modes of the same frequency which have the same number of quanta n_σ, where n_σ is the number of nodes in the normal mode oscillator wavefunction.

4.4 N-electron atom

The N-electron atom was previously discussed using low-order many-body dimensional perturbation theory by Loeser[80]. In this section, we give details necessary to derive the results in Ref.[80], to which we direct the interested reader for specific numerical results. The confining potential is provided by the Coulomb attraction of the electrons to the nucleus:

$$V_{\mathrm{conf}}(r_i) = -\frac{Z}{r_i}, \tag{4.61}$$

and the interaction potential is the Coulomb repulsion of the electrons:

$$V_{\text{int}}(r_{ij}) = \frac{1}{\sqrt{r_i^2 + r_j^2 - 2r_i r_j \gamma_{ij}}}. \tag{4.62}$$

Substitution of the following charge/dimensionally scaled variables into the similarity transformed Schrödinger equation (4.13) in atomic units ($\hbar = m = 1$):

$$\bar{r}_i = \frac{Z}{\Omega} r_i, \quad \bar{E} = \frac{\Omega}{Z^2} E, \quad \Omega = (D-1)(D-2N-1)/4, \tag{4.63}$$

places all of the dimension-dependence in the second-derivative parts of the kinetic energy and gives the following scaled equation:

$$\left(\mathcal{T}^{(A)} + U^{(A)} + V^{(A)}\right)\Phi = \bar{E}\Phi, \tag{4.64}$$

where

$$\begin{aligned}
\mathcal{T}^{(A)} &= -\frac{1}{2\Omega}\sum_{i=1}^{N}\left[\frac{\partial^2}{\partial \bar{r}_i{}^2} + \sum_{j\neq i}\sum_{k\neq i}\frac{\gamma_{jk} - \gamma_{ij}\gamma_{ik}}{\bar{r}_i^2}\frac{\partial^2}{\partial\gamma_{ij}\partial\gamma_{ik}}\right] \\
U^{(A)} &= \frac{1}{2}\sum_{i=1}^{N}\frac{1}{\bar{r}_i^2}\frac{\Gamma^{(i)}}{\Gamma} \\
V^{(A)} &= -\sum_{i=1}^{N}\frac{1}{\bar{r}_i} + \frac{1}{Z}\sum_{i=1}^{N-1}\sum_{j=i+1}^{N}\frac{1}{\sqrt{\bar{r}_i^2 + \bar{r}_j^2 - 2\bar{r}_i\bar{r}_j\gamma_{ij}}}.
\end{aligned} \tag{4.65}$$

The superscript A refers to the N-electron atom system (to distinguish these quantities from those in the systems to follow). From this equation, it can be seen that if D, and hence Ω, become infinitely large, the differential part $\mathcal{T}^{(A)}$ of the kinetic energy ($U^{(A)}$ being the centrifugal-like part of the kinetic energy) will drop out of the similarity transformed Hamiltonian. In effect it is as though the particles become infinitely heavy, and, because of this, any function from the basis set of all delta functions in configuration space is an eigenfunction of the Hamiltonian. The energy of such an eigenfunction is just the value of the effective potential at that specific point in configuration space which that delta function selects, and, as mentioned in Section 4.2, this point is the minimum of the infinite-D effective potential:

$$\bar{E}_{\infty}^{(A)} = V_{\text{eff}}^{(A)}\Big|_{\infty} = \left[U^{(A)} + V^{(A)}\right]_{\infty}, \tag{4.66}$$

where the effective potential $V_{\text{eff}}^{(A)}$ corresponds to Eq. (4.18) in scaled units.

4.4.1 Atomic infinite-D analysis

We have chosen a particularly simple infinite-D configuration: the totally symmetric configuration characterized by the equality of all $\bar{r}_i$ and γ_{ij}. The effective potential is an extremum when its derivatives with respect to all $\bar{r}_i$ and γ_{ij} are zero at $\bar{r}_\infty$ and γ_∞. Using the conditions imposed in Eqs. (4.20) and (4.21), we find:

$$\begin{aligned} -\frac{1}{\bar{r}_\infty^3}\frac{1+(N-2)\gamma_\infty}{(1+(N-1)\gamma_\infty)(1-\gamma_\infty)} + \frac{1}{\bar{r}_\infty^2}\left[1-\frac{N-1}{2^{3/2}Z\sqrt{1-\gamma_\infty}}\right] = 0, \\ \frac{1}{\bar{r}_\infty^2}\frac{(2+(N-2)\gamma_\infty)\gamma_\infty}{(1+(N-1)\gamma_\infty)^2(1-\gamma_\infty)^2} + \frac{1}{\bar{r}_\infty}\frac{1}{2^{3/2}Z(1-\gamma_\infty)^{3/2}} = 0, \end{aligned} \tag{4.67}$$

where we have used the infinite-D symmetric-minimum Gramian results given in Eqs. (E12) of Appendix E.

One can eliminate $\bar{r}_\infty$ from the above equations and then γ_∞ is the negative solution of smallest magnitude of the following equation:

$$8Z^2\gamma_\infty^2[2+(N-2)\gamma_\infty]^2 + \gamma_\infty - 1 = 0. \tag{4.68}$$

For $Z = N$ it has been verified that this extremum is a minimum. If we consider Z to be a parameter and we decrease this parameter, the system becomes more and more unstable and at some point the above extremum is no longer a minimum. This critical value $Z_{\mathbf{local}}$ can be obtained via Eq. (4.68) from the negative real solution of the following equation:

$$(4-6\gamma_\infty)(1-\gamma_\infty)^3+N\gamma_\infty(22-9\gamma_\infty)(1-\gamma_\infty)^2+20N^2\gamma_\infty^2(1-\gamma_\infty)+5N^3\gamma_\infty^3 = 0, \tag{4.69}$$

which is simply the condition under which the smallest eigenvalue of the Hessian[83] changes sign. $Z_{\mathbf{local}}$ is always less than N for neutral atoms, and hence the totally symmetric state is indeed in an energetic (local) minimum for neutral atoms.

The infinite-D radius and energy can be written in terms of the solution γ_∞ of the quartic equation (4.68) as follows:

$$\bar{r}_\infty^{(A)} = [1+(N-1)\gamma_\infty]^{-2} \tag{4.70}$$

$$\frac{\bar{E}_\infty^{(A)}}{N} = -\frac{1}{2}[1+(N-1)\gamma_\infty]^3[1+(N-2)\gamma_\infty]/(1-\gamma_\infty). \tag{4.71}$$

We should remark here on the fact that we are considering a minimum in the effective potential, which allows us to eliminate Z from the above expressions. Specifically, we have employed the conditions (4.20) and (4.21) at the minimum that

$$\frac{\partial V^{(A)}}{\partial \gamma_{ij}}\Big|_{\infty} = -\frac{\partial U^{(A)}}{\partial \gamma_{ij}}\Big|_{\infty}, \tag{4.72}$$

which leads to

$$\frac{1}{Z} = -\frac{2^{3/2}\gamma_{\infty}[2+(N-2)\gamma_{\infty}]}{\sqrt{1-\gamma_{\infty}}}. \tag{4.73}$$

4.4.2 Atomic normal modes

We can determine the elements of **G** by comparing the differential terms in Eq. (4.30) with $\mathcal{T}^{(A)}$ in Eq. (4.65) expanded to first order in $1/D$ as in Eq. (4.29). The non-zero elements of the **G** matrix are:

$$\begin{aligned} G_a &= 1 \\ G_g = 2\frac{1-\gamma_{\infty}^2}{\left(\bar{r}_{\infty}^{(A)}\right)^2} &= 2[1+(N-1)\gamma_{\infty}]^4(1+\gamma_{\infty})(1-\gamma_{\infty}) \\ G_h = \frac{\gamma_{\infty}(1-\gamma_{\infty})}{\left(\bar{r}_{\infty}^{(A)}\right)^2} &= [1+(N-1)\gamma_{\infty}]^4\gamma_{\infty}(1-\gamma_{\infty}), \end{aligned} \tag{4.74}$$

where the matrix elements have been evaluated at the infinite-D symmetric minimum and we have used the notation in Eq. (4.34). The factor of 2 in G_g comes from the fact that each (ij,ij) term appears twice in $\mathcal{T}^{(A)}$ of Eq. (4.65) (e.g., (21, 21) as well as (12, 12)), but it is only counted once in the **G** matrix (e.g., only (12, 12) is counted). In a similar manner to the **G**-matrix elements, the non-zero **F**-matrix elements are:

$$\begin{aligned} F_a &= \frac{[1+(N-1)\gamma_{\infty}]^6}{(1-\gamma_{\infty})^2} \times \\ &\quad \left(\frac{2+2(5N-7)\gamma_{\infty}+(5N-6)(N-3)\gamma_{\infty}^2-3(N-1)(N-2)\gamma_{\infty}^3}{2}\right) \\ F_b &= \frac{[1+(N-1)\gamma_{\infty}]^6}{(1-\gamma_{\infty})^2}\left(\frac{-\gamma_{\infty}(3-\gamma_{\infty})[2+(N-2)\gamma_{\infty}]}{2}\right) \\ F_e &= \frac{[1+(N-1)\gamma_{\infty}]^4}{(1-\gamma_{\infty})^2}\left(\frac{-\gamma_{\infty}[2+3(N-2)\gamma_{\infty}]}{2}\right) \end{aligned}$$

$$
\begin{aligned}
F_f &= \frac{[1+(N-1)\gamma_\infty]^4}{(1-\gamma_\infty)^2}\left(2\gamma_\infty^2\right) \qquad (4.75)\\
F_g &= \frac{[1+(N-1)\gamma_\infty]}{(1-\gamma_\infty)^3}\times \\
&\quad \left(\frac{4+6(2N-5)\gamma_\infty+(12N^2-53N+64)\gamma_\infty^2+(4N^3-23N^2+49N-38)\gamma_\infty^3}{2}\right)\\
F_h &= -\frac{[1+(N-1)\gamma_\infty]}{(1-\gamma_\infty)^3}\gamma_\infty\left(3+(5N-14)\gamma_\infty+(2N^2-9N+11)\gamma_\infty^2\right)\\
F_\iota &= \frac{[1+(N-1)\gamma_\infty]}{(1-\gamma_\infty)^3}4\gamma_\infty^2\left(2+(N-2)\gamma_\infty\right),
\end{aligned}
$$

where we have used Eqs. (E13) from Appendix E to evaluate the Gramian second-order derivatives. Again we have used the fact that we are considering a minimum in the effective potential, which allows us to use Eq. (4.73) to eliminate Z from the above expressions. Pulling out the common term among the **GF** matrix elements, we define the matrix $(\mathbf{GF})'$ as:

$$
(\mathbf{GF})' \equiv \tau \mathbf{GF}, \qquad (4.76)
$$

where

$$
\tau \equiv \frac{2(1-\gamma_\infty)^2}{[1+(N-1)\gamma_\infty]^6}\Omega. \qquad (4.77)
$$

Using the above equations along with Eqs. (4.42) we find the following for the elements of $(\mathbf{GF})'$:

$$
\begin{aligned}
a &= 2+2(5N-7)\gamma_\infty+(5N-6)(N-3)\gamma_\infty^2-3(N-1)(N-2)\gamma_\infty^3\\
b &= -\gamma_\infty(3-\gamma_\infty)[2+(N-2)\gamma_\infty]\\
c &= -\gamma_\infty(1-\gamma_\infty)[2+(3N-4)\gamma_\infty][2+(N-2)\gamma_\infty][1+(N-1)\gamma_\infty]^2\\
d &= 2\gamma_\infty^2(1-\gamma_\infty)[2+(N-2)\gamma_\infty][1+(N-1)\gamma_\infty]^2\\
e &= -\gamma_\infty[2+3(N-2)\gamma_\infty][1+(N-1)\gamma_\infty]^{-2} \qquad (4.78)\\
f &= 4\gamma_\infty^2[1+(N-1)\gamma_\infty]^{-2}\\
g &= 2[4+2(4N-11)\gamma_\infty+(4N^2-17N+24)\gamma_\infty^2+3(N-2)\gamma_\infty^3]\\
h &= -\gamma_\infty[8+6(N-3)\gamma_\infty-(3N-10)\gamma_\infty^2]\\
\iota &= 8\gamma_\infty^2(1-\gamma_\infty).
\end{aligned}
$$

The eigenvalues of $(\mathbf{GF})'$ will be equal to the eigenvalues of $\mathbf{GF}$ multiplied by the common factor τ in Eq. (4.77).

Using the matrix elements of Eq. (4.78), we obtain the two multiplicity-1 modes from Eqs. (4.58) and (4.59):

$$\lambda_{0\pm}^{(A)} = 5(1-\gamma_\infty)^2 + 2N\gamma_\infty(1-\gamma_\infty) + N^2\gamma_\infty^2 + \pm\sqrt{\begin{array}{c} 3(1-\gamma_\infty)^4(3+8\gamma_\infty) - 12N\gamma_\infty(1-\gamma_\infty)^3(1-3\gamma_\infty) \\ -2N^2\gamma_\infty^2(1-\gamma_\infty)^2(1-6\gamma_\infty) + 4N^3\gamma_\infty^3(1-\gamma_\infty) + N^4\gamma_\infty^4 \end{array}}. \quad (4.79)$$

For the modes with multiplicity $N-1$ ($\lambda_{1\pm}^{(A)}$) and multiplicity $N(N-3)/2$ ($\lambda_2^{(A)}$) we find from Eqs. (4.55, 4.56, and 4.57):

$$\lambda_{1\pm}^{(A)} = 5(1-\gamma_\infty)^2 + 9N\gamma_\infty(1-\gamma_\infty) + \frac{7}{2}N^2\gamma_\infty^2 + \pm\sqrt{\begin{array}{c} 3(1-\gamma_\infty)^4(3+8\gamma_\infty) - 6N\gamma_\infty(1-\gamma_\infty)^3(1-8\gamma_\infty) \\ -2N^2\gamma_\infty^2(1-\gamma_\infty)^2(4-9\gamma_\infty) + 3N^3\gamma_\infty^3(1-\gamma_\infty) + \frac{9}{4}N^4\gamma_\infty^4 \end{array}} \quad (4.80)$$

$$\lambda_2^{(A)} = 4(1-\gamma_\infty)(2-5\gamma_\infty) + 2N\gamma_\infty(8-11\gamma_\infty) + 8N^2\gamma_\infty^2. \quad (4.81)$$

With τ given in Eq. (4.77), from Eq. (4.32) the normal-mode frequencies ω are related to these λ's by

$$\bar{\omega}^{(A)} = \sqrt{\frac{\lambda^{(A)}}{\tau}}. \quad (4.82)$$

Having obtained the normal-mode frequencies from Eqs. (4.79), (4.80), (4.81), and (4.82), the energy through first order is given by Eqs. (4.60) and (4.71).

4.5 N-electron Quantum Dot

We follow the N-electron atom with an analogous many-electron system, the quantum dot, or, as it is sometimes called, the artificial atom[85]. Quantum dots are nanostructures in which a controllable number of electrons are attracted to a central location. But instead of the Coulomb attraction of a nucleus, the quantum dot

electrons are attracted to the center of an external trapping potential. Another difference between quantum dots and atoms is their size: quantum dots are typically much larger than atoms. Furthermore, the quantum dot electrons typically interact in some medium such as a semiconductor; thus, we use the effective-mass approximation where the electrons, each with mass m^*, move in a medium with dielectric constant ϵ. McKinney and Watson have used dimensional perturbation theory to solve for the two-electron quantum dot spectrum[86]. In their paper, they outline how one could use the many-body techniques previously introduced by Loeser[80] and detailed in this chapter, to apply dimensional perturbation theory to a quantum dot with an arbitrary number of electrons. We now provide the details sketched in Ref. [86] .

The electrons, each of effective mass m^*, are confined by a spherical harmonic trap with trapping frequency $\omega_{\rm ho}$:

$$V_{\rm conf}(r_i) = \frac{1}{2} m^* \omega_{\rm ho}^2 {r_i}^2, \tag{4.83}$$

and we take the interelectron potential to be

$$V_{\rm int}(r_{ij}) = \frac{e^2}{\epsilon \sqrt{r_i^2 + r_j^2 - 2 r_i r_j \gamma_{ij}}}, \tag{4.84}$$

where e is the electric charge and ϵ is the dielectric constant. Unlike the N-electron atom problem, where we used dimensionally scaled atomic units, for the quantum dot we use dimensionally scaled harmonic oscillator units. We can transfer all of the explicit dimension dependence to the differential part of the kinetic energy and regularize the large-dimension limit by substituting the following dimensionally-scaled variables into the similarity transformed Schrödinger equation (4.13):

$$\bar{r}_i = \frac{r_i}{\Omega l_{\rm ho}} \qquad \bar{E} = \frac{\Omega}{\hbar \bar{\omega}_{\rm ho}} E \qquad \Omega = (D-1)(D-2N-1)/4, \tag{4.85}$$

where the dimensionally scaled harmonic oscillator length and trap frequency are, respectively,

$$l_{\rm ho} = \sqrt{\frac{\hbar}{m^* \bar{\omega}_{\rm ho}}} \qquad \bar{\omega}_{\rm ho}^2 = \Omega^3 \omega_{\rm ho}^2. \tag{4.86}$$

That is, we obtain

$$(T^{(\rm QD)} + U^{(\rm QD)} + V^{(\rm QD)})\Phi = \bar{E}\Phi, \tag{4.87}$$

where

$$
\begin{aligned}
T^{(\mathrm{QD})} &= -\frac{1}{2\Omega}\sum_{i=1}^{N}\left[\frac{\partial^2}{\partial \bar{r}_i{}^2}+\sum_{j\neq i}\sum_{k\neq i}\frac{\gamma_{jk}-\gamma_{ij}\gamma_{ik}}{\bar{r}_i^2}\frac{\partial^2}{\partial\gamma_{ij}\partial\gamma_{ik}}\right] \\
U^{(\mathrm{QD})} &= \frac{1}{2}\sum_{i=1}^{N}\frac{1}{\bar{r}_i^2}\frac{\Gamma^{(i)}}{\Gamma} \\
V^{(\mathrm{QD})} &= \sum_{i=1}^{N}\frac{1}{2}\bar{r}_i^2+\frac{1}{\xi}\sum_{i=1}^{N-1}\sum_{j=i+1}^{N}\frac{1}{\sqrt{\bar{r}_i^2+\bar{r}_j^2-2\bar{r}_i\bar{r}_j\gamma_{ij}}},
\end{aligned}
\tag{4.88}
$$

and where

$$
\xi=\frac{a^*}{l_{\mathrm{ho}}} \qquad a^*=\frac{\epsilon\hbar^2}{m^*e^2} \tag{4.89}
$$

are the coupling constant and the effective bohr radius, respectively. From Eq. (4.88), it can be seen that if D and, hence, Ω becomes infinitely large, the differential part $T^{(\mathrm{QD})}$ of the kinetic energy will drop out of the Hamiltonian, just as for the N-electron atom. The particles behave as though they become infinitely heavy and the infinite-D energy becomes the value of the effective potential,

$$
V_{\mathrm{eff}}^{(\mathrm{QD})}=U^{(\mathrm{QD})}+V^{(\mathrm{QD})}, \tag{4.90}
$$

at its minimum:

$$
\bar{E}_{\infty}^{(\mathrm{QD})}=V_{\mathrm{eff}}^{(\mathrm{QD})}\Big|_{\infty}=\left[U^{(\mathrm{QD})}+V^{(\mathrm{QD})}\right]_{\infty}. \tag{4.91}
$$

4.5.1 Quantum Dot infinite-D analysis

As before, we choose the totally symmetric configuration for which all $\bar{r}_i$ and γ_{ij} are equal to some $\bar{r}_\infty$ and γ_∞. The effective potential is an extremum when its derivatives with respect to all $\bar{r}_i$ and γ_{ij} are zero at this $\bar{r}_\infty$ and γ_∞. Using Eq. (4.90) in Eqs. (4.20) and (4.21), we find:

$$
-\frac{1}{\bar{r}_\infty^3}\frac{1+(N-2)\gamma_\infty}{(1+(N-1)\gamma_\infty)(1-\gamma_\infty)}+\left[\bar{r}_\infty-\frac{N-1}{2^{3/2}\xi\bar{r}_\infty^2\sqrt{1-\gamma_\infty}}\right]=0, \tag{4.92}
$$

$$
\frac{1}{\bar{r}_\infty^2}\frac{(2+(N-2)\gamma_\infty)\gamma_\infty}{(1+(N-1)\gamma_\infty)^2(1-\gamma_\infty)^2}+\frac{1}{\bar{r}_\infty}\frac{1}{2^{3/2}\xi(1-\gamma_\infty)^{3/2}}=0, \tag{4.93}
$$

where we have used the infinite-D symmetric minimum Gramian results given in Eqs. (E12) of Appendix E.

One can eliminate $\bar{r}_\infty$ from the above equations and then, just as for the N-electron atom, γ_∞ is the negative solution of smallest magnitude of a quartic equation:

$$8\xi^2\gamma_\infty^2[2+(N-2)\gamma_\infty]^2-(1-\gamma_\infty)(1+(N-1)\gamma_\infty)^3=0. \tag{4.94}$$

The infinite-D radius and energy per atom are then given by

$$\bar{r}_\infty^{(\mathrm{QD})}=[1+(N-1)\gamma_\infty]^{-1/2} \tag{4.95}$$

$$\frac{\bar{E}_\infty^{(\mathrm{QD})}}{N}=-\frac{1}{2}\frac{(N-1)(N-2)\gamma_\infty^2+2N\gamma_\infty-2}{(1-\gamma_\infty)[1+(N-1)\gamma_\infty]}, \tag{4.96}$$

where we use the superscript (QD) to distinguish similar quantities in the atomic and hard-sphere systems. Just as in the N-electron atom analysis, we have used the fact that we are considering a minimum in the effective potential, which allows us to eliminate the coupling constant ξ from the above expressions. Specifically, we have employed the conditions (4.20) and (4.21) at the minimum that

$$\frac{\partial V^{(\mathrm{QD})}}{\partial\gamma_{ij}}\Big|_\infty=-\frac{\partial U^{(\mathrm{QD})}}{\partial\gamma_{ij}}\Big|_\infty, \tag{4.97}$$

which leads to

$$\xi=-\frac{2^{3/2}\gamma_\infty[2+(N-2)\gamma_\infty]}{\sqrt{1-\gamma_\infty}[1+(N-1)\gamma_\infty]^{3/2}}. \tag{4.98}$$

4.5.2 Quantum Dot Normal Modes

We can determine the elements of $\mathbf{G}$ by comparing the differential term in Eq. (4.30) with $T^{(\mathrm{QD})}$ in Eq. (4.88) expanded to first order in $1/D$ as in Eq. (4.29). The non-zero elements of the $\mathbf{G}$ matrix are:

$$\begin{aligned}
G_a &= 1 \\
G_g=2\frac{1-\gamma_\infty^2}{\left(\bar{r}_\infty^{(\mathrm{QD})}\right)^2} &= 2(1-\gamma_\infty)(1+\gamma_\infty)[1+(N-1)\gamma_\infty] \\
G_h=\frac{\gamma_\infty(1-\gamma_\infty)}{\left(\bar{r}_\infty^{(\mathrm{QD})}\right)^2} &= \gamma_\infty(1-\gamma_\infty)[1+(N-1)\gamma_\infty],
\end{aligned} \tag{4.99}$$

where the matrix elements have been evaluated at the infinite-D symmetric minimum and we have used the notation in Eq. (4.34). (See the discussion after Eq. (4.74) for

an explanation of the factor of 2 in G_g.) Likewise, the non-zero **F** matrix elements are:

$$\begin{aligned}
F_a &= \frac{1}{2(1-\gamma_\infty)^2}\left(8+2(5N-13)\gamma_\infty+(5N^2-21N+24)\gamma_\infty^2-3(N-1)(N-2)\gamma_\infty^3\right)\\
F_b &= \frac{\gamma_\infty(\gamma_\infty-3)(2+(N-2)\gamma_\infty)}{2(1-\gamma_\infty)^2}\\
F_e &= \frac{-\gamma_\infty}{2(1-\gamma_\infty)^2(1+(N-1)\gamma_\infty)^{1/2}}\left(2+3(N-2)\gamma_\infty\right)\\
F_f &= \frac{2{\gamma_\infty}^2}{(1-\gamma_\infty)^2(1+(N-1)\gamma_\infty)^{1/2}} \qquad (4.100)\\
F_g &= \frac{1}{2(1-\gamma_\infty)^3(1+(N-1)\gamma_\infty)^2}\Big(4+6(2N-5)\gamma_\infty+(64-53N+12N^2){\gamma_\infty}^2+\\
&\quad (-38+49N-23N^2+4N^3){\gamma_\infty}^3\Big)\\
F_h &= \frac{-2\gamma_\infty}{(1-\gamma_\infty)^3(1+(N-1)\gamma_\infty)^2}\left(3+(5N-14)\gamma_\infty+(11-9N+2N^2){\gamma_\infty}^2\right)\\
F_i &= \frac{[1+(N-1)\gamma_\infty]}{(1-\gamma_\infty)^3}4\gamma_\infty^2\left(2+(N-2)\gamma_\infty\right),
\end{aligned}$$

where we have used Eqs. (E13) from Appendix E to evaluate the Gramian second-order derivatives. Again, since we are considering a minimum in the effective potential, we employed Eq. (4.98) to replace the coupling constant ξ of Eq. (4.89) in favor of γ_∞. Using the above equations for **F** and **G** along with Eqs. (4.42) we find:

$$\begin{aligned}
a &= \frac{1}{2(1-\gamma_\infty)^2}\left(8+2(5N-13)\gamma_\infty+(5N^2-21N+24)\gamma_\infty^2-3(N-1)(N-2)\gamma_\infty^3\right)\\
b &= \frac{\gamma_\infty(\gamma_\infty-3)(2+(N-2)\gamma_\infty)}{2(1-\gamma_\infty)^2}\\
c &= \frac{-\gamma_\infty(1+\gamma_\infty)(1+(N-1)\gamma_\infty)^{1/2}}{2(1-\gamma_\infty)}\left(4+3(N-2)^2{\gamma_\infty}^2\right)\\
d &= \frac{{\gamma_\infty}^2(1+\gamma_\infty)(1+(N-1)\gamma_\infty)^{1/2}}{(1-\gamma_\infty)}\left(2+(N-6)\gamma_\infty\right)\\
e &= \frac{-\gamma_\infty}{2(1-\gamma_\infty)^2(1+(N-1)\gamma_\infty)^{1/2}}\left(2+3(N-2)\gamma_\infty\right) \qquad (4.101)\\
f &= \frac{2{\gamma_\infty}^2}{(1-\gamma_\infty)^2(1+(N-1)\gamma_\infty)^{1/2}}\\
g &= \frac{1}{(1-\gamma_\infty)^2(1+(N-1)\gamma_\infty)}\Big(4+2(6N-13)\gamma_\infty+(50-37N+2N^2+2N^3){\gamma_\infty}^2+\\
&\quad (-30+20N+27N^2-12N^3+2N^4){\gamma_\infty}^3+(50-107N+89N^2-22N^3+2N^4){\gamma_\infty}^4\Big)\\
h &= \frac{\gamma_\infty}{2(1-\gamma_\infty)^2(1+(N-1)\gamma_\infty)}\Big(4+6(2N-7)\gamma_\infty+(16-17N+2N^2+2N^3){\gamma_\infty}^2+
\end{aligned}$$

$$\iota = \frac{(-14-35N+45N^2-14N^3+2N^4){\gamma_\infty}^3)}{-4{\gamma_\infty}^2(1+\gamma_\infty)} \left(-1-(N-6)\gamma_\infty+(3N-5){\gamma_\infty}^2\right).$$
$$(1-\gamma_\infty)^2(1+(N-1)\gamma_\infty)$$

Substituting these **GF** matrix elements in Eqs. (4.32), (4.55), (4.56), and (4.58), we now write down the quantum dot normal-mode frequencies. The multiplicity-$N(N-3)/2$ mode is a vector mode with frequency

$$\bar{\omega}_2^{(QD)} = \sqrt{g-2h+i}. \tag{4.102}$$

The multiplicity-$(N-1)$ asymmetric stretch and bend frequencies take the form

$$\bar{\omega}_{1\pm}^{(QD)} = \sqrt{\eta_1 \pm \sqrt{{\eta_1}^2-\Delta_1}}, \tag{4.103}$$

and the two multiplicity-1 symmetric stretch and bend frequencies take the form

$$\bar{\omega}_{0\pm}^{(QD)} = \sqrt{\eta_0 \pm \sqrt{{\eta_0}^2-\Delta_0}}, \tag{4.104}$$

where η_1 and Δ_1 are given in Eq. (4.57), and η_0 and Δ_0 are given in Eq. (4.59).

Having obtained the frequencies from Eqs. (4.102), (4.103), and (4.104) and the Lewis structure energy in Eq. (4.96), the energy through first order is given by Eq. (4.60). Although this is only a low order approximation, two-body studies suggest that when the coupling constant $\xi << 1$ (i.e., the strongly interacting regime where the repulsive energy of the electrons dominates the confinement energy of the trap) low order dimensional perturbation may be very accurate[86]. Dimensional perturbation theory has a non-perturbative character in the sense that the leading-order term of DPT includes a contribution from the Coulomb potential.

Chapter 5

Many-body dimensional perturbation theory for Bose-Einstein condensates

The achievement of Bose-Einstein condensation (BEC) in magnetically trapped alkali-metal atoms has generated a considerable amount of experimental and theoretical activity in recent years. In typical BEC experiments, the average distance between the bose atoms is much larger than the range of the atomic interactions, which is characterized by the s-wave scattering length a. The mean-field Gross-Pitaevskii (GP) equation has been instrumental in describing the properties of these weakly interacting condensates (see Ref. [6] for an extended review). A fundamental assumption underlying the derivation of the GP equation is that the interatomic potential is well described by the shape-independent approximation, also called the pseudopotential approximation, which uses a zero-range potential, as opposed to an extended potential with a well-defined shape:

$$V_{\text{pseudo}}(\mathbf{r}) = \frac{4\pi\hbar^2 a}{m}\delta(\mathbf{r}), \tag{5.1}$$

where a is the s-wave scattering length and m is the mass of the identical bosons. Despite its success in the weakly interacting regime, the GP equation does not adequately treat correlation, and its assumed shape-independent approximation breaks down in the strongly interacting regime[87]. Moreover, recent experiments involving atoms with tunable interactions have obtained stable condensates in a regime in which the predictions of the mean-field theory are measurably lacking[4], allowing BEC to act as a test bed for fundamental many-body physics beyond the mean-field approach. Recent theoretical studies, performed to quantify the breakdown of the mean-field theory and the shape-independent approximation, have included analytical corrections to the GP equation due to quantum fluctuations about the mean-field[88, 89]

and a related approach from density functional theory[90], while others are based on numerical calculations such as the diffusion Monte Carlo method(DMC)[91, 92] or the correlated basis function approach[93, 94]. In this chapter, we further explore beyond-mean-field effects using many-body dimensional perturbation theory (DPT), a novel many-body approach that includes correlation beyond mean-field at low orders. We use a shape-dependent interatomic potential, and the number of condensate atoms N appears as a parameter in our results, which are analytical, thus making our many-body calculations for any N much less involved than even solving the mean-field GP equation. We also calculate excitation frequencies, which naturally arise out of our first-order, harmonic energy correction.

In our discussion of the inhomogeneous (trapped) atomic BEC, it proves useful to mention properties of the homogeneous (uniform) bose gas theory, since the two systems will share many features, at least qualitatively, when the density of the inhomogeneous gas is slowly varying. The low-density expansion of a homogeneous bose gas of hard spheres of mass m is well known[14, 95, 96]. The expansion relies on an improved, though still shape-independent, potential over the pseudopotential of Eq. (5.1), called the regularized Fermi pseudopotential (derived in Appendix F):

$$V_{\mathbf{reg-pseudo}}(\mathbf{r}) = \frac{4\pi\hbar^2 a}{m}\delta(\mathbf{r})\frac{\partial}{\partial r}r. \tag{5.2}$$

The ground-state energy per particle, expanded in terms of the gas parameter $\sqrt{na^3}$, is

$$\begin{aligned}\frac{E}{N} &= \frac{2\pi\hbar^2 na}{m}\times \\ &\left[1+\frac{128}{15\sqrt{\pi}}(na^3)^{1/2}+\frac{8(4\pi-3\sqrt{3})}{3}(na^3)\ln(na^3)+O(na^3)\right],\end{aligned} \tag{5.3}$$

where n is the uniform number density. In this approximation, it is assumed that the gas is dilute, that is, the average interatomic spacing is much larger than the s-wave scattering length, stated mathematically as $na^3 \ll 1$. For larger densities, higher-order terms in the expansion beyond those in Eq. (5.3) are needed, and these terms depend on the detailed shape of the potential[97]. The leading-order term of (5.3) was first derived by Bogoliubov[14] and is equivalent to the mean-field term in the Gross-Pitavskii equation(see below). The term in Eq. (5.3) of order $(na^3)^{3/2}$ was derived by Lee, Huang, and Yang[95], and the logarithmic term

was first obtained by Wu[96]. Lieb and Yngvason[98] showed that for a repulsive, non-negative, finite range, spherical, two-body potential, the Bogoliubov mean-field term, $E/N = 2\pi\hbar^2 na/m$, is the lower bound for the exact ground-state energy of a homogeneous bose gas. Giorgini *et al.*[91] found that Eq. (5.3) continues to be a good approximation for higher densities provided the logarithmic term is dropped. At intermediate densities ($na^3 > 1.385\times10^{-3}$) the logarithmic term causes the overall correction (second and third terms in brackets in Eq. (5.3)) to the Bogoliubov mean-field energy to become negative, thus, violating the lower bound. For a narrow range of na^3 the logarithmic term does actually improve the energy over the mean-field term.

The validity condition for a homogeneous gas to be described by the shape-independent approximation of Eq. (5.3) is given by the diluteness condition $na^3 \ll 1$. This condition is often invoked for the inhomogeneous system as well except, since the density is not uniform, one uses some other characteristic density of the gas n, usually the peak density at the center of the trap $n(0)$[92, 94, 99]. However, it is possible for the condensate to be in a strongly interacting regime, wherein the shape-independent approximation fails, and yet for the condensate to still be dilute (i.e., $na^3 < 1$). A more appropriate validity-condition rigorously obtained by Proukakis and Burnett[100] for inhomogeneous gases is $4\pi\hbar^2 na/m \ll \hbar\omega_{\rm ho}$, where n is some characteristic number density in the trap and $\omega_{\rm ho}$ is the harmonic trap frequency. If one takes the characteristic density of the trapped gas to be the average density, which is on the order $N/a_{\rm ho}^3$, where $a_{\rm ho} = \sqrt{\hbar/m\omega_{\rm ho}}$ is the trap length-scale, the validity condition for an inhomogeneous gas becomes $4\pi Na/a_{\rm ho} \ll 1$. The limit of strong interaction in the mean-field approach ($Na/a_{\rm ho} \gg 1$) corresponds to the TF limit of the GP equation[6]. That is, $Na/a_{\rm ho}$, which is the ratio of the mean-field interaction energy to the kinetic energy, satisfies $Na/a_{\rm ho} \gg 1$ in the TF limit. These two opposing limits – the small $Na/a_{\rm ho}$ limit in which the mean-field approach is valid on the one hand and the large-$Na/a_{\rm ho}$ TF limit of the GP equation on the other – suggest that while the TF approximation is an excellent approximation of the GP equation in the strongly interacting limit, the GP equation itself is not a good approximation of the BEC in this limit. Thus, the TF approximation and the GP equation are not physically relevant in the large-N limit. Other approaches are needed to describe the strongly interacting (large-N or large-a) systems. We use DPT to study both weakly and strongly interacting systems. In the latter case, for which $4\pi Na \ll 1$, we examine both large-N and large-a systems.

We investigate beyond-mean-field effects in inhomogeneous BEC's by analyzing three scattering lengths for the ^{87}Rb atom: the natural scattering length, and multiples 10 and 100 times the natural value. As mentioned earlier, the shape-independent approximation is one of the underlying weaknesses of the GP equation. Ideally, one would use a detailed interatomic potential in a many-body calculation in the strongly interacting, shape-dependent regime, but using such a potential poses a difficult challenge. In our large-N calculations, we use a simple shape-dependent potential as the interatomic potential, namely, a hard sphere with radius equal to the s-wave scattering length. In the previous chapter, we derived the methods of many-body dimensional perturbation theory (DPT) for a general system of identical, interacting particles under spherically symmetric quantum confinement[101]. In this chapter, we use this many-body formalism to calculate the ground-state energy for spherical condensates in both the strongly and weakly interacting regimes.

We compare our many-body results with two nonlinear Schrödinger equations that describe inhomogeneous condensates: the mean-field Gross-Pitaevskii equation and a modified GP equation that contains beyond-mean-field quantum corrections. The GP energy for an isotropically trapped BEC is calculated from the following energy functional:

$$E_{\rm GP}[\psi] = \int d\mathbf{r} \left[\frac{\hbar^2}{2m} |\nabla\psi|^2 + \frac{1}{2} m\omega_{\rm ho}^2 r^2 |\psi|^2 + \frac{2\pi\hbar^2(N-1)a}{m} |\psi|^4 \right], \qquad (5.4)$$

where $\omega_{\rm ho}$ is the harmonic frequency of the isotropic trap and ψ is the ground-state wavefunction, which is given by the solution of the GP equation:

$$\left(-\frac{\hbar^2}{2m} \nabla^2 + \frac{1}{2} m\omega_{\rm ho}^2 r^2 + \frac{4\pi\hbar^2(N-1)a}{m} |\psi|^2 \right) \psi = \mu\psi. \qquad (5.5)$$

In Eq. (5.5), μ is interpreted as the chemical potential in the Bogoliubov approach and as the ground-state orbital energy in the Hartree-Fock approach[11]. The presence of the quantity $(N-1)$ in the nonlinear term, rather than N, follows from number-conserving Schrödinger quantum mechanics with a product of orbitals as the initial state[11]. The so-called modified GP (MGP) equation includes an analytical quantum correction to the mean-field contribution to the GP equation[88, 89]. This correction takes the form of an additional nonlinear term to the GP energy functional, which

arises from the ground-state depletion of the condensate due to excitations. The MGP energy is calculated from the following energy functional:

$$E_{\rm MGP}[\psi] = \int d\mathbf{r}\left[\frac{\hbar^2}{2m}|\nabla\psi|^2+\frac{1}{2}m\omega_{\rm ho}^2r^2|\psi|^2+\frac{2\pi\hbar^2(N-1)a}{m}|\psi|^4\times\left(1+\frac{128}{15\sqrt{\pi}}a^{\frac{3}{2}}(N-1)^{\frac{1}{2}}\psi\right)\right], \tag{5.6}$$

where the wave function is given by the following nonlinear Schrödinger equation:

$$\left[-\frac{\hbar^2}{2m}\nabla^2+\frac{1}{2}m\omega_{\rm ho}^2r^2+\frac{4\pi\hbar^2(N-1)a}{m}|\psi|^2\times\left(1+\frac{32}{3\sqrt{\pi}}a^{\frac{3}{2}}(N-1)^{\frac{1}{2}}\psi\right)\right]\psi=\mu\psi \tag{5.7}$$

The MGP energy was derived by Braaten and Nieto[88] by carrying out a self-consistent one-loop calculation through second order in the gradient expansion. In Eqs. (5.7) and (5.6) we have dropped the additional nonlocal term in Eq. (2) of Ref. [88] that accounts for edge effects since it is found to be small[88, 92]. The stationary MGP solution of Eq. (5.7) minimizes the MPG energy functional (5.6). The nonlinear mean-field term in the GP energy functional (5.4) reproduces the leading-order term of the homogeneous energy density expansion (5.3) in the uniform limit. Likewise, the nonlinear terms in the MGP energy functional (5.6) reproduce the homogeneous-gas energy per particle of Eq. (5.3) with the logarithmic term neglected (see Appendix G). Equation (5.6) is the inhomogeneous generalization of the first two terms in Eq. (5.3).

We compare our results with the GP and MGP equations (5.5 and 5.7), and discuss the relevance of the logarithmic term in Eq. (5.3) to the range of validity of our DPT results. In addition to predicting ground-state properties of the condensate, we also calculate excitation properties, such as frequencies, which arise naturally from our first-order calculation. An advantage of many-body DPT over purely numerical methods is the analytical nature of its results which offer insight into the many-body physics of BEC.

5.1 Formalism

5.1.1 The dimensionally scaled Schrödinger equation

The N-body Schrödinger equation for a system of identical, trapped, interacting particles in D-dimensional Cartesian coordinates is

$$H\Psi = \left[\sum_{i=1}^{N} h_i + \sum_{i=1}^{N-1}\sum_{j=i+1}^{N} g_{ij}\right]\Psi = E\Psi, \tag{5.8}$$

$$h_i = -\frac{\hbar^2}{2m}\sum_{\nu=1}^{D}\frac{\partial^2}{\partial x_{i\nu}^2} + V_{\text{conf}}\left(\sqrt{\sum_{\nu=1}^{D} x_{i\nu}^2}\right) \tag{5.9}$$

$$g_{ij} = V_{\text{int}}\left(\sqrt{\sum_{\nu=1}^{D}\left(x_{i\nu} - x_{j\nu}\right)^2}\right), \tag{5.10}$$

where V_{conf} is the trapping potential, V_{int} is the two-body interatomic potential, H is the D-dimensional Hamiltonian, and $x_{i\nu}$ is the ν^{th} Cartesian component of the i^{th} particle. We have also assumed equal masses m for the condensate atoms at $T = 0$K, which are confined by an isotropic, harmonic trap with frequency ω_{ho}:

$$V_{\text{conf}}(r_i) = \frac{1}{2}m\omega_{\text{ho}}^2 {r_i}^2. \tag{5.11}$$

We take the interatomic potential to be a hard sphere of radius a:

$$V_{\text{int}}(r_{ij}) = \begin{cases} \infty, & r_{ij} < a \\ \\ 0, & r_{ij} \geq a. \end{cases}, \tag{5.12}$$

where a is the s-wave scattering length of the condensate atoms. In the many-electron systems of the previous chapter, the dimensionally continued Laplacian is dimension dependent while the potential energy maintains the same form as it has at $D = 3$. In the hard-sphere system, we dimensionally continue the hard-sphere potential so that it is differentiable away from $D = 3$, allowing us to perform the dimensional

perturbation analysis (see the previous chapter as well as a later discussion in this chapter). Thus, we take the interaction to be

$$V_{\text{int}}(r_{ij}) = \frac{V_o}{1-3/D}\left[1-\tanh\left[\frac{c_o}{1-3/D}\left(r_{ij}-\alpha-\frac{3}{D}(a-\alpha)\right)\times \left(1+(1-3/D)\sum_{n=1}^{s-3}c_n r_{ij}^{2n}\right)\right]\right], \tag{5.13}$$

where D is the Cartesian dimensionality of space. This interaction becomes a hard-sphere of radius a in the physical, $D = 3$, limit. The other s constants (V_o, α, and $\{c_n;\ \forall n:\ 0 \le n \le s-3\}$) are parameters that allow us to fine-tune the large-D shape of the potential and optimize our results through Langmuir (first) order (see Section 5.3). The simplest possibility could have as few as two parameters: V_o and c_o, with $\alpha = a$ and the remaining $c_n = 0$; however, we can have any number of parameters for the most general and flexible potential.

As in the previous chapter, we restrict our attention to spherically symmetric states (i.e., S-wave states), and we transform the Schrödinger equation to a form more suitable for dimensional perturbation theory analysis. The transformation, discussed in more detail in the previous chapter, takes place in three steps. The first step is to transform the variables of all N particles, each with D Cartesian components $x_i = (x_{i1}, x_{i2}, \ldots, x_{iD})$ $(1 \le i \le N)$, to internal coordinates, defined as the D-dimensional scalar radii r_i of the N particles and the angle cosines γ_{ij} of the $N(N-1)/2$ angles between the radial vectors:

$$r_i = \sqrt{\sum_{\nu=1}^{D} x_{i\nu}^2} \quad (1 \le i \le N), \quad \text{and} \quad \gamma_{ij} = cos(\theta_{ij}) = \left(\sum_{\nu=1}^{D} x_{i\nu}x_{j\nu}\right)/r_i r_j \quad (1 \le i < j \le N). \tag{5.14}$$

The second step is to carry out a similarity transformation of the Schrödinger equation resulting from step 1. The transforming function,

$$\chi = (r_1 r_2 \ldots r_N)^{-\frac{(D-1)}{2}}\Gamma^{-\frac{(D-1)}{4}}, \tag{5.15}$$

results in a Schrödinger equation in terms of Φ $(= \chi^{-1}\Psi)$, in which the first derivative terms of the Laplacian are removed.

The third step is to regularize the large-D limit of the similarity transformed hamiltonian $(\chi^{-1}H\chi)$. We use dimensionally scaled harmonic oscillator units similar to the N-electron quantum dot system with the difference that we use D^2 in the

dimensional scaling instead of Ω of Eq. (4.85). Ideally, one would use Ω in order to remove all of the dimension dependence from the centrifugal-like term in the kinetic energy, but in order to simplify the scaling of our dimensionally continued hard-sphere potential, we allow some dimension dependence in the centrifugal-like term (see U in (5.18) below). We regularize the large-D limit of the Schrödinger equation by using the following dimensionally scaled variables (bars):

$$\begin{aligned} &\bar{r}_i = \tfrac{r_i}{D^2\bar{a}_{\rm ho}} \quad \bar{E} = \tfrac{D^2}{\hbar\bar{\omega}_{\rm ho}}E, \quad \bar{H} = \tfrac{D^2}{\hbar\bar{\omega}_{\rm ho}}H, \quad \bar{a} = \tfrac{a}{\sqrt{2}D^2\bar{a}_{\rm ho}}, \\ &\bar{V}_o = \tfrac{D^2}{\hbar\bar{\omega}_{\rm ho}}V_o, \quad \bar{\alpha} = \tfrac{\alpha}{\sqrt{2}D^2 a_{\rm ho}}, \quad \bar{c}_o = \sqrt{2}D^2\bar{a}_{\rm ho}c_o, \quad \bar{c}_n = (\sqrt{2}D^2\bar{a}_{\rm ho})^{2n}c_n, \end{aligned} \tag{5.16}$$

where

$$\bar{a}_{\rm ho} = \sqrt{\frac{\hbar}{m\bar{\omega}_{\rm ho}}} \quad \text{and} \quad \bar{\omega}_{\rm ho} = D^3\omega_{\rm ho} \tag{5.17}$$

are the dimensionally scaled harmonic oscillator length and dimensionally scaled trap frequency, respectively. The dimensionally scaled harmonic oscillator units of energy, length and time are $\hbar\bar{\omega}_{\rm ho}$, $\bar{a}_{\rm ho}$, and $1/\bar{\omega}_{\rm ho}$, respectively. All barred constants ($\bar{a}$, $\bar{a}_{\rm ho}$, $\bar{\omega}_{\rm ho}$, $\bar{V}_o$, $\bar{\alpha}$, $\bar{c}_o$ and $\bar{c}_n$) are held fixed as D varies. For example, as D varies $\bar{a}$ is held fixed at a value by requiring that it give the physical unscaled scattering length at $D = 3$. Finally, we arrive at

$$\bar{H}\Phi = (\mathcal{T} + U + V)\Phi = \bar{E}\Phi, \tag{5.18}$$

where

$$\mathcal{T} = -\frac{1}{2}\delta^2\sum_{i=1}^{N}\left[\frac{\partial^2}{\partial\bar{r}_i{}^2} + \sum_{j\neq i}\sum_{k\neq i}\frac{\gamma_{jk}-\gamma_{ij}\gamma_{ik}}{\bar{r}_i^2}\frac{\partial^2}{\partial\gamma_{ij}\partial\gamma_{ik}}\right] \tag{5.19}$$

$$U = \sum_{i=1}^{N}\frac{(\delta-1)[(2N+1)\delta-1]}{8\bar{r}_i^2}\frac{\Gamma^{(i)}}{\Gamma} \tag{5.20}$$

$$\begin{aligned} V = &\sum_{i=1}^{N}\frac{1}{2}\bar{r}_i^2 + \frac{\bar{V}_o}{1-3\delta}\sum_{i=1}^{N}\sum_{j=i+1}^{N} \\ &\left(1-\tanh\left[\frac{\bar{c}_o}{1-3\delta}\left(\frac{\bar{r}_{ij}}{\sqrt{2}}-\bar{\alpha}-3\delta(\bar{a}-\bar{\alpha})\right)\left(1+(1-3\delta)\sum_{n=1}^{s-3}\frac{\bar{c}_n\bar{r}_{ij}^{2n}}{2^n}\right)\right]\right), \end{aligned} \tag{5.21}$$

where the perturbation parameter is

$$\delta = 1/D \tag{5.22}$$

and $\bar{r}_{ij} = \sqrt{\bar{r}_i^2 + \bar{r}_j^2 - 2\bar{r}_i\bar{r}_j\gamma_{ij}}$ is the interatomic separation. The quantity $\mathcal{T}$ is the derivative portion of the kinetic energy $T = \mathcal{T} + U$. As D becomes infinitely large, and $\delta \to 0$, the entire differential part of the kinetic energy as well as a portion of the interatomic and centrifugal-like potentials will drop out of the Hamiltonian. In the infinite-dimension limit, the particles behave as though they become infinitely heavy and rest at the bottom of the infinite-D effective potential, a potential that includes the trap potential and contributions from the centrifugal-like and hard-sphere potentials. The infinite-D energy becomes the minimum value of the effective potential (see Appendix A of Ref. [55]).

As noted above, for a given set of trap parameters at $D = 3$, the energy of the $D = 3$ Bose-Einstein condensate only depends on the scattering length of the interatomic potential, and not the detailed shape of the potential. This is due to the long wavelength nature of BEC's: for small to moderate scattering lengths, the atomic wavelengths are not short enough to "resolve" the short-range detail of the potential. However, for large D the atomic wavelengths become very short, since according to Eqs. (5.18), (5.19) and (5.22) the scaled, similarity-transformed Hamiltonian displays an effective mass term equal to D^2. Thus, unlike at $D = 3$, the energy of the large-D system is sensitive to the details of the potential.

One may think, prima facie, that this is an indication that the large-dimension limit is a poor starting point for a series expansion in terms of a perturbation parameter, in this case δ, since it appears not to reflect the long wavelength nature of the condensate and displays a sensitivity to the details of the interatomic potential. These concerns are particularly acute since a large-order calculation for a large-N system seems infeasible. These concerns, though, are resolved upon closer inspection of the issues involved. Suppose one had actually found a perturbation scheme in some parameter which at low orders displays an insensitivity to the precise shape of the interatomic potential, as long as the perturbation parameter and scattering length are unchanged. Now what is most important in a low-order perturbation calculation is that the energy be as close as possible to the actual $D = 3$ result. One could not, however, reasonably ask for both the energy to be insensitive to the precise shape of the interatomic potential for fixed scattering length and, at the same time, for the

energy at low orders of a perturbation theory to differ only a small amount from the actual $D = 3$ condensate energy. The energy at low orders would almost certainly be different from the actual $D = 3$ condensate.

In fact, instead of being a liability, this large-D sensitivity to the details of the interatomic potential is actually to our advantage, enabling us to optimize our dimensional continuation of the hard-sphere potential so that the low-order DPT energy is as close as possible to the actual $D = 3$ result. We discuss this in detail in Section 5.4.

It is also seen that the issue of long wavelengths at $\delta = 1/3$ and short wavelengths for extremely small δ is a spurious concern. At $D = 3$ the zeroth-order wavefunction does have a large-wavelength character, but further discussion of this issue is put off until Section 5.1.3.

5.1.2 Leading-order energy term

The infinite-D ($\delta \to 0$) effective potential in dimensionally scaled harmonic oscillator units is

$$V_{\mathit{eff}} = \sum_{i=1}^{N} \left(\frac{1}{8\bar{r}_i^2} \frac{\Gamma^{(i)}}{\Gamma} + \frac{1}{2}\bar{r}_i^2 \right) + \bar{V}_o \sum_{i=1}^{N-1} \sum_{j=i+1}^{N} \left(1 - \tanh \left[\bar{c}_o \left(\frac{\bar{r}_{ij}}{\sqrt{2}} - \bar{\alpha} \right) \left(1 + \sum_{n=1}^{s-3} \frac{\bar{c}_n \bar{r}_{ij}^{2n}}{2^n} \right) \right] \right). \tag{5.23}$$

As one can see from the double-sum term in V_{eff}, the interaction potential becomes a soft sphere of radius approximately $\bar{\alpha}$ and height $2\bar{V}_o$. The slope of the soft wall is determined by $\bar{c}_o$, while, as discussed earlier, the remaining $s - 3$ parameters act to further refine the shape of the interaction potential[102].

The parameters are chosen with the goal of optimizing the energy perturbation series through first order in δ. In Sec. 5.4 we optimize the potential by fitting the energies through first order to DMC energies[92] at low atom number, and since in our DPT analysis the number of atoms N is a parameter, we can readily extrapolate to larger N without large amounts of calculation. Further discussion on the optimization procedure and the range of validity of the extrapolation to larger N will follow in Sections 5.3 and 5.4, respectively.

Again choosing the totally symmetric configuration for which all $\bar{r}_i$ and γ_{ij} are equal to some $\bar{r}_\infty$ and γ_∞:

$$\bar{r}_i = \bar{r}_\infty \ (1 \le i \le N) \quad \text{and} \quad \gamma_{ij} = \gamma_\infty \ (1 \le i < j \le N), \tag{5.24}$$

and using Eqs. (E12) from Appendix E in Eqs. (4.20) and (4.21), we find that the large-D radii and energy per atom are:

$$\bar{r}_\infty = [2(1+(N-1)\gamma_\infty)]^{-1/2} \tag{5.25}$$

$$\frac{\bar{E}_\infty}{N} = \frac{1+(N-2)\gamma_\infty}{(1-\gamma_\infty)(1+(N-1)\gamma_\infty)}\frac{1}{8\bar{r}_\infty^2} + \frac{1}{2}\bar{r}_\infty^2 + \frac{N-1}{2}\bar{V}_o[1-\tanh(\Theta)] \tag{5.26}$$

where for simplicity of presentation we have defined the following:

$$\Theta = \bar{c}_o\left(\bar{r}_\infty\sqrt{1-\gamma_\infty} - \bar{\alpha}\right)\left(1+\sum_{n=1}^{s-3}\bar{c}_n\bar{r}_\infty^{2n}(1-\gamma_\infty)^n\right). \tag{5.27}$$

The large-D direction cosine, γ_∞, of the hyperangle between the infinite-dimensional radii is given by the negative solution of smallest magnitude of

$$\bar{V}_o\bar{c}_o\Upsilon\mathrm{sech}^2\Theta + \gamma_\infty\frac{2(2+(N-2)\gamma_\infty)^2}{(1-\gamma_\infty)^3(1+(N-1)\gamma_\infty)} = 0, \tag{5.28}$$

where

$$\Upsilon = \left[1+\sum_{n=1}^{s-3}\left((2n+1)\bar{c}_n\bar{r}_\infty^{2n}(1-\gamma_\infty)^n - 2n\bar{\alpha}\bar{c}_n\bar{r}_\infty^{2n-1}(1-\gamma_\infty)^{n-1/2}\right)\right]. \tag{5.29}$$

5.1.3 Normal modes and first quantum energy correction

To obtain the $1/D$ quantum correction to the energy for large but finite values of D, we expand about the minimum of the $D\to\infty$ effective potential (5.23) and use the FG matrix method[78] to obtain the normal-mode frequencies of the condensate. We first define a configuration vector consisting of all $\mathrm{P} = N(N+1)/2$ internal coordinates:

$$\bar{y}^T = (\bar{r}_1, \bar{r}_2, \ldots, \bar{r}_N, \gamma_{12}, \gamma_{13}, \ldots, \gamma_{N-1,N}), \tag{5.30}$$

where T is the transpose operator. We make the following substitutions for all radii and angle cosines:

$$\bar{r}_i = \bar{r}_\infty + \delta^{1/2}\bar{r}_i' \tag{5.31}$$

$$\gamma_{ij} = \gamma_\infty + \delta^{1/2}\gamma_{ij}', \tag{5.32}$$

where $\delta = 1/D$ is the expansion parameter, and we define a displacement vector consisting of the internal displacement coordinates (primed in Eqs. (5.31) and (5.32)):

$$\bar{y}'^T = (\bar{r}'_1, \bar{r}'_2, \ldots, \bar{r}'_N, \gamma'_{12}, \gamma'_{13}, \ldots, \gamma'_{N-1,N}), \tag{5.33}$$

The first-order term in the hamiltonian (in $\delta = 1/D$) becomes

$$\hat{H}_1 = -\frac{1}{2}\sum_{\mu=1}^{P}\sum_{\nu=1}^{P} \partial_{\bar{y}'_\mu} [G_{\mu,\nu}]_\infty \partial_{\bar{y}'_\nu} + \frac{1}{2}\sum_{\mu=1}^{P}\sum_{\nu=1}^{P} \bar{y}'_\mu [F_{\mu,\nu}]_\infty \bar{y}'_\nu + v_o, \tag{5.34}$$

where the elements of **G** are found by comparing with $\mathcal{T}$ of Eq. (5.19), and the elements of **F** are found by evaluating the Hessian matrix of the effective potential at the infinite-D symmetric minimum[101]:

$$[F_{\mu\nu}]_\infty = \left[\frac{\partial^2 V_{\mathit{eff}}}{\partial \bar{y}'_\mu \partial \bar{y}'_\nu}\right]_\infty . \tag{5.35}$$

The quantity v_o is a constant first-order energy shift (see Eq. (5.59) below), and the subscripts μ and ν refer to the components of the displacement vector $\bar{y}'$, whose elements are the internal displacement coordinates defined in Eqs. (5.31), (5.32), and (5.33).

To make the connection with internal coordinates more explicit we adopt the following subscripts to identify the elements of **F**, **G**, and the product **GF**, which we will need shortly: (i,j) refers to elements associated with (r_i, r_j); (i,jk) refers to (r_i, γ_{jk}); and (ij,kl) refers to $(\gamma_{ij}, \gamma_{kl})$, etc. See Chapter 4 for more details on the indical structure of the **FG** matrices.

The first-order Hamiltonian, $\hat{H}_1$, of equation (5.34) gives the first-order energy correction, $\bar{E}_0$, and zeroth-order similarity transformed wave function, Φ_0, through the Schrödinger equation

$$\hat{H}_1 \Phi_0 = \bar{E}_0 \Phi_0. \tag{5.36}$$

The Wilson FG method shows that under a linear transformation

$$\bar{q}' = \mathbf{T}\bar{y}', \tag{5.37}$$

the large-D similarity transformed Schrödinger equation of eq. (5.36) takes on the separable form

$$\left[-\frac{1}{2}\partial^T_{\bar{q}'}\partial_{\bar{q}'} + \frac{1}{2}\bar{q}'^T \mathbf{\Lambda} \bar{q}' + v_0\right] \Phi_0 = \bar{E}_0 \Phi_0 , \tag{5.38}$$

where $\mathbf{\Lambda}$ is a positive-definite diagonal matrix (see Appendix A of Ref. [101] with the identification $\mathbf{T} = \mathbf{UA}$). Thus the large-dimension similarity-transformed Schrödinger equation is separable into one-dimensional harmonic oscillator wave functions in each of the P normal modes $\bar{q}'_p$, where $1 \leq p \leq \mathrm{P}$. If $\bar{\omega}_p$ is the corresponding normal-mode frequency, then the wave function is a product of $\mathrm{P} = N(N+1)/2$ harmonic oscillator wave functions

$$\Phi_0(\bar{y}') = \prod_{p=1}^{\mathrm{P}} h_{n_p}\left(\bar{\omega}_p^{1/2}\bar{q}'_p\right), \tag{5.39}$$

where $h_{n_p}\left(\bar{\omega}_p^{1/2}q'_p\right)$ is a one-dimensional harmonic oscillator wave function of frequency $\bar{\omega}_p$ and n_p is the oscillator quantum number, $0 \leq n_p < \infty$, which counts the number of quanta in each normal mode.

Having obtained equation (5.39) we are now in a position to address the above noted concern (in Sec. 5.1.1) that low-order DPT might not contain the right physics for the macroscopic, long-wave-length $D = 3$ condensate since DPT is a perturbation expansion based on solutions to the semi-classical short wavelength problem in a large number of spatial dimensions. In the notation of equation (5.30) and (5.33), equations (5.31) and (5.32) can be written as

$$\bar{y}^T = \bar{y}^T_\infty + \delta^{1/2}\bar{y}'^T, \tag{5.40}$$

where

$$\bar{y}^T_\infty = \bar{y}^T \Big|_{\substack{\bar{r}_i = \bar{r}_\infty \\ \gamma_{jk} = \gamma_\infty}} \quad \forall\, 1 \leq i \leq N \text{ and } 1 \leq j < k \leq N. \tag{5.41}$$

Inserting equation (5.40) into equation (5.37) one obtains

$$\bar{q}^T = \bar{q}^T_\infty + \delta^{1/2}\bar{q}'^T, \tag{5.42}$$

where

$$\bar{q}_\infty = \mathbf{T}\bar{y}_\infty. \tag{5.43}$$

Then using equation (5.42) in equation (5.39) one obtains

$$\Phi_0(\bar{y}) = \prod_{p=1}^{\mathrm{P}} h_{n_p}\left(\left\{\frac{\bar{\omega}_p}{\delta}\right\}^{1/2}(\bar{q}_p - [\bar{q}_\infty]_p)\right). \tag{5.44}$$

Equation (5.44) represents oscillations about the Lewis structure configuration $\bar{q}_\infty$ with frequencies $\{\bar{\omega}_p/\delta\}$. When δ is small (large dimensions) the frequencies $\{\bar{\omega}_p/\delta\}$

are very large and so according to equation (5.44) the zeroth-order wave function is strongly localized about $\bar{q} = \bar{q}_\infty$ (i.e., it features short wavelengths). However as δ takes on increasing positive values, $\{\bar{\omega}_p/\delta\}$ becomes less and less large, and so the zeroth-order wave function becomes increasingly extensive. That is, the wavelengths of the zeroth-order wave function at $\delta = 1/3$ have become macroscopic. Thus, the zeroth-order DPT wave function for the Bose-Einstein condensate at $D = 3$ appropriately has a macroscopic, long-wave-length character.

The Wilson FG method shows that the normal-mode coordinates are the solutions of the eigenvalue equation

$$\mathbf{GF}\vec{q}'_p = \lambda_p \vec{q}'_p , \tag{5.45}$$

where the eigenvalues λ_p are the diagonal entries of the diagonal force-constant matrix $\mathbf{\Lambda}$ in equation (5.38). Thus the normal-mode frequencies are related to the λ_p in equation (5.45) by

$$\lambda_p = \bar{\omega}_p^2 . \tag{5.46}$$

Equation (5.45) leads to the secular equation

$$\det(\lambda_p \mathbf{I} - \mathbf{GF}) = 0 \tag{5.47}$$

for the λ_p.

Equation (5.47) provides a general formula for calculating the normal-mode frequencies in terms of the elements of the product $\mathbf{GF}$. Recall from the previous chapter that we derived analytical expressions for the normal-mode frequencies in terms of

the highly symmetric **GF** matrix elements. To simplify the analytical expressions for the normal-mode frequencies, we define the scalar quantities a through ι:

$$
\begin{aligned}
a = (GF)_{i,i} &= G_a F_a \\
b = (GF)_{i,j} &= G_a F_b && (i<j) \\
c = (GF)_{ij,i} &= G_g F_e + (N-2) G_h F_e + (N-2) G_g F_f && (i<j) \\
d = (GF)_{jk,i} &= G_g F_f + 2 G_h F_e + 2(N-3) G_h F_f && (i \neq j < k \neq i) \\
e = (GF)_{i,ij} &= G_a F_e && (i<j) \\
f = (GF)_{i,jk} &= G_a F_f && (i \neq j < k \neq i) \\
g = (GF)_{ij,ij} &= G_g F_g + 2(N-2) G_h F_f && (i<j) \\
h = (GF)_{ij,jk} &= G_g F_h + G_h F_e + (N-2) G_h F_h + (N-3) G_h F_\iota && (i<j<k) \\
\iota = (GF)_{ij,kl} &= G_g F_\iota + 4 G_h F_h + 2(N-4) G_h F_\iota && (i<j,\ k<l),
\end{aligned}
\tag{5.48}
$$

where the expressions in Eq. (5.48) for the **GF** matrix elements of the Schrödinger equation (5.18) in terms of the **F** and **G** matrix elements were derived in Eq. (4.42). The **G** and **F** matrices are defined by the first-order $1/D$ Hamiltonian of Eq. (5.34). We can determine the elements of **G** by comparing the differential term in Eq. (5.34) with $\mathcal{T}$ of Eq. (5.19) expanded to first order in $1/D$. Using the notation in Eq. (4.34), the non-zero elements of the **G** matrix are found to be:

$$
\begin{aligned}
G_a &= 1 \\
G_g = 2\tfrac{1-\gamma_\infty{}^2}{r_\infty^2} &= 4(1-\gamma_\infty)(1+\gamma_\infty)[1+(N-1)\gamma_\infty] \\
G_h = \tfrac{\gamma_\infty(1-\gamma_\infty)}{r_\infty^2} &= 2\gamma_\infty(1-\gamma_\infty)[1+(N-1)\gamma_\infty],
\end{aligned}
\tag{5.49}
$$

where the matrix elements have been evaluated at the infinite-D symmetric minimum. Likewise, using Eq. (5.35), the non-zero $\mathbf{F}$ matrix elements are:

$$
\begin{aligned}
F_a &= 1+\frac{3}{4\bar{r}_\infty^4}\frac{1+(N-2)\gamma_\infty}{(1-\gamma_\infty)(1+(N-1)\gamma_\infty)}+\frac{\bar{V}_o\bar{c}_o}{2}(N-1)\mathrm{sech}^2\Theta\Bigg[\bar{c}_o(1-\gamma_\infty)\Upsilon^2\tanh\Theta+ \\
&\quad -\frac{1+\gamma_\infty}{2\bar{r}_\infty\sqrt{1-\gamma_\infty}}+\sum_{n=1}^{s-3}\Bigg(\frac{2n+1}{2}\bar{r}_\infty^{2n-1}(1-\gamma_\infty)^{n-1/2}[(2n-1)\gamma_\infty-(2n+1)]+ \\
&\quad 2n\bar{\alpha}\bar{r}_\infty^{2n-2}(1-\gamma_\infty)^{n-1}[(n-1)\gamma_\infty-n)]\Bigg)\bar{c}_n\Bigg] \\
F_b &= \frac{\bar{V}_o\bar{c}_o}{2}\mathrm{sech}^2\Theta\Bigg[\bar{c}_o(1-\gamma_\infty)\Upsilon^2\tanh\Theta+\frac{1+\gamma_\infty}{2\bar{r}_\infty\sqrt{1-\gamma_\infty}}+ \\
&\quad +\sum_{n=1}^{s-3}\Bigg(\frac{2n+1}{2}\bar{r}_\infty^{2n-1}(1-\gamma_\infty)^{n-1/2}[(2n+1)\gamma_\infty-(2n-1)]+ \\
&\quad -2n\bar{\alpha}\bar{r}_\infty^{2n-2}(1-\gamma_\infty)^{n-1}[n\gamma_\infty-(n-1))]\Bigg)\bar{c}_n\Bigg] \\
F_e &= -\frac{\gamma_\infty}{2\bar{r}_\infty^3}\frac{1+(N-2)\gamma_\infty}{(1-\gamma_\infty)^2(1+(N-1)\gamma_\infty)^2}+\frac{\bar{V}_o\bar{c}_o}{2}\mathrm{sech}^2\Theta\Bigg[-\bar{c}_o\bar{r}_\infty\Upsilon^2\tanh\Theta+ \\
&\quad +\frac{1}{2\sqrt{1-\gamma_\infty}}+\sum_{n=1}^{s-3}\frac{1}{2}\Bigg((2n+1)^2\bar{r}_\infty^{2n}(1-\gamma_\infty)^{n-1/2}-(2n)^2\bar{\alpha}\bar{r}_\infty^{2n-1}(1-\gamma_\infty)^{n-1}\Bigg)\bar{c}_n\Bigg] \\
F_f &= \frac{{\gamma_\infty}^2}{2\bar{r}_\infty^3(1-\gamma_\infty)^2(1+(N-1)\gamma_\infty)^2} \qquad (5.50) \\
F_g &= \frac{1}{2\bar{r}_\infty^2(1-\gamma_\infty)^3(1+(N-1)\gamma_\infty)^3}\Big(1+3(N-2)\gamma_\infty+(13-11N+3N^2){\gamma_\infty}^2+ \\
&\quad (N-2)(4-3N+N^2){\gamma_\infty}^3\Big)+\frac{\bar{V}_o\bar{c}_o}{2}\mathrm{sech}^2\Theta\Bigg[\frac{\bar{c}_o\bar{r}_\infty}{1-\gamma_\infty}\Upsilon^2\tanh\Theta+\frac{\bar{r}_\infty}{2(1-\gamma_\infty)^{3/2}}+ \\
&\quad -\sum_{n=1}^{s-3}\Bigg(\frac{(2n-1)(2n+1)}{2}\bar{r}_\infty^{2n-1}(1-\gamma_\infty)^{n-3/2}+ \\
&\quad +2n(n-1)\bar{\alpha}\bar{r}_\infty^{2n}(1-\gamma_\infty)^{n-2}\Bigg)\bar{c}_n\Bigg] \\
F_h &= \frac{-\gamma_\infty}{4\bar{r}_\infty^2(1-\gamma_\infty)^3(1+(N-1)\gamma_\infty)^3}\left[3+(5N-14)\gamma_\infty+(11-9N+2N^2){\gamma_\infty}^2\right], \\
F_i &= \frac{\gamma_\infty^2(2+(N-2)\gamma_\infty)}{\bar{r}_\infty^2(1-\gamma_\infty)^3(1+(N-1)\gamma_\infty)^3},
\end{aligned}
$$

where we have used Eqs. (E13) from Appendix E to evaluate the Gramian second derivatives. For transparency we leave the $\bar{r}_\infty$ terms in Eq. (5.50) instead of using the explicit γ_∞ dependent form of $\bar{r}_\infty$.

Although there are $N(N+1)/2$ different normal modes, there are only five distinct normal-mode frequencies[101, 80]! The five distinct eigenfrequencies of $\mathbf{GF}$ belong to

three different irreducible representations of the symmetric group S_N[80, 101]. One distinct frequency, given by

$$\bar{\omega}_2 = \sqrt{g - 2h + \iota}, \tag{5.51}$$

has a multiplicity of $N(N-3)/2$ (i.e., there are $N(N-3)/2$ normal modes with the same frequency ω_2). We designate the set of normal-modes with this frequency with the label **2** [80, 101]. Another two frequencies, with multiplicities $(N-1)$, are given by

$$\bar{\omega}_{1\pm} = \sqrt{\eta_1 \pm \sqrt{{\eta_1}^2 - \Delta_1}}, \tag{5.52}$$

where

$$\eta_1 = \frac{1}{2}[a - b + g + (N-4)h - (N-3)\iota] \tag{5.53}$$

$$\Delta_1 = (N-2)(c-d)(e-f) + (a-b)[g + (N-4)h - (N-3)\iota]. \tag{5.54}$$

The normal modes with the frequencies $\bar{\omega}_{1\pm}$ are a mixture of asymmetric stretching and bending motions, and we designate them by the labels $\mathbf{1}^-$ and $\mathbf{1}^+$[80, 101]. The last two frequencies have multiplicity of unity (i.e., singlet) and are given by

$$\bar{\omega}_{0\pm} = \sqrt{\eta_0 \pm \sqrt{{\eta_0}^2 - \Delta_0}}, \tag{5.55}$$

where

$$\eta_0 = \frac{1}{2}\left[a - (N-1)b + g + 2(N-2)h - \frac{(N-2)(N-3)}{2}\iota\right] \tag{5.56}$$

$$\Delta_0 = (a-(N-1)b)\left[g + 2(N-2)h - \frac{(N-2)(N-3)}{2}\iota\right] + -\frac{N-2}{2}(2c + (N-2)d)(2e + (N-2)f). \tag{5.57}$$

The normal modes with the frequencies $\bar{\omega}_{0+}$ and $\bar{\omega}_{0-}$ are a mixture of symmetric stretching and bending motions, and correspond to the center of mass and breathing mode of the condensate, respectively. We designate them by $\mathbf{0}^-$ and $\mathbf{0}^+$[80, 101].

Because of the factors of δ in the centrifugal-like and hard-sphere potentials (U and V of Eq. (5.18)), there is also a constant shift, v_o, in the first-order energy:

$$\begin{aligned} \bar{E}^{(\mathrm{DPT})} &= \bar{E}_\infty + \delta\bar{E}_o + O(\delta^2) \\ &= V_{\mathrm{eff}}(\bar{r}_\infty, \gamma_\infty) + \delta\left[\sum_\sigma \sum_{n_\sigma} (n_\sigma + \frac{1}{2}) d_{\sigma,n_\sigma}\bar{\omega}_\sigma + v_o\right] + O(\delta^2), \end{aligned} \tag{5.58}$$

where the n_σ ($1 \le \sigma \le 5$) are the vibrational quantum numbers of the normal modes of the same frequency $\bar{\omega}_\sigma$, and d_{σ,n_σ} is the occupancy of the manifold of normal modes with vibrational quantum number n_σ and normal mode frequency $\bar{\omega}_\sigma$. The contribution from v_o acts as an order-δ shift in the energy, which is given by:

$$v_o = -\frac{N(N+1)(1+(N-2)\gamma_\infty)}{4\bar{r}_\infty^2(1+(N-1)\gamma_\infty)(1-\gamma_\infty)} + 3\bar{V}_o\frac{N(N-1)}{2}\Bigg(1-\tanh\Theta + \\ +\bar{c}_o\left[(\bar{a}-\bar{\alpha})\left(\sum_{n=1}^{s-3}\bar{c}_n\bar{r}_\infty^{2n}(1-\gamma_\infty)\right) - (\bar{r}_\infty\sqrt{1-\gamma_\infty}-\bar{a})\right]\mathrm{sech}^2\Theta\Bigg), \quad (5.59)$$

where Θ is give by Eq. (5.27).

Using the definitions of the dimensionally scaled harmonic oscillator units in Eqs. (5.16) and (5.17), we can undo the scalings to write the through-first-order DPT energy of Eq. (5.58) in regular oscillator units ($\hbar\omega_{\rm ho}$) we arrive at

$$E^{(\rm DPT)} = DV_{\rm eff}(\bar{r}_\infty,\gamma_\infty) + \left[\sum_\sigma(n_\sigma+\frac{1}{2})d_{\sigma,n_\sigma}\bar{\omega}_\sigma + v_o\right] + O(\delta). \quad (5.60)$$

Since the normal-mode frequencies $\bar{\omega}_\sigma$ do not depend on D, Eq. (5.60) shows that their values are equal to the physical ($D = 3$) excitation frequencies of the condensate. It is also noteworthy that in the noninteracting limit the DPT energy series truncates at first order and gives the exact isotropic D-dimensional N-particle harmonic oscillator energy. At its minimum the effective potential in regular oscillator units ($\hbar\omega_{\rm ho}$) in the noninteracting limit becomes $E_\infty = D\bar{E}_\infty = DV_{\rm eff}(\bar{r}_\infty = 1/\sqrt{2}, \gamma_\infty = 0) = DN/2$, the ideal-gas energy. In the infinite-D limit, $r_\infty = \sqrt{D/2}$ is the infinite-D radius in regular oscillator units, also the expectation value $< r^2 >$ for the ground-state D-dimensional spherical harmonic oscillator. In addition, the excitation frequencies become the N-atom harmonic oscillator frequencies: $\bar{\omega}_\sigma = 2$ for all σ. As the interatomic interaction increases, the strength of the interaction is reflected in the deviation from the above noninteracting values of the infinite-D radius and direction cosine as well as the excitation frequencies of the leading-order energy correction.

5.2 Motivation for low-order method

Recall that the dimensionally-continued interatomic potential becomes a hard sphere at $D = 3$ with radius equal to the scattering length, but takes on the shape of

a soft-sphere for larger D. The reason for choosing this dimensional continuation of the hard sphere is to facilitate the DPT analysis, which requires a differentiable effective potential. The exact shape of the soft sphere for dimensions departing from $D = 3$ is determined by s built-in parameters. In this study we consider three scattering lengths: the ^{87}Rb scattering length $a_{\rm Rb} = 0.00433a_{\rm ho}$ and two larger multiples, $a = 10 \times a_{\rm Rb}$ and $a = 100 \times a_{\rm Rb}$. For these three scattering lengths, we optimize the s interatomic potential parameters by fitting our analytical energy through first order (Eq. (5.58)) at the physical ($D = 3$) dimension to accurate, low-N, hard-sphere DMC energies[92].

The fitted interatomic parameters for each scattering length are given in the Sec. 5.4 where we extrapolate our fitted energies to large values of N. Note that our extrapolating function is not an arbitrary fitting function to the data. Rather, it is based on the dynamical approximation to the real system that is intrinsic to DPT, which includes contributions from all components of the Hamiltonian, including the kinetic, trap and interaction terms, as well as correlation effects beyond the mean-field approximation. Furthermore, this low-order approximation is well defined and in principle can be systematically refined by using higher-order DPT[55, 103].

5.3 Optimization of the interatomic parameters

A chi-square statistic is used to optimize the parameters of the dimensionally-continued interatomic potential. We fit to six accurate low-N DMC energies[92] for each scattering length (see column 1 of Tables 5.1, 5.2, and 5.3) by minimizing the following quantity[104] with respect to the set of parameters $\{V_o, \alpha\} \bigcup \{c_n;\ \forall n:\ 0 \leq n \leq s-3\}$:

$$\chi^2_s = \sum_{i=1}^{6} \left(\frac{\left(E_i^{(\rm DMC)} - E^{(\rm DPT)}(N_i; V_o, \alpha, \{c_n\})\right)^2}{\sigma_i} \right), \tag{5.61}$$

where $E_i^{(\rm DMC)}$ is the DMC energy within statistical uncertainty σ_i[1] for a condensate with atom number N_i. That is, the DMC energy $E_i^{(\rm DMC)}$ has an error of $\pm\sigma_i$. The quantity $E^{(\rm DPT)}(N_i; V_o, \alpha, \{c_n\})$ is the DPT energy approximation through first-order given by Eq. (5.58) with interatomic potential parameters $\{V_o, \alpha\} \bigcup \{c_n;\ \forall n:\ 0 \leq$

[1]Each DMC-calculated energy for a given number of atoms N_i represents a collection of independent random walks. The uncertainty σ_i in the energy $E_i^{(\rm DMC)}$ arises from overall statistical fluctuations due to the finite number of random walks.

$n \leq s-3\}$. The Q-probability is used to constrain the number of parameters s in the fitting function $E^{(\mathrm{DPT})}(N_i; V_o, \alpha, \{c_n\})$, where

$$Q\left(\frac{\nu}{2}, \frac{\chi_s^2}{2}\right) \equiv \frac{\Gamma(\frac{\nu}{2}, \frac{\chi_s^2}{2})}{\Gamma(\frac{\nu}{2})} \equiv \frac{1}{\Gamma(\frac{\nu}{2})} \int_{\chi_s^2/2}^{\infty} e^{-t} t^{\nu/2-1} dt \tag{5.62}$$

is the probability that χ_s^2 should exceed a particular value by chance, and in our case[2] the quantity $\nu = 6 - s$ is the number of degrees of freedom in the fitting function[105]. We want to use the minimum number of parameters which extract all of the relevant physical information from the DMC energies, while not overfitting the DMC energies. Thus, the number of parameters s is constrained to be the minimum number of parameters whose χ_s^2 gives a Q-probability greater than 0.5. The value of $Q = 0.5$ is chosen as the cutoff in order to avoid overfitting the DMC energies. Overfitting is a serious concern as we are extrapolating our energies to large N, and we wish to capture the essential information without fitting to statistical fluctuations in the DMC energies. We found $s = 4$ to be the minimum number of parameters in the $E^{(\mathrm{DPT})}$ fitting function that gives a Q-probability of at least 0.5 from the weighted least-squares-fit to the six low-N ($N < 100$) DMC energies for all three scattering lengths considered in this study. In fact, there is a dramatic increase in Q when going from three to four parameters, suggesting that four parameters is the optimum number.

5.4 Ground-state energy

In this section we report calculations for ^{87}Rb atoms in a spherical condensate with trap frequency $\omega_{\mathrm{ho}} = 2\pi \times 77.87$ Hz. We consider three scattering lengths: one equal to the natural ^{87}Rb value of approximately $a = 100$ a.u. or $0.00433 a_{\mathrm{ho}}$ in oscillator units ($a_{\mathrm{ho}} = \sqrt{\hbar/m\omega_{\mathrm{ho}}}$); one roughly 10 times the natural ^{87}Rb value, at $a = 1\,000$ a.u. or $0.0433 a_{\mathrm{ho}}$ in oscillator units; and one roughly 100 times the natural ^{87}Rb value, at $a = 10\,000$ a.u. or $0.433 a_{\mathrm{ho}}$ in oscillator units. The scattering length $a = 0.433 a_{\mathrm{ho}}$ is especially relevant to experiments observing beyond-mean-field effects, because stable condensates with a scattering length of 10 000 a.u. have been achieved in nonspherical traps[4].

[2]Equation (5.61) assumes one can achieve an exact fit ($Q = 1.0$) with $s = 6$ parameters, which is not quite possible with our fitting function. However, the fit with $s = 6$ parameters is close enough to effectively give $Q = 1.0$

5.4.1 Small scattering length

For $a = 0.00433a_{\rm ho}$, we determine the $s = 4$ interatomic potential parameters to be $V_o = 0.0257$, $\alpha = -0.464$, $c_o = 1.402$, and $c_1 = 0.109$, with $\chi^2 = .20$ and $Q = 0.90$. Table 5.1 shows a low-N comparison of energies for $a = 0.00433a_{\rm ho}$. Column 1 contains accurate DMC energies for a hard-sphere potential calculated previously in Ref. [92], where the statistical uncertainty is given in parenthesis. Column 3 contains our many-body DPT energies, while columns 4 and 5 contain GP and MGP energies, which are calculated by using the wave functions from Eqs. (5.5) and (5.7), respectively, in the corresponding energy functionals[6]. In Fig. 5.1, we plot the energy shift per atom due to the interatomic interactions (i.e., we subtract the ideal-gas energy $3N/2$, in units of $\hbar\omega_{\rm ho}$) for the DPT, GP, and MGP for larger N. There is very little difference between any of these interaction energies because, for such a small scattering length and moderate atom number, the condensate is very dilute and weakly interacting. Consistent with low-N DMC calculations by Blume and Greene[92], the many-body DPT energy is slightly above the MGP and GP energies for low and moderate N, with the MGP energy being slightly above the GP energy. Going to higher N (beyond that shown in the plot), near 10^4 atoms the DPT energy falls below the GP energy.

Table 5.1: Ground-state energies in units $\hbar\omega_{\rm ho}$ for small scattering length and low N. Column 2 contains DMC energies from Ref. [92] (statistical uncertainty in parenthesis). Column 3 contains our many-body DPT energies. Columns 4 and 5 contain the GP (Eq. 5.5) and MGP energies (Eq. 5.7), respectively. We use ^{87}Rb mass and let $a = 100$ a.u. and $\omega_{\rm ho} = 2\pi \times 77.87$ Hz, which corresponds to $a = 0.00433a_{\rm ho}$, in oscillator units.

N	DMC	DPT	GP	MGP
3	4.51036(2)	4.51035	4.51032	4.51032
5	7.53443(4)	7.53441	7.53432	7.53434
10	15.1537(2)	15.1537	15.1534	15.1535
20	30.640(1)	30.6396	30.638	30.639
50	78.96(1)	78.964	78.953	78.962
100	165.07(5)	165.089	165.06	165.11

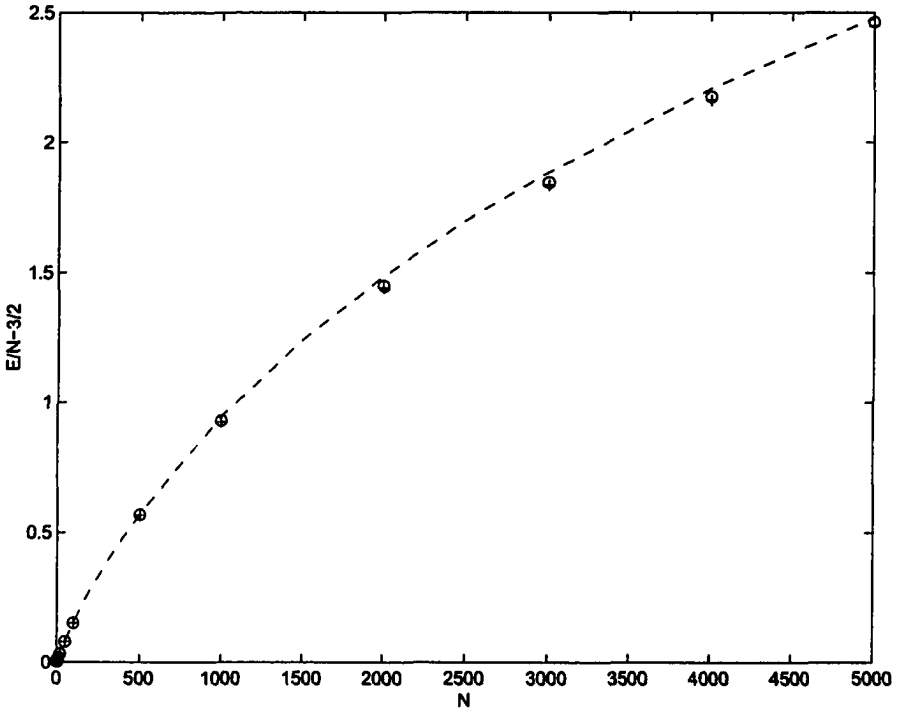


Figure 5.1: Interatomic energy per atom versus number of condensate atoms for small scattering length. We use ^{87}Rb mass and let $a = 100$ a.u. and $\omega_{\rm ho} = 2\pi \times 77.87$ Hz, which corresponds to $a = 0.00433 a_{\rm ho}$, in oscillator units. Circles refer to the MGP energy from the solution of Eq. (5.7), plus signs, slightly below the circles, refer to the GP energy from the solution of Eq. (5.5), and the dashed line refers to the many-body DPT energy. Interaction energies are obtained by subtracting the ideal gas energy $3N/2$ from the total energy. Energies are given in oscillator units ($\hbar\omega_{\rm ho}$).

5.4.2 Large and intermediate scattering length

The $s = 4$ interatomic potential parameters for the large scattering length $a = 0.433 a_{\rm ho}$ are found to be $V_o = 4.617 \times 10^7$, $\alpha = -4.211$, $c_o = 1.555$, and $c_1 = 5.00 \times 10^{-3}$, with $\chi^2 = 0.23$ and $Q = 0.89$. In Table 5.2 and Fig. 5.2 for $a = 0.433 a_{\rm ho}$, it can again be seen that the MGP interaction energy lies above GP, but the DPT interaction energy is now sandwiched between MGP and GP. These results are also consistent with accurate low-N DMC calculations in Ref. [92], which show MGP overestimating the ground-state energy for $a = 0.433 a_{\rm ho}$ for small N. However, as one increases the number of atoms beyond that displayed in Fig 5.2, one finds that

the low-order many-body DPT interaction energy eventually falls below GP above 10^4 atoms.

Table 5.2: Ground-state energies in units $\hbar\omega_{\text{ho}}$ for large scattering length and low N. Column 2 contains DMC energies from Ref. [92] (statistical uncertainty in parenthesis). Column 3 contains our many-body DPT energies. Columns 4 and 5 contain the GP (Eq. 5.5) and MGP energies (Eq. 5.7), respectively. We use ^{87}Rb mass and let $a = 10\,000$ a.u. and $\omega_{\text{ho}} = 2\pi \times 77.87$ Hz, which corresponds to $a = 0.433 a_{\text{ho}}$, in oscillator units.

N	DMC	DPT	GP	MGP
2	3.3831(7)	3.38319	3.3040	3.3950
3	5.553(3)	5.5519	5.329	5.611
5	10.577(2)	10.5771	9.901	10.772
10	26.22(8)	26.2151	23.61	26.84
20	66.9(4)	67.01538	57.9	68.5
50	239.2(3)	239.18	196.12	243.45

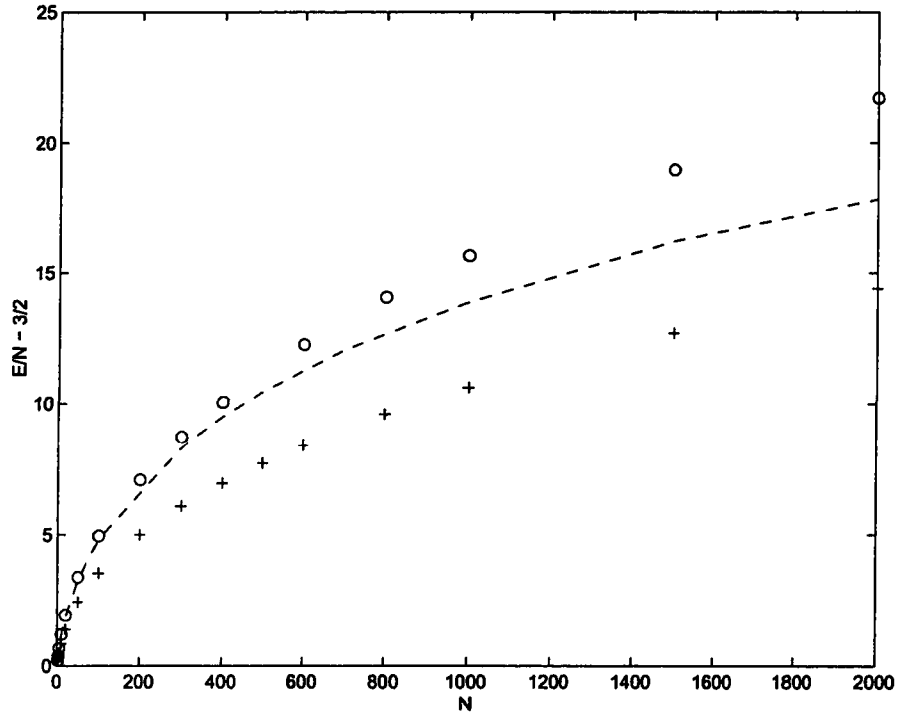


Figure 5.2: Interatomic energy per atom versus number of condensate atoms for large scattering length. We use ^{87}Rb mass and let $a = 10\,000$ a.u. and $\omega_{\mathrm{ho}} = 2\pi \times 77.87$ Hz, which corresponds to $a = 0.433 a_{\mathrm{ho}}$, in oscillator units. Circles refer to the MGP energy from the solution of Eq. (5.7), plus signs refer to the GP energy from the solution of Eq. (5.5), and the dashed line refers to the many-body DPT energy. Interaction energies are obtained by subtracting the ideal gas energy $3N/2$ from the total energy. Energies are given in oscillator units ($\hbar\omega_{\mathrm{ho}}$).

The intermediate-a ($a = 0.0433 a_{\mathrm{ho}}$) interaction parameters are found to be $V_o = 0.645$, $\alpha = -0.837$, $c_o = 1.3875$, and $c_1 = 0.0889$, where $\chi^2 = 0.0047$ and $Q = 0.998$. Figure 5.3 shows the DPT interatomic energy falling below GP at a few hundred atoms, as opposed to approximately 10^4 atoms for large and small a. The interatomic interaction parameters were determined from accurate DMC energies (see Table 5.3) near a shape-independent density regime and then extrapolated to a shape-dependent regime. As we discuss below in more depth, this lack of shape-dependent information in the DPT energies for intermediate-a helps to explain the smaller range of validity versus the small- and large-a extrapolations.

Table 5.3: Ground-state energies in units $\hbar\omega_{\mathrm{ho}}$ for intermediate scattering length and low N. Column 2 contains DMC energies from Ref. [92] (statistical uncertainty in parenthesis). Column 3 contains our many-body DPT energies. Columns 4 and 5 contain the GP (Eq. 5.5) and MGP energies (Eq. 5.7), respectively. We use ^{87}Rb mass and let $a = 1\,000$ a.u. and $\omega_{\mathrm{ho}} = 2\pi \times 77.87$ Hz, which corresponds to $a = 0.0433 a_{\mathrm{ho}}$, in oscillator units.

N	DMC	DPT	GP	MGP
3	4.6033(5)	4.6032	4.6007	4.6024
5	7.8356(15)	7.8356	7.8265	7.8340
10	16.426(6)	16.426	16.383	16.426
20	35.475(15)	35.474	35.297	35.497
50	103.99(3)	103.991	102.96	104.21
100	245.4(1)	245.402	241.85	246.24

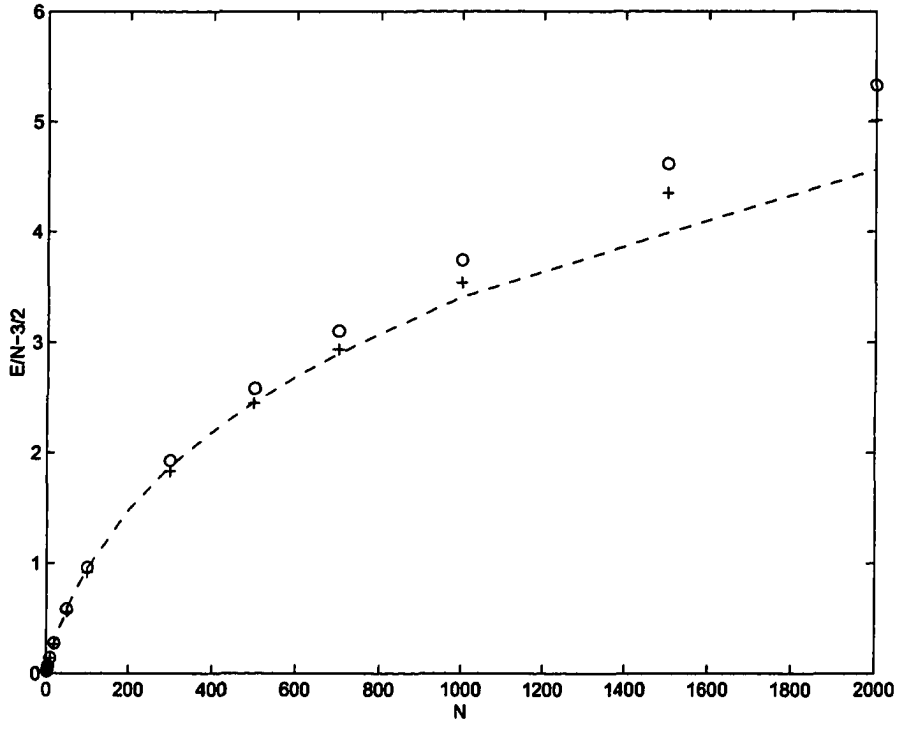


Figure 5.3: Interatomic energy per atom versus number of condensate atoms for intermediate scattering length. We use ^{87}Rb mass and let $a = 1\,000$ a.u. and $\omega_{\rm ho} = 2\pi \times 77.87$ Hz, which corresponds to $a = 0.0433 a_{\rm ho}$, in oscillator units. Circles refer to the MGP energy from the solution of Eq. (5.7), plus signs refer to the GP energy from the solution of Eq. (5.5), and the dashed line refers to the many-body DPT energy. Interaction energies are obtained by subtracting the ideal gas energy $3N/2$ from the total energy. Energies are given in oscillator units ($\hbar\omega_{\rm ho}$).

5.4.3 Discussion

For large scattering lengths such as $a = 0.433 a_{\rm ho}$, the condensate has entered a density regime where, even for small atom number, the gas parameter na^3 becomes large enough that shape-dependent corrections can no longer be ignored. For a homogeneous condensate in this shape-dependent regime, the truncated series of Eq. (5.3) becomes invalid and the logarithmic term causes the mean-field lower-bound to be violated. To connect with the low-density expansion of (5.3), we use its validity condition ($na^3 \ll 1$) for the inhomogeneous gases considered in this study. We use the TF peak density as the characteristic density in order to write the gas parameter

in terms of the physical parameters of the system. The gas parameter can then be approximated by

$$n_{\rm TF}(0)a^3 = \frac{(15N(a/a_{\rm ho})^6)^{2/5}}{8\pi}. \tag{5.63}$$

The TF peak density is often a surprisingly good estimate of the bose number density at the center of the trap, even when the the TF energy is a poor approximation. DuBois and Glyde[99] show that for $Na/a_{\rm ho} > 5$ and $n(0)a^3 < 10^{-3}$, $n_{\rm TF}(0)$ is a good estimate and it is sufficient for our qualitative purposes of using Eq. (5.3). Using Eq. (5.63) as the estimate for na^3, the correction to the mean-field in Eq. (5.3) is already negative for $a = 0.433a_{\rm ho}$ for only a single atom. And so higher-order, shape-dependent terms are needed in the local-density approximation corresponding to Eq. (5.3). That is, the energies depend on the detailed shape of the potential, in this case the hard-sphere potential. Again, strictly speaking, the truncated low-density expansion (5.3) is only valid for homogeneous hard-core bose gases. However, we assume the spatial variations of the inhomogeneous gas are not too large, in which case Eq. (5.3) will share features of the inhomogeneous gas theory. Within this context, we use Eq. (5.3) to interpret our DPT results for the trapped BEC.

The optimization procedure discussed earlier gives the best energy at low order for low and moderate N, but terms beyond first-order become more significant at large atom number in which case higher-order DPT is needed for all scattering lengths. When the number of atoms is extended beyond that shown in Figs. 5.1 and 5.2 for both large and small scattering lengths, one finds that the low-order many-body DPT interaction energy eventually falls below the GP interaction energy above 10^4 atoms due to the neglected higher-order terms. At these larger values of N, higher-order perturbation theory is needed.

However, as can be seen from Fig. 5.3, for intermediate-a (i.e., $a = 0.0433a_{\rm ho}$) the DPT interatomic energy falls below GP at a few hundred atoms, as opposed to approximately 10^4 atoms for large and small a. For this intermediate a, the interaction parameters are determined from accurate DMC energies, but near a shape-independent density regime (i.e., $n_{\rm TF}(0)a^3 < 10^{-4}$), and then extrapolated to a shape-dependent regime (i.e., $n_{\rm TF}(0)a^3 > 10^{-3}$). Since the intermediate-a potential parameters were calculated in a shape-independent density regime, the extrapolated energies follow the local-density approximation that includes the logarithmic term in Eq. (5.3) but not higher-order, shape-dependent corrections. Fig. 5.3 shows the DPT interatomic energy falling below GP, and thus violating the lower bound, at a

few hundred atoms, as opposed to approximately 10^4 atoms for both large and small a. It should be noted that the reduced extrapolation range for intermediate a is not due to overfitting, the large Q-probability for four-parameters notwithstanding. The dramatic increase in Q from $s = 3$ to $s = 4$ parameters indicates underfitting for any $s < 4$. Moreover, varying the fourth parameter above and below the optimal fit to lower the Q-probability to 0.5 results in the same reduced range of validity noted above.

The low-a (i.e., $a = 0.00433a_{\text{ho}}$) parameters were also determined in a shape-independent regime, but the extrapolated energies never reach the shape-dependent regime (which the local-density approximation suggests does not occur until there are more than 10^9 atoms) before higher-order $1/D$ perturbation theory is needed. The increased range of validity of our large-a results over intermediate-a is likely explained by noting that the large-a (e.g., $a = 0.433a_{\text{ho}}$) DPT parameters contain shape-dependent information as they were determined in a shape-dependent density regime.

5.5 Excitations

In addition to ground-state properties, we can easily calculate excitation properties of the condensate, such as frequencies, from the normal-mode structure of many-body DPT. The analytical frequencies in Eq. (5.55), $\bar{\omega}_{0-}$ and $\bar{\omega}_{0+}$, correspond to the center-of-mass and breathing modes of the condensate, respectively. In units of the trap frequency ω_{ho}, the center-of-mass frequency equals 2. We also calculate the frequencies of small oscillation about the ground-state wave function within the mean-field approximation by solving the linearized GP equation[6].

Using the hydrodynamic theory of superfluids[106] based on the GP equation, Stringari found the following large-N approximation to the mean-field dispersion relation[107]:

$$\omega(n_r, l) = \omega_{\text{ho}} \left(2{n_r}^2 + 2n_r l + 3n_r + l \right)^{1/2}, \tag{5.64}$$

where n_r is the number of radial nodes and l is the angular momentum of the excitation. Despite the significant departure from the non-interacting case ($\omega = \omega_{\text{ho}}(2n_r + l)$), the mean-field frequency does not depend on the scattering length or the number of atoms in the TF limit. This curious lack of dependence on the mean-field interaction strength Na/a_{ho} in the strongly interacting limit can be seen as a

consequence of the relationship between the spatial extent of the condensate and the speed of sound at the center of the condensate[6]. The excitation frequency in the phonon regime is given by $\omega \sim c(r=0; Na/a_{\rm ho})/\lambda(Na/a_{\rm ho})$, where the wavelength $\lambda(Na/a_{\rm ho})$ associated with the excitation and the speed of sound at the center of the the gas $c(r=0; Na/a_{\rm ho})$ are both functions of $Na/a_{\rm ho}$. In the phonon regime, the excitation wavelength for an inhomogeneous gas is on the order of the size of the gas, which increases with increasing $Na/a_{\rm ho}$. As the mean-field interaction strength increases, the speed of sound increases in the same ratio as the increase in the wavelength of the phonon-like excitation. This lack of dependence on the number of atoms and the scattering length clearly becomes a problem in the strongly-interacting regime, as can be seen in Fig. 5.4. For intermediate scattering lengths and moderate number of atoms, the excitation frequency is accurately described by the hydrodynamic approximation of Eq. (5.64), which is independent of N. However, just like the TF approximation for the ground-state energy of the GP equation, Eq. (5.64) is a good approximation of the mean-field theory in the strongly-interacting limit but the mean-field theory itself breaks down.

In Ref. [23], Stringari and Pitaevskii consider beyond-mean-field corrections to the collective excitation frequencies in Eq. 5.64). Defining $\omega_{\rm M}$ as the mean-field monopole frequency in the hydrodynamic limit ($n_r = 1$, $l = 0$ in Eq. 5.64), ω as the hydrodynamic-limit beyond-mean-field frequency, and writing $\omega = \omega_{\rm M} + \delta\omega_{\rm M}$ (δ is not to be confused with $1/D$ as $\delta\omega_{\rm M}$ is the shift from the mean-field monopole frequency), Stringari and Pitaevskii use the homogeneous gas first-order correction (i.e., the second term in Eq. (5.3)) to the Bogoliubov equation to find the following beyond-mean-field, but still shape independent, fractional shift of the monopole (breathing mode) frequency in the hydrodynamic limit[23]:

$$\frac{\delta\omega_{\rm M}}{\omega_{\rm M}} = \frac{63}{256\sqrt{2}}(15N(a/a_{\rm ho})^6)^{1/5}. \tag{5.65}$$

In Fig. 5.4 we compare the DPT breathing mode frequency ω_{0+} in Eq. (5.55) with the mean-field (i.e., the solution of the linearized GP equation[6]) and the beyond-mean-field correction (5.65) to the monopole (breathing) mode of frequency in the strongly interacting regime, $a = 0.433a_{\rm ho}$. The lack of dependence on the interaction strength for the mean-field excitation frequency in Eq. (5.64) is clearly a detriment in this regime, in which a large beyond-mean-field shift of the breathing mode frequency is predicted by both DPT and the beyond-mean-field calculation by Stringari and

Pitaevksii. For $N = 2\,000$ atoms we predict a fractional shift of 74% above the mean-field prediction while Eq. (5.65) gives a 50% shift.

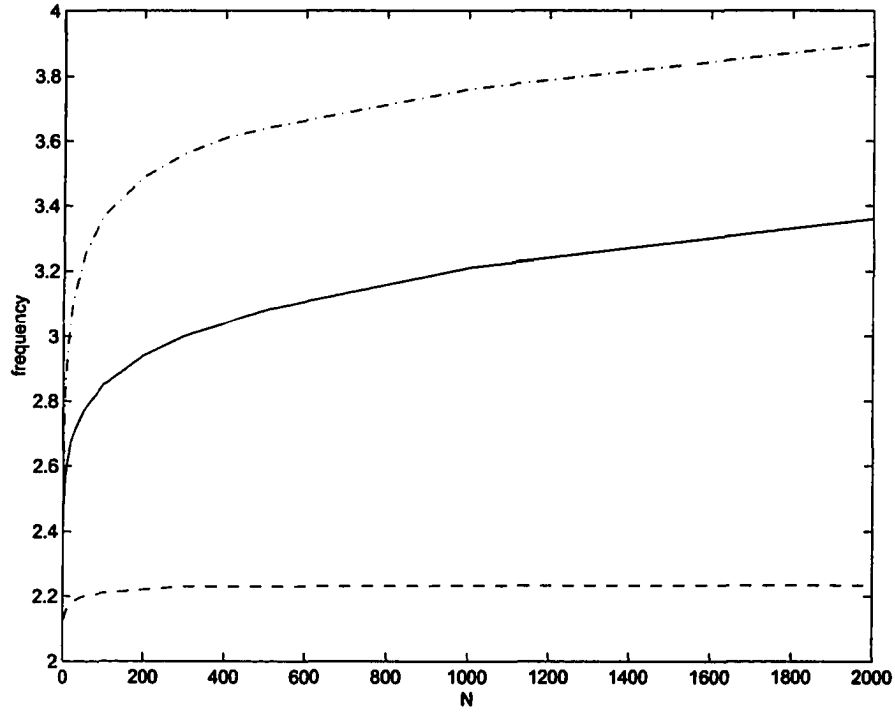


Figure 5.4: Breathing mode frequency in units of ω_{ho} versus N for large scattering length. We use ^{87}Rb mass and let $a = 10\,000$ a.u. and $\omega_{ho} = 2\pi \times 77.87$ Hz, which corresponds to $a = 0.433 a_{ho}$, in oscillator units. The solid line corresponds to Eq. (5.65), the first correction to the monopole frequency calculated by Pitaevskii and Stringari[23]. The dashed line is the numerical solution of the linearized GP equation. The dash-dotted line refers to the DPT normal mode frequency ω_{0+} from Eq. (5.55).

Chapter 6

Summary

This dissertation has developed a comprehensive many-body approach to isotropically confined systems of identical, interacting particles. In this final chapter, we summarize the most important results and give an outlook for further development and applications of many-body DPT.

DPT has advantages over traditional methods that either neglect all of the interaction (conventional perturbation theory) or all of the kinetic energy (classical TF approximation) at lowest order. The infinite-dimension (leading-order) limit of DPT results in an effective potential that keeps contributions from the confinement, interaction, and kinetic terms of the Hamiltonian. The remaining kinetic contribution is a centrifugal-like $(1/r^2)$ term that allows the leading order of DPT to satisfy the minimum uncertainty principle. In the infinite-dimension limit, we choose a symmetric configuration in which all of the particles are localized and equivalent. The first-order energy correction corresponds to small oscillations about the large-D structure, where the vibrational frequencies are determined by the Wilson FG matrix method. Analytical results through first order are obtained for a spherical system of identical particles with a general confining potential and general interaction potential. Many-body DPT includes beyond-mean-field correlation at all orders.

Many-body DPT was first applied to two N-electron systems: the N-electron atom where the confinement is supplied by the attraction of the nucleus and the N-electron quantum dot where the confinement is supplied by an external harmonic potential. Numerical results for the N-electron atom are given in Ref. [80]. Our two-electron quantum dot study suggests that our low-order many-body results will be quite accurate for typical many-electron quantum dots whose length scales are in the mesoscopic regime (i.e., in the strongly interacting or strongly confined regime), but higher order perturbation theory would most likely be needed to accurately describe

many-electron quantum dots in the weakly interacting or weakly confined regime. Moreover, because N is a parameter in our formalism, the challenge of calculating the physical properties of a system with DPT does not increase as one adds more particles to the system.

The main focus of this dissertation is on obtaining results for the N-atom inhomogeneous bose condensate that go beyond the mean-field and shape-independent approximations. For BEC we use a shape dependent interatomic potential, namely, a hard sphere. Like the N-electron quantum dot, the condensate atoms are confined by an external harmonic trap. Unlike either N-electron system, however, the hard sphere potential has explicit dimension dependence. Both the atom and quantum dot interact via a repulsive Coulomb potential that maintains its three-dimensional form as D varies (an alternative generalization of the three-dimensional Coulomb potential might be $1/r^{D-2}$). In order to make the hard sphere amenable to DPT analysis, we dimensionally continue the hard-sphere potential so that it is differentiable in the infinite-D limit and becomes a hard-sphere with radius equal to the scattering length in the physical $D = 3$ limit. This dimensional continuation results in a shape-dependent soft-sphere interatomic potential at large-D. The large-D soft-sphere potential parameters are optimized for the ground-state energy. No adjusting of parameters is needed for the N-electron systems because their interparticle potentials do not vary with dimension. This makes the N-electron systems easier to deal with, but it also makes them less fiexible.

We compare our semi-analytical ground-state energy results with numerical solutions of the GP equation and modified GP equations for Bose-Einstein condensates with three different scattering lengths, in the weak, intermediate, and strongly interacting regimes. As expected, there is practically no deviation from the mean-field ground-state energy for small scattering length up to very large N. For intermediate and large scattering length, though, the breakdown of the mean-field becomes quite noticeable even for a low number of atoms. We also calculate collective excitation frequencies from our first-order normal-mode frequencies. For large scattering length, we predict a large beyond-mean-field correction to the condensate breathing mode frequency. For $a = 0.433a_{ho}$ for example, we predict a 75% fractional shift above the mean-field breathing mode frequency for $N = 2\,000$ atoms. Our many-body DPT results are accurate up to moderate atom number. For larger N, higher order DPT terms, which are small for low and moderate N, become more important as N increases. Our studies suggest that the regime of validity is further reduced for

intermediate scattering lengths, which is related to the presence of the logarithmic correction in the low-density expansion (5.3). In future work, we will incorporate higher-order, anharmonic terms to the perturbation series, which will extend the range of validity to larger N.

While the treatment of these physical systems has been in many respects quite general, this dissertation leaves open many opportunities for further development and application of the many-body DPT formalism. One extension might be to relax the spherical symmetry constraint by allowing confining potentials with axial symmetry. This is a particularly important extension for describing actual experiments, especially for BEC's, which predominantly have axial symmetry. With axial symmetry, one has an extra N degrees of freedom due to the z-components of the N particles, but the many-body formalism presented in this dissertation readily accommodates this generalization. Instead of generalized spherical coordinates with a D-dimensional radius, one uses generalized cylindrical coordinates, which consists of a $(D-1)$-dimensional sphere plus a z-coordinate. Another extension involves the choice of confining potential. Our main focus has been on harmonic traps of the form r^2 because this is the most prevalent form of confinement in experiments today, but there is no reason why one could not also consider more general external confining potentials. Yet another extension involves the use of the DPT formalism for higher angular momentum[108, 109] ($L > 0$) states, which would correspond to quantized vortex states. Using this formalism, it is possible to find analytical, low-order energies for the N-atom condensate similar to the analytical ground-state results found in this thesis but for quantized vortices in a BEC. Finally, the calculation of higher-order perturbation terms is the last extension of the results of this thesis that we mention. As discussed in Sec. 5.1.3, the leading-order DPT wavefunction is a product of one-dimensional harmonic-oscillator wavefunctions with frequencies given by the first-order term of the energy series. From this wavefunction, one can then use ordinary perturbation theory to extend our results to include anharmonic corrections beyond first order. This is also an important extension as it will increase the range of validity of our dimensionally continued hard sphere results to larger N as well as improve numerical results for many-electron systems.

Reference List

[1] H. Metcalf and P. van der Straten. *Physics Reports*, 244:203, 1994.

[2] S. N. Bose. *Zeitschrift für Physik*, 26:178, 1924.

[3] A. Einstein. *Sitzungsber. der Preuss. Akad. der Wiss.*, page 3, 1924.

[4] S. L. Cornish, N. R. Claussen, J. L. Roberts, E. A. Cornell, and C.E. Wieman. *Phys. Rev. Lett.*, 85:1795, 2000.

[5] T. C. Germann. PhD thesis, Harvard University, 1995.

[6] F. Dalfovo, S. Giorgini, L. P. Pitaevskii, and S. Stringari. *Rev. Mod. Phys.*, 71:463, 1999.

[7] A. Leggett. *Rev. Mod. Phys.*, 73:307, 2001.

[8] M. Inguscio, S. Stringari, and C. E. Wieman, editors. *Proceedings of the International School of Physics (Enrico Fermi) Bose-Einstein Condensation in Atomic Gases.* IOS, Washington DC, 1999.

[9] B. H. Bransden and C. J. Joachain. *Physics of Atoms and Molecules.* Longman, 1983.

[10] H. Friedrich. *Theoretical Atomic Physics, 2nd ed.* Springer, 1998.

[11] B. D. Esry. *Phys. Rev. A*, 55:1147, 1997.

[12] A. L. Fetter and J. D. Walecka. *Quantum Theory of Many-Particle Systems.* McGraw-Hill, New York, 1971.

[13] J. Weiner, V. S. Bagnato, S. Zilio, and P. S. Julienne. *Rev. Mod. Phys*, 71:1, 1996.

[14] N. N. Bogoliubov. *J. Phys. (U.S.S.R.)*, 11:23, 1947.

[15] E. P. Gross. *Nuovo Cimento*, 20:454, 1961.

[16] L. P. Pitaevskii. *Zh. Eksp. Teor. Fiz.*, 40:646, 1961.

[17] B. A. McKinney and D. K. Watson. *Phys. Rev. A*, 65:33604, 2002.

[18] P. Schuck and X. Vi nas. *Phys. Rev. A*, 61:43603, 2000.

[19] G. Baym and C. J. Pethick. *Phys. Rev. Lett.*, 76:6, 1996.

[20] D. S. Jin, J. R. Ensher, M. R. Matthews, C. E. Wieman, and E. A. Cornell. *Phys. Rev. Lett.*, 77:420, 1996.

[21] M. R. Andrews, D. M. Kurn, H. J. Miesner, D. S. Durfee, C. G. Townsend, S. Inouye, and W. Ketterle. *Phys. Lett.*, 77:988, 1996.

[22] J-P. Blaizot and G. Ripka. *Quantum theory of finite systems.* MIT press, Cambridge, MA, 1986.

[23] L. Pitaevskii and S. Stringari. *Phys. Rev. Lett.*, 81:4541, 1998.

[24] D. K. Watson and B. A. McKinney. *Phys. Rev. A*, 59:4091, 1999.

[25] B. A. McKinney and D. K. Watson. *Phys. Rev. B*, 61:4958, 2000.

[26] M. Edwards and K. Burnett. *Phys. Rev. A*, 51:1382, 1995.

[27] H. T. C. Stoof. *J. Stat. Phys.*, 87:1353, 1997.

[28] A. L. Fetter. *J. Low Temp. Phys.*, 106:643, 1997.

[29] V. M. Pérez-García, H. Michinel, J. I. Cirac, M. Lewenstein, and P. Zoller. *Phys. Rev. A*, 56:1424, 1997.

[30] A. Gonzalez. *J. Phys.: Condens. Matter*, 9:4643, 1997.

[31] K. K. Das. *Phys. Rev. A*, 66:53612, 2002.

[32] D.R. Herschbach, J. Avery, and O. Goscinski, editors. *Dimensional Scaling in Chemical Physics.* Kluwer, Dordrecht, 1992.

[33] C. A. Tsipis, V. S. Popov, D. R. Herschbach, and J. Avery, editors. *New Methods in Quantum Theory.* Kluwer, Dordrecht, 1996.

[34] A. Chatterjee. *Phys. Rep.*, 186:249, 1990.

[35] F. Dalfovo, L. Pitaevskii, and S. Stringari. *Phys. Rev. A*, 54:4213, 1996.

[36] E. Lundh, C. J. Pethick, and H. Smith. *Phys. Rev. A*, 55:2126, 1997.

[37] A. L. Fetter and D. L. Feder. *Phys. Rev. A*, 58:3185, 1998.

[38] M. O. Mewes, M. R. Andrews, N. J. van Druten, D. M. Kurn, D. S. Durfee, C. G. Townsend, and W. Ketterle. *Phys. Lett.*, 77:988, 1996.

[39] C. J. Myatt, E. A. Burt, R. W. Ghrist, E. A. Cornell, and C. E. Wieman. *Phys. Rev. Lett.*, 78:586, 1997.

[40] B. Jackson, J. F. McCann, and C. S. Adams. *Phys. Rev. Lett.*, 80:3903, 1998.

[41] J. L. Bohn, B. D. Esry, and C. H. Greene. *Phys. Rev. A*, 58:584, 1998.

[42] J. Avery, editor. *Hyperspherical Harmonics: Applications in Quantum Theory.* Kluwer, Dordrecht, 1989.

[43] L. H. Thomas and D. F. Walls. *Philos. Soc.*, 23:542, 1926.

[44] E. Fermi. *Z. Phys.*, 48:73, 1928.

[45] A. Chatterjee. *J. Phys. A*, 18:735, 1985.

[46] R. Peterson M. Crescimanno, C. G. Koay and R. Walsworth. *Phys. Rev. A*, 62:63612, 2000.

[47] S. Sinha. *Phys. Rev. A*, 55:4325, 1997.

[48] J. L. Bohn, B. D. Esry, and C. H. Greene. *Phys. Rev. A*, 58:584, 1998.

[49] V.S. Popov, V.D. Mur, , and A.V. Sergeev. *Phys. Lett.*, 149A:425, 1990.

[50] L.D. Mlodinow and N. Papanicolaou. *Ann. Phys. (N.Y.)*, 128:314, 1980.

[51] T.H. Berlin and M. Kac. *Phys. Rev.*, 86:821, 1952.

[52] H.E. Stanley. *Phys. Rev.*, 176:718, 1968.

[53] J. Rudnick and G. Gaspari. *Science*, 237:384, 1987.

[54] Y.Y. Goldschmidt. *Nucl. Phys. B*, 393:507, 1993.

[55] M. Dunn, T.C. Germann, D.Z. Goodson, C.A. Traynor, J.D.Morgan III, D.K. Watson, , and D.R. Herschbach. *J. Chem. Phys.*, 101:5987, 1994.

[56] Y.F. Smirnov and K.V. Shitkova. *Sov. J. Part. Nucl.*, 8:344, 1977.

[57] A. L. Fetter. *J. Low Temp. Phys.*, 106:643, 1997.

[58] M. Ueda and A.J. Leggett. *Phys. Rev. Lett.*, 80:1576, 1998.

[59] C.C. Bradley, C.A. Sackett, and R.G. Hulet. *Phys. Rev. Lett.*, 78:985, 1997.

[60] J. L. Bohn. private communication.

[61] D. Pfannkuche, V. Gudmundsson, and P.A. Makasym. *Phys. Rev. B*, 47:2244, 1993.

[62] P. A. Maksym and T. Chakraborty. *Phys. Rev. Lett.*, 65:108, 1990.

[63] D. A. Broido, K. Kempa, and P. Bakshi. *Phys. Rev. B*, 42:11400, 1990.

[64] V. Gudmundsson and R. R. Gerhardts. *Phys. Rev. B*, 43:12098, 1991.

[65] S. Klama and E. G. Mishchenko. *J. Phys.: Condens. Matter*, 10:3411, 1998.

[66] R. M. G. García-Castelán, W. S. Choe, and Y. C. Lee. *Phys. Rev. B*, 57:9792, 1998.

[67] E. Anisimovas and A. Matulis. *J. Phys.: Condens. Matter*, 10:601, 1998.

[68] L. Quiroga, A. Camacho, and A. Gonzalez. *J. Phys.: Condens. Matter*, 7:7517, 1995.

[69] O. Mustafa. *J. Phys.: Condens. Matter*, 5:1327, 1993.

[70] X-F He. *Phys. Rev. B*, 43:2063, 1991.

[71] H. Mathieu, P. Lefebvre, and P. Christol. *Phys. Rev. B*, 46:4092, 1992.

[72] M. de Dios-Leyva, A. Bruno-Alfonso, A. Matos-Abiague, and L.E. Oliveira. *J. Phys.: Condens. Matter*, 9:8477, 1997.

[73] D. K. Watson, M. Dunn, T. C. Germann, D. R. Herschbach, D. Z. Goodson, and J. R. Walkup. *New Methods in Quantum Theory.* Kluwer, Dordrecht, 1996.

[74] C. M. Bender, L. D. Mlodinow, and N. Papanicolaou. *Phys. Rev. A*, 25:1305, 1982.

[75] J. L. Zhu, Z. Q. Li, J.Z. Yu, K. Ohno, and Y. Kawazoe. *Phys. Rev. B*, 55:15819, 1997.

[76] A. A. Svidzinky and A. L. Fetter. *Phys. Rev. A*, 58:3168, 1998.

[77] G. W. Bryant. *Phys. Rev. Lett.*, 59:1140, 1987.

[78] E. B. Wilson Jr., J. C. Decius, and P. C. Cross. *Molecular vibrations: The theory of infrared and raman vibrational spectra.* McGraw-Hill, New York, 1955.

[79] W. Häusler. *Z. Phys. B*, 99:551, 1996.

[80] J. G. Loeser. *J. Chem. Phys.*, 86:5635, 1987.

[81] J. Avery, D. Z. Goodson, and D. R. Herschbach. *Theor. Chim. Acta*, 81:1, 1991.

[82] M. Dunn, B. A. McKinney, and D. K. Watson. *to be submitted*, 2003.

[83] G. Strang. *Linear algebra and its applications, Third ed.* Harcourt Brace Jovanovich College Publishers, Orlando, FL, 1988.

[84] M. Hamermesh. *Group theory and its application to physical problems.* Addison-Wesley, Reading, MA, 1962.

[85] R. C. Ashoori. *Nature*, 379:413, 1996.

[86] B. A. McKinney and D. K. Watson. *Phys. Rev. B*, 61:4958, 2000.

[87] B. D. Esry and C. H. Greene. *Phys. Rev. A*, 60:1451, 1999.

[88] E. Braaten and A. Nieto. *Phys. Rev. B*, 56:14745, 1997.

[89] E. Timmermans, P. Tommasini, and K. Huang. *Phys. Rev. A*, 55:3645, 1997.

[90] G. S. Nunes. *J. Phys. B: At. Mol. Opt. Phys.*, 32:4293, 1999.

[91] S. Giorgini, J. Boronat, and J. Casulleras. *Phys. Rev. A*, 60:5129, 1999.

[92] D. Blume and C. H. Greene. *Phys. Rev. A*, 63:63061, 2001.

[93] A. Fabrocini and A. Polls. *Phys. Rev. A*, 60:2319, 1999.

[94] A. Fabrocini and A. Polls. *Phys. Rev. A*, 64:63610, 1999.

[95] T. D. Lee, K. Huang, and C. N. Yang. *Phys. Rev.*, 106:1135, 1957.

[96] T. T. Wu. *Phys. Rev.*, 115:1390, 1959.

[97] N. Hugenholtz and D. Pines. *Phys. Rev.*, 116:489, 1959.

[98] E. H. Lieb and J. Yngvason. *Phys. Rev. Lett.*, 80:2504, 1998.

[99] J. L. DuBois and H. R. Glyde. *Phys. Rev. A*, 63:23602, 2001.

[100] N. P. Proukakis and K. Burnett. *Phys. Rev. A*, 57:1230, 1998.

[101] B. A. McKinney, M. Dunn, D. K. Watson, J. G. Loeser, and et. al. *Annals of Physics (submitted)*, 2003.

[102] B. A. McKinney, M. Dunn, and D. K. Watson. *to be sumbitted*, 2003.

[103] J. R. Walkup, M. Dunn, and D. K. Watson. *Phys. Rev. A*, 63:25405, 2001.

[104] P. R. Bevington and D. K. Robinson. *Data reduction and error analysis for the physical sciences.* McGraw-Hill, 1992.

[105] W. H. Press, S. A. Teukolsky, W. T. Vetterling, and B. P. Flannery. *Numerical Recipes, Second Edition.* Cambridge University Press, Cambridge, 1992.

[106] P. Nozières and D. Pines. *The Theory of Quantum Liquids, Vol. II.* Addison-Wesley, Reading, MA, 1990.

[107] S. Stringari. *Phys. Rev. Lett.*, 77:2360, 1996.

[108] M. Dunn and D. K. Watson. *Ann. Phys. (N.Y.)*, 251:266, 1996.

[109] M. Dunn and D. K. Watson. *Ann. Phys. (N.Y.)*, 251:319, 1996.

[110] H. Sachs D. M. Cvetković, M. Doob. *Spectra of Graphs: Theory and Application.* Academic Press, New York, 1980.

[111] M. Marcus and H. Ming. *A survey of matrix theory and matrix inequalities.* Allyn and Bacon Inc., Boston, 1964.

[112] F. R. Gantmacher. *The theory of matrices, Vol. 1.* Chelsea, New York, 1959.

[113] T. Busch, B-G Englert, K. Rzazewski, and M. Wilkens. *Foundations of Physics*, 28:549, 1998.

Appendices

Appendix A

Hydrodynamic approximation for inhomogeneous bose gas

In this appendix we derive the TF approximation for the mean-field collective modes of the condensate in the hydrodynamic limit. This approximation provides a valid description of the mean-field theory for a BEC with a large number of atoms with positive scattering length. We begin by writing the time-dependent GP equation (2.34) as two coupled hydrodynamic equations in terms of the density $n = N\psi^2$ and the local velocity, which is proportional to the gradient of the phase ϕ (i.e., $\mathbf{v} = \frac{\hbar}{m}\nabla\phi$, see Eq. (A3) below). Inserting the ansatz

$$\Psi = \sqrt{n(\mathbf{r},t)}e^{i\phi(\mathbf{r},t)} \tag{A1}$$

into Eq. (2.34) results in a new equation whose imaginary part is given by

$$\hbar\frac{\partial n}{\partial t} = -\hbar\left[n\frac{\hbar}{m}\nabla^2\phi + \frac{\hbar}{m}\nabla n\cdot\nabla\phi\right]. \tag{A2}$$

Noting the identity $\nabla\times(\nabla\times A) = \nabla(\nabla\cdot A) - \nabla^2 A$ for a vector A and noting that ϕ is irrotational (i.e., $\nabla\times\phi = 0$), we can replace $\nabla^2\phi$ in Eq. (A2) with $\nabla(\nabla\cdot\phi)$. Further, using the definition

$$v = \frac{\hbar}{m}\nabla\phi, \tag{A3}$$

Eq. (A2) becomes

$$\frac{\partial n}{\partial t} = -\left[n\nabla\cdot v + \nabla n\cdot v\right]. \tag{A4}$$

We recognize the product rule in the bracketed term in the above equation, which allows us to write it as a continuity equation for $j = nv$:

$$\frac{\partial n}{\partial t} + \nabla\cdot(nv) = 0. \tag{A5}$$

The real part of the time-dependent GP equation after insertion of the ansatz of Eq. (A1) is

$$-\hbar\sqrt{n}\frac{\partial\phi}{\partial t} = -\frac{\hbar^2}{2m}\nabla^2 + \frac{1}{2}m\omega_o^2 r^2\sqrt{n} + U_3 n\sqrt{n} +$$

$$-\frac{\hbar^2}{2m}\left[\frac{(\nabla n)^2}{\sqrt{n}} - \frac{1}{4n^{3/2}}(\nabla n)^2 - \sqrt{n}(\nabla\phi)^2\right]. \tag{A6}$$

This equation simplifies greatly when we recognize that the right-hand-side on the first line is simply the time-independent GP Hamiltonian, which we can replace with $\mu\sqrt{n}$. Also, since $\nabla n = 2\sqrt{n}\nabla\sqrt{n}$, the first two terms in the bracket cancel, and Eq. (A6) simplifies to

$$-\hbar\frac{\partial\phi}{\partial t} = \mu + \frac{1}{2}mv^2. \tag{A7}$$

Taking the gradient of this equation and using the definition $v = \frac{\hbar}{m}\nabla\phi$ gives the equation of motion:

$$m\frac{\partial v}{\partial t} = -\nabla\left(\mu + \frac{1}{2}mv^2\right), \tag{A8}$$

where

$$\mu = \frac{1}{2}m\omega_o^2 r^2 + nU_3 - \frac{\hbar^2}{2m}\frac{1}{\sqrt{n}}\nabla^2\sqrt{n}. \tag{A9}$$

Next we linearize the hydrodynamic equations (A5), (A8), and (A9). This is equivalent to linearizing the time-independent GP equation as we did in Eqs. (2.52) and (2.53). We write the density as

$$n = n_{\rm eq} + \delta n, \tag{A10}$$

where $n_{\rm eq}$ is the equilibrium density and δn is a small departure from the equilibrium. We assume that δn and v are small quantities and we neglect terms that are higher than linear in δn and v. Using Eq. (A10) with the assumed small quantities, the continuity equation (A5) gives

$$\frac{\partial\delta n}{\partial t} = -\nabla\cdot(n_{\rm eq}v), \tag{A11}$$

where we have neglected $\delta n v$ as second-order small. Similarly, Eq. (A8) gives

$$m\frac{\partial v}{\partial t} = -\nabla\delta\mu, \tag{A12}$$

where we have neglected $mv^2/2$ as second-order small and $\delta\mu = (\partial\mu/\partial n)\delta n$. Taking the time derivative of Eq. (A11) and noting that $\partial n_{\rm eq}/\partial t = 0$, we find the linearized equation of motion:

$$m\frac{\partial^2\delta n}{\partial t^2} = \nabla\cdot(n_{\rm eq}\nabla\delta\mu), \tag{A13}$$

where we have used Eq. (A12) in the right-hand side.

Recall that in the TF ($Na/a_{\rm ho} \gg 1$) limit one neglects the quantum pressure. In the TF limit, Eq. (A9) reduces to

$$\mu = \frac{1}{2}m\omega_o^2 r^2 + nU_3, \tag{A14}$$

and hence we find

$$\delta\mu = U_3\delta n, \tag{A15}$$

which when used in Eq. (A13) we find that the density fluctuation satisfies

$$m\frac{\partial^2\delta n}{\partial t^2} = U_3\nabla\cdot(n_{\rm eq}\nabla\delta n). \tag{A16}$$

If we consider oscillations with time dependence $\delta n(r,t) = \delta n(r)\cos(\omega t+\gamma)$, where ω is the frequency of the excitation and γ is a phase shift, the previous equation becomes

$$-\omega^2\delta n = \frac{U_3}{m}\left[\nabla n_{\rm eq}\cdot\nabla\delta n + n_{\rm eq}\nabla^2\delta n\right]. \tag{A17}$$

We now use the TF equilibrium density

$$n_{\rm eq} = \frac{\mu_{\rm TF} - \frac{1}{2}m\omega_o^2 r^2}{U_3}, \tag{A18}$$

where $\mu_{\rm TF} = m\omega_o^2R^2/2$ with R being the TF radius, and Eq. (A17) then becomes

$$\epsilon\delta n = r\frac{d}{dr}\delta n - \frac{1}{2}\left(R^2-r^2\right)\left(\frac{d^2}{dr^2}+\frac{2}{r}\frac{d}{dr}\right)\delta n, \tag{A19}$$

where we have defined $\epsilon = \omega^2/\omega_o^2$. Due to the spherical symmetry of this equation, the general solution for the density fluctuations is

$$\delta n(r) = P(r)r^lY_{lm}(\theta,\phi). \tag{A20}$$

Assuming this form for the solution in Eq. (A19) and introducing the new variable $u = r^2/R^2$, one finds the following equation

$$u(1-u)P'' + \left(\frac{2l+3}{2} - \frac{2l+5}{2}u\right)P' + \frac{\epsilon-l}{2}P = 0, \tag{A21}$$

which is in the form of the differential equation for the hypergeometric function $F(\alpha,\beta,\gamma,u)$:

$$u(1-u)F'' + (\gamma - (\alpha+\beta+1)u)\,F' - \alpha\beta F = 0. \tag{A22}$$

To ensure that F or P is well behaved, we set $\alpha = -n$ where n_r is an integer. Then comparing Eqs. (A21) and (A22), we find that $\beta = l+n_r+3/2$, $\gamma = l+3/2$, and $\epsilon - l = 2n(l+n_r+3/2)$. Thus, the TF excitation frequencies in terms of the trap frequency ω_o are given by

$$\omega = \omega_o(l+3n_r+2n_rl+2n_r^2)^{1/2}, \tag{A23}$$

where n_r is the number of radial nodes and l is the angular momentum of the excitation. The density fluctuation is given by

$$\delta n(r,t) = Cr^lF(-n,l+n+3/2,l+3/2,r^2/R^2)Y_{l,m}(\theta,\phi)\cos(\omega t+\gamma), \tag{A24}$$

where C is a normalization constant.

Appendix B

Wilson FG matrix method

In this appendix, we derive the Wilson FG matrix method[78] which is at the heart of our obtaining the normal mode frequencies and, thereby, the first-order energy correction. The derivation involves a transformation to the set of coordinates called normal-coordinates in which both the differential term and the potential term of Eq. (4.30) are diagonal. We begin by defining a symmetric transformation, $\mathbf{A}$, that transforms from the vector $\bar{y}'$, defined by Eq. (4.26), to $\bar{z}'$ ($\bar{z}' = \mathbf{A}\bar{y}'$). $\mathbf{A}$ is an active transformation and has the property that it diagonalizes the symmetric $\mathbf{G}$ matrix to unity. That is, $\mathbf{A}$ satisfies

$$\mathbf{A}^T\mathbf{G}\mathbf{A} = \mathbf{I}, \tag{B1}$$

which can also be written as

$$\mathbf{G} = \mathbf{A}^{-1}(\mathbf{A}^{-1})^T, \tag{B2}$$

where we have used the property that $\mathbf{A}$ is symmetric ($\mathbf{A} = \mathbf{A}^T$) in the derivation of Eq. (B2). $\hat{H}_1$ then becomes

$$\hat{H}_1 \rightarrow -\frac{1}{2}\partial_{\bar{z}'}^T\partial_{\bar{z}'} + \frac{1}{2}\bar{z}'^T(\mathbf{A}^{-1})^T\mathbf{F}\mathbf{A}^{-1}\bar{z}'. \tag{B3}$$

Next we focus our attention on the potential term, the term involving the matrix $\mathbf{F}$. We introduce another transformation, $\mathbf{U}$ ($\bar{\mathbf{q}}' = \mathbf{U}\bar{z}'$), that diagonalizes the potential term while simultaneously leaving the differential term unchanged. This orthogonal transformation ($\mathbf{U}^T\mathbf{U} = \mathbf{I}$, where $\mathbf{I}$ is the identity matrix) leaves the differential term in the same form as in Eq. (B3), and the potential term becomes

$$\mathbf{U}(\mathbf{A}^{-1})^T\mathbf{F}\mathbf{A}^{-1}\mathbf{U}^T = \mathbf{\Lambda}, \tag{B4}$$

where Λ is a diagonal matrix. That is,

$$\hat{H}_1 \rightarrow -\frac{1}{2}\partial_{\bar{\mathbf{q}}'}^T\partial_{\bar{\mathbf{q}}'} + \frac{1}{2}\bar{\mathbf{q}}'^T\mathbf{\Lambda}\bar{\mathbf{q}}'. \tag{B5}$$

The eigenvalue equation corresponding to Eq. (B4) is

$$\left(\mathbf{U}(\mathbf{A}^{-1})^T\mathbf{F}\mathbf{A}^{-1}\mathbf{U}^T\right)\bar{\mathbf{q}}' = \lambda\bar{\mathbf{q}}', \tag{B6}$$

where $\bar{\mathbf{q}}'$ is the eigenvector with eigenvalue λ. Equation (B4) is a matrix eigenvalue equation expressed in the basis of the normal coordinates. We can change the basis back to the original internal displacement coordinates with the passive similarity transformation $\bar{q}' = \mathbf{A}^{-1}\mathbf{U}^T\bar{\mathbf{q}}'$, under which Eq. (B6) now reads

$$\mathbf{U}(\mathbf{A}^{-1})^T\mathbf{F}\bar{q}' = \lambda\mathbf{U}\mathbf{A}\bar{q}'. \tag{B7}$$

Multiplying on the left by $\mathbf{U}^T$ followed by $\mathbf{A}^{-1}$ gives

$$\mathbf{A}^{-1}(\mathbf{A}^{-1})^T\mathbf{F}\bar{q}' = \lambda\bar{q}'. \tag{B8}$$

Inserting Eq. (B2), gives the eigenvalue equation for the normal mode coordinate $\bar{q}'$:

$$\mathbf{G}\mathbf{F}\bar{q}' = \lambda\bar{q}'. \tag{B9}$$

Thus, the FG matrix method consists of finding the roots of the characteristic polynomial in λ:

$$\det(\lambda\mathbf{I} - \mathbf{G}\mathbf{F}) = 0, \tag{B10}$$

which is carried out for a general N-body system in Sec. 4.3 and applied to the systems of Secs. 4.4 and 4.5 and Ch. 5.

Appendix C

Spectral graph theory and the symmetry of the Q matrices

In this appendix, we introduce the relevant aspects of graph theory in order to derive several quantities used throughout the main text and to show the connection of graphs to the large-D symmetric configuration of N particles. A more complete treatment of the mathematics of graph theory with an emphasis on chemical physics applications may be found in Ref. [110].

A graph $\mathcal{G} = (V, E)$ consists of a finite set of vertices $\{v_1, v_2, \ldots, v_n\} \epsilon V(\mathcal{G})$ and a set of not necessarily distinct unordered pairs $\{(v_i, v_j), \forall (1 \leq i < j \leq n)\} \epsilon E(\mathcal{G})$ connecting the vertices to form the corresponding edges. A graph is complete on n vertices, denoted by $K_n(\mathcal{G})$, if every distinct pair of vertices is connected by an edge; K_n is sometimes called a simplex of n points. Notice that K_n contains $n(n-1)/2$ edges. Our large-dimension symmetric minimum configuration of N atoms forms a simplex on N vertices in D-dimensional space. For example, the $N = 4$ simplex is a hypertetrahedron. The line graph $L(\mathcal{G})$ of a graph $\mathcal{G}$ is the graph whose vertices correspond to the edges of $\mathcal{G}$ with two vertices being adjacent if and only if the corresponding edges in $\mathcal{G}$ have a vertex in common.

Derivation of Eq. (4.42): The $\mathbf{Q}$ matrices display a high degree of symmetry in the large-dimension configuration, but it is not trivial to write down the elements of $\mathbf{GF}$ in terms of its constituents $\mathbf{G}$ and $\mathbf{F}$ as we have done in Eq. (4.42). We now derive this result in a two-step process. The first step is to write the $(N+M)$-square matrices $\mathbf{G}$ and $\mathbf{F}$, where $M = N(N-1)/2$, as block matrices of the following form:

$$\mathbf{Q} = \begin{pmatrix} \mathbf{Q}_1 & \mathbf{Q}_2 \\ \mathbf{Q}_3 & \mathbf{Q}_4 \end{pmatrix}, \tag{C1}$$

where the blocks, each of which will be discussed in turn, have the same indical structure as the blocks of $\mathbf{y}\mathbf{y}^T$ in Eq. (4.33).

From Eq. (4.34), the $(N \times N)$ $\mathbf{Q}_1$ block is composed of two distinct elements: the diagonal elements $Q_a = F_{ii}$ and the off-diagonal elements $Q_b = Q_{ij}$ $(i \neq j)$. $\mathbf{Q}_1$ can

be written in terms of the more basic matrices $\mathbf{I}_N$ (the $(N \times N)$ identity matrix) and $\mathbf{J}_N$ (the $(N \times N)$ matrix consisting of all ones):

$$\mathbf{Q}_1 = (Q_a - Q_b)\mathbf{I}_N + Q_b\mathbf{J}_N. \tag{C2}$$

The matrix $\mathbf{J}_N$ contains all ones, so for the diagonal parts of $\mathbf{Q}_1$ the Q_b's cancel and one is correctly left with Q_a. The off-diagonal parts of $\mathbf{Q}_1$ correctly become Q_b since the off-diagonal of $\mathbf{I}_N$ is zero. Specifically, taking the $\mathbf{Q}$ matrix to be $\mathbf{F}$, we find

$$\mathbf{F}_1 = (F_a - F_b)\mathbf{I}_N + F_b\mathbf{J}_N. \tag{C3}$$

One can write down the $\mathbf{G}_1$ block in similar fashion noting that the off-diagonal entries of $\mathbf{G}_1$ are zero:

$$\mathbf{G}_1 = G_a\mathbf{I}_N. \tag{C4}$$

The $(N \times M)$ $\mathbf{Q}_2$ block according to Eq. (4.34) is also composed of two distinct elements: the "incident" elements $Q_e = Q_{i,ij}$ $(i \neq j)$ and the "non-incident" elements $Q_f = Q_{i,jk}$ $(i \neq j \neq k)$. The elements F_e are termed "incident" because the repeated index i means that the vertex i is incident with edge (ij), while for Q_f the vertex designated i is not incident with the edge (jk) since $i \neq j \neq k$. To write $\mathbf{Q}_2$ in terms of basic matrices, we need the $(N \times M)$ vertex-edge matrix $\mathbf{R}$, defined as $R_{i,jk} = \delta_{ij} + \delta_{ik}$, which equals one when vertex i is incident with edge (jk) (i.e., when $i = j$ or $i = k$) and zero otherwise. Thus, the following equation accurately describes the $\mathbf{Q}_2$ block:

$$\mathbf{Q}_2 = (Q_e - Q_f)\mathbf{R} + Q_f\mathbf{J}_{NM}. \tag{C5}$$

Specifically, letting the $\mathbf{Q}$ matrix be $\mathbf{F}$, we find

$$\mathbf{F}_2 = (F_e - F_f)\mathbf{R} + F_f\mathbf{J}_{NM}. \tag{C6}$$

And since there is no mixing of radial and angular derivatives in the Schrödinger equation (4.13), we have

$$\mathbf{G}_2 = \mathbf{G}_3 = 0. \tag{C7}$$

By definition, the Hessian matrix $\mathbf{F}$ is symmetric; hence, from Eq. (C6) we find

$$\mathbf{F}_3 = (F_e - F_f)\mathbf{R}^T + F_f\mathbf{J}_{MN}, \tag{C8}$$

where $\mathbf{J}_{MN} = \mathbf{J}_{NM}^T$. However, for a more general $\mathbf{Q}$-matrix (e.g., $\mathbf{GF}$ which, unlike $\mathbf{F}$, is not symmetric), an analysis analogous to that leading to Eq. (C5) yields

$$\mathbf{Q}_3 = (Q_c - Q_d)\mathbf{R}^T + Q_d\mathbf{J}_{MN}, \tag{C9}$$

where $Q_c = Q_{ij,i}$ $(i \neq j)$ and $Q_d = Q_{jk,i}$ $(i \neq j \neq k)$. The $\mathbf{Q}_3$ block can be interpreted in the same was as $\mathbf{Q}_2$ where the "incident" elements are now Q_c and the "non-incident" elements are Q_d

For the fourth block of $\mathbf{Q}$, we need to introduce the adjacency matrix of the line graph of the simplex, i.e., the quantity $\mathbf{R}^T\mathbf{R} - 2\mathbf{I}_M$. A more intuitive way to interpret this quantity is to think of it as an edge-edge matrix that is unity when two edges

are adjacent and zero otherwise. For the purposes of constructing the $\mathbf{Q}_4$ matrix, which has indices of the form (ij, kl), it helps to then think of the index (ij) as an edge of the simplex connecting vertices i and j, and likewise for edge (kl). Two edges are adjacent if they share a vertex. $\mathbf{Q}_4$ is comprised of three distinct elements: the diagonal elements $Q_g = Q_{ij,ij}$ $(i \neq j)$, the adjacent-edge elements $Q_h = Q_{ij,jk}$ $(i \neq j \neq k)$, and the non-adjacent-edge elements $Q_\iota = Q_{ij,kl}$ $(i \neq j \neq k \neq l)$, which have no repeated indices and, hence, no adjacent edges. The matrix $\mathbf{R}^T\mathbf{R}$, whose $(ij, kl)^{th}$ element is given by $I_{ik}(J_N)_{jl} + I_{il}(J_N)_{jk} + I_{jk}(J_N)_{il} + I_{jl}(J_N)_{ik}$, gives the adjacent edges, but it double counts the diagonal; hence, the term $Q_h(\mathbf{R}^T\mathbf{R} - 2\mathbf{I}_M)$ of $\mathbf{Q}_4$ accounts for the adjacent edges. To get the diagonal elements of $\mathbf{Q}_4$, we need the term $Q_g\mathbf{I}_M$. And for the non-adjacent edges we need $Q_\iota[\mathbf{J}_M - (\mathbf{R}^T\mathbf{R} - \mathbf{I}_M)]$. Putting these terms together gives:

$$\mathbf{Q}_4 = (Q_g - 2Q_h + Q_\iota)\mathbf{I}_M + (Q_h - Q_\iota)\mathbf{R}^T\mathbf{R} + Q_\iota\mathbf{J}_M. \tag{C10}$$

Specifically, one has

$$\mathbf{F}_4 = (F_g - 2F_h + F_\iota)\mathbf{I}_M + (F_h - F_\iota)\mathbf{R}^T\mathbf{R} + F_\iota\mathbf{J}_M, \tag{C11}$$

and likewise for $\mathbf{G}_4$, noting that $G_\iota = 0$:

$$\mathbf{G}_4 = (G_g - 2G_h)\mathbf{I}_M + G_h\mathbf{R}^T\mathbf{R}. \tag{C12}$$

The second step to derive Eq. (4.42) is to find the blocks of $\mathbf{GF}$ by matrix multiplication of $\mathbf{G}$ and $\mathbf{F}$, whose blocks are given above. That is, we multiply the following

$$\mathbf{G} = \begin{pmatrix} \mathbf{G}_1 & \mathbf{0} \\ \mathbf{0} & \mathbf{G}_4 \end{pmatrix} \quad \mathbf{F} = \begin{pmatrix} \mathbf{F}_1 & \mathbf{F}_2 \\ \mathbf{F}_3 & \mathbf{F}_4 \end{pmatrix}. \tag{C13}$$

Then by analyzing each block of $\mathbf{GF}$ we can write down its elements in terms of the elements of $\mathbf{G}$ and $\mathbf{F}$. The first block of $\mathbf{GF}$ gives a and b of Eq. (4.42) and is given by

$$(\mathbf{GF})_1 = \mathbf{G}_1\mathbf{F}_1 = (G_aF_a - G_aF_b)\mathbf{I}_N + G_aF_b\mathbf{J}_N. \tag{C14}$$

Taking the diagonal part of $(\mathbf{GF})_1$ gives

$$a \equiv (GF)_a \equiv (GF)_{i,i} = G_aF_a, \tag{C15}$$

while the off-diagonal $(i \neq j)$ gives

$$b \equiv (GF)_b \equiv (GF)_{i,j} = G_aF_b. \tag{C16}$$

The second block gives e and f of Eq. (4.42) and is given by

$$(\mathbf{GF})_2 = \mathbf{G}_1\mathbf{F}_2 = (G_aF_e - G_aF_f)\mathbf{R} + G_aF_f\mathbf{J}_{NM}. \tag{C17}$$

Noting that $R_{i,ij}$ is unity when $i \neq j$ and that all elements of $\mathbf{J}_{NM}$ are unity, we find the following from $(\mathbf{GF})_2$ when $i \neq j$:

$$e \equiv (GF)_e \equiv (GF)_{i,ij} = G_a F_e. \tag{C18}$$

For $i \neq j \neq k$, $R_{i,jk} = 0$; hence,

$$f \equiv (GF)_f \equiv (GF)_{i,jk} = G_a F_f. \tag{C19}$$

When deriving $(\mathbf{GF})_3$ and $(\mathbf{GF})_4$ below, the following relations prove useful:

$$\mathbf{R}\mathbf{R}^T = \mathbf{J}_N + (N-2)\mathbf{I}_N \quad \mathbf{R}^T\mathbf{J}_N = 2\mathbf{J}_{MN} \quad \mathbf{R}\mathbf{J}_{MN} = (N-1)\mathbf{J}_N \tag{C20}$$

$$\mathbf{R}\mathbf{J}_M = (N-1)\mathbf{J}_{NM} \quad \mathbf{R}^T\mathbf{J}_{NM} = 2\mathbf{J}_M \quad . \tag{C21}$$

Equations c and d of Eq. (4.42) can be found from the third block of $\mathbf{GF}$, which is given by

$$\begin{aligned}(\mathbf{GF})_3 = \mathbf{G}_4\mathbf{F}_3 = \; & [G_g F_e - G_g F_f + (N-4)(G_h F_e - G_h F_f)]\,\mathbf{R}^T \\ & + [G_g F_f + 2G_h F_e + 2(N-3)G_h F_f]\,\mathbf{J}_{MN}.\end{aligned} \tag{C22}$$

For the (ij,i) elements $(i \neq j)$, $\mathbf{R}^T$ is unity; thus, to get $(GF)_c$ one adds both bracketed terms in Eq. (C22):

$$c \equiv (GF)_c \equiv (GF)_{ij,i} = G_g F_e + (N-2)G_h F_e + (N-2)G_h F_f. \tag{C23}$$

For the (jk,i) elements $(i \neq j \neq k)$, $\mathbf{R}^T$ is zero; hence, $(GF)_d$ is simply given by the second bracketed term in Eq. (C22):

$$d \equiv (GF)_d \equiv (GF)_{jk,i} = G_g F_f + 2G_h F_e + 2(N-3)G_h F_f. \tag{C24}$$

Equations g, h, and ι of Eq. (4.42) can be found from the fourth block of $\mathbf{GF}$, which is given by

$$\begin{aligned}(\mathbf{GF})_4 = \mathbf{G}_4\mathbf{F}_4 = \; & [(G_g - 2G_h)(F_g - 2F_h + F_\iota)]\,\mathbf{I}_M \\ & + [G_g F_\iota + 4G_h F_h + 2(N-4)G_h F_\iota]\,\mathbf{J}_M \\ & + [(N-6)G_h F_h - (N-5)G_h F_\iota + G_g(F_h - F_\iota) + G_h F_g]\,\mathbf{R}^T\mathbf{R}.\end{aligned} \tag{C25}$$

As noted earlier, $\mathbf{R}^T\mathbf{R}$ double counts the diagonal elements (i.e., (ij,ij) elements where $i \neq j$). Thus, the $(GF)_{ij,ij}$ elements are given by the sum of the first two bracketed terms in Eq. (C25) plus twice the third term:

$$g \equiv (GF)_{ij,ij} \equiv (GF)_{ij,ij} = G_g F_g + 2(N-2)G_h F_h. \tag{C26}$$

For the (ij,jk) elements $(i \neq j \neq k)$, we note that the $\mathbf{R}^T\mathbf{R}$ elements are unity and the elements of $\mathbf{I}_N$ are zero. Thus, to get $(GF)_{ij,jk}$ we take the sum of the second and third bracketed term in Eq. (C25):

$$h \equiv (GF)_h \equiv (GF)_{ij,jk} = G_g F_h + G_h F_g + (N-2)G_h F_h + (N-3)G_h F_\iota. \quad \text{(C27)}$$

Finally, the (ij,kl) elements $(i \neq j \neq k \neq l)$ of $\mathbf{R}^T\mathbf{R}$ and $\mathbf{I}_N$ are zero, and thus the last equation in (4.42) is simply given by the second bracketed term in Eq. (C25):

$$\iota \equiv (GF)_\iota \equiv (GF)_{ij,kl} = G_g F_\iota + 4G_h F_h + 2(N-4)G_h F_\iota. \quad \text{(C28)}$$

Derivation of Eq. (4.49): A graph with a given structure corresponds to a spectrum. That is, a graph may be represented by a matrix whereby its spectrum, or eigenvalues, may be calculated. $P_{\mathcal{G}}(\lambda)$ denotes the characteristic polynomial of the adjacency matrix $\mathbf{A}$ of graph $\mathcal{G}$:

$$P_{\mathcal{G}}(\lambda) \equiv \det(\lambda\mathbf{I} - \mathbf{A}). \quad \text{(C29)}$$

The element (i,j) of the adjacency matrix is the number of edges connecting vertices i and j of the graph $\mathcal{G}$. The spectrum of $\mathcal{G}$ is found by solving $P_{\mathcal{G}}(\lambda) = 0$.

To prove the relationships involving determinants in this appendix and the next, we quote the following result from p.72 of Ref. [110] for the complete graph K_n:

$$P_{K_n}(\lambda) = (\lambda - n + 1)(\lambda + 1)^{n-1}. \quad \text{(C30)}$$

The adjacency matrix of a simplex of n points, K_n, is an $n \times n$ matrix of ones except along the diagonal which contains all zeros. That is, $P_{K_n}(\lambda)$ takes the following form:

$$P_{K_n}(\lambda) = \det \begin{pmatrix} \lambda & -1 & \cdots & -1 \\ -1 & \lambda & \ddots & \vdots \\ \vdots & \ddots & \ddots & -1 \\ -1 & \cdots & -1 & \lambda \end{pmatrix}. \quad \text{(C31)}$$

Using Eq. (C30) one can easily derive Eq. (4.49) of Sec. 4.3 , which states

$$\det(\mathbf{XYEZ}) = \det \begin{pmatrix} \frac{t}{v}\mathbf{I}_N + \frac{u}{v}\mathbf{J}_N & \mathbf{0} \\ \cdots & v\mathbf{I}_M \end{pmatrix} = t^{N-1}(t+Nu)v^{M-N}, \quad \text{(C32)}$$

where the integer M is defined in Eq. (4.35). First we note that

$$\det\begin{pmatrix} \frac{t}{v}\mathbf{I}_N + \frac{u}{v}\mathbf{J}_N & \mathbf{0} \\ \cdots & v\mathbf{I}_M \end{pmatrix} = \det(v\mathbf{I}_M)\det\left(\frac{t}{v}\mathbf{I}_N + \frac{u}{v}\mathbf{J}_N\right). \tag{C33}$$

Then, $\det(\frac{t}{v}\mathbf{I}_N + \frac{u}{v}\mathbf{J}_N)$ can be written as an $(N \times N)$ matrix of the same form as $P_{K_n}(\lambda)$ in Eq. (C31):

$$\begin{aligned} \det(\frac{t}{v}\mathbf{I}_N + \frac{u}{v}\mathbf{J}_N) &= \det\begin{pmatrix} \frac{t+u}{v} & \frac{u}{v} & \cdots & \frac{u}{v} \\ \frac{u}{v} & \frac{t+u}{v} & \ddots & \vdots \\ \vdots & \ddots & \ddots & \frac{u}{v} \\ \frac{u}{v} & \cdots & \frac{u}{v} & \frac{t+u}{v} \end{pmatrix} \\ &= \left(-\frac{u}{v}\right)^N \det\begin{pmatrix} -1-\frac{t}{u} & -1 & \cdots & -1 \\ -1 & -1-\frac{t}{u} & \ddots & \vdots \\ \vdots & \ddots & \ddots & -1 \\ -1 & \cdots & -1 & -1-\frac{t}{u} \end{pmatrix}, \end{aligned} \tag{C34}$$

so that, noting $\det(v\mathbf{I}_M) = v^M$, and setting $\lambda = -1 - \frac{t}{u}$ and $n = N$ in Eq. (C30) leads directly to $\det(\mathbf{XYEZ}) = t^{N-1}(t + Nu)v^{M-N}$.

Appendix D

Gaussian reduction of Eq. (4.44)

The characteristic equation for the GF eigenvalues is $\det(\mathbf{E}) = 0$, where $\mathbf{E}$ is given by Eq. (4.44). The Gaussian elimination to reduce $\mathbf{E}$ of Eq. (4.44) to the form $\mathbf{XYEZ}$ of Eq. (4.45) allows us to find analytic expressions for the normal-mode frequencies. The goal is to transform $\mathbf{E}$ to a lower-triangular matrix, whose determinant we can compute exactly with Eq. (4.49), while leaving the characteristic determinant invariant by imposing that the transforming matrices have unit determinant. The elimination process consists of three steps.

Step 1: We first define $\mathbf{Z}$:

$$\mathbf{Z} \equiv \begin{pmatrix} \mathbf{I}_N & w\mathbf{J}_{NM} \\ \mathbf{0} & \mathbf{I}_M \end{pmatrix}, \tag{D1}$$

whose determinant is unity, which we now show. It is known from matrix theory (for example, see Ref. [111]) that the determinant of an $(N+M)$-square matrix with an $(N \times M)$ zero matrix $(\mathbf{0}_{N,M})$ in the upper right block or an $(M \times N)$ zero matrix $(\mathbf{0}_{M,N})$ in the lower left block is the product of the determinant of the diagonal block of matrices. That is,

$$\det \begin{pmatrix} \mathbf{A} & \mathbf{0}_{NM} \\ \mathbf{C} & \mathbf{B} \end{pmatrix} = \det \begin{pmatrix} \mathbf{A} & \mathbf{C} \\ \mathbf{0}_{MN} & \mathbf{B} \end{pmatrix} = \det(\mathbf{A}) \det(\mathbf{B}), \tag{D2}$$

where $\mathbf{A}$ and $\mathbf{B}$ are square matrices. For $\mathbf{Z}$, we have $\det(\mathbf{A}) = \det(\mathbf{I}_N) = 1$ and $\det(\mathbf{B}) = \det(\mathbf{I}_M) = 1$; thus, $\det(\mathbf{Z}) = 1$.

Multiplying $\mathbf{E}$ on the right by $\mathbf{Z}$ and using the multiplication rules above leads to

$$\mathbf{EZ} = \begin{pmatrix} (\lambda - a + b)\mathbf{I}_N - b\mathbf{J}_N & (f-e)\mathbf{R} + [w(\lambda - a - (N-1)b) - f]\mathbf{J}_{NM} \\ (d-c)\mathbf{R}^T - d\mathbf{J}_{NM}^T & (\lambda - g + 2h - \iota)\mathbf{I}_M - (h-\iota)\mathbf{R}^T\mathbf{R} \\ & \quad + [(2(d-c) - Nd)w - \iota]\mathbf{J}_M \end{pmatrix}. \tag{D3}$$

We choose w equal to $f/(\lambda - a - (N-1)b)$, such that the upper-right $\mathbf{J}_{NM}$ term vanishes. This results in:

$$\mathbf{EZ} = \begin{pmatrix} (\lambda - a + b)\mathbf{I}_N - b\mathbf{J}_N & (f-e)\mathbf{R} \\ (d-c)\mathbf{R}^T - d\mathbf{J}_{NM}^T & v\mathbf{I}_M - (h-\iota)\mathbf{R}^T\mathbf{R} + \zeta\mathbf{J}_M \end{pmatrix}, \tag{D4}$$

where

$$\zeta \equiv f\left(\frac{2(d-c) - Nd}{\lambda - a - (N-1)b}\right) - \iota \tag{D5}$$

$$v \equiv \lambda - g + 2h - \iota. \tag{D6}$$

Step 2: Next multiply on the left by $\mathbf{Y}$, which by Eq. (D2) has unit determinant:

$$\mathbf{Y} \equiv \begin{pmatrix} \mathbf{I}_N & \mathbf{0} \\ x\mathbf{R}^T + y\mathbf{J}_{NM}{}^T & \mathbf{I}_M \end{pmatrix}, \tag{D7}$$

where we impose

$$x = \frac{h-i}{f-e} \quad y = -\frac{\zeta}{2(f-e)} = -\frac{1}{2(f-e)}\left[f\left(\frac{2(d-c) - Nd}{\lambda - a - (N-1)b}\right) - \iota\right] \tag{D8}$$

to eliminate the lower-right $\mathbf{R}^T\mathbf{R}$ and $\mathbf{J}_M$ terms from $\mathbf{EM}$. This results in

$$\mathbf{YEZ} = \begin{pmatrix} (\lambda - a + b)\mathbf{I}_N - b\mathbf{J}_N & (f-e)\mathbf{R} \\ l\mathbf{R}^T + m\mathbf{J}_{NM}^T & v\mathbf{I}_M \end{pmatrix}, \tag{D9}$$

where

$$\begin{aligned} l &\equiv \frac{h-\iota}{f-e}(\lambda - a + b) + (d-c) \\ m &\equiv y(\lambda - a - (N-1)b) - 2b\frac{h-\iota}{f-e} - d \\ &= -\frac{1}{2(f-e)}[f(2(d-c) - Nd) - \iota(\lambda - a - (N-1)b)] - 2b\frac{h-\iota}{f-e} - d. \end{aligned} \tag{D10}$$

Step 3: The final step is to eliminate the upper right term from **YEZ** by multiplying **YEZ** by **X**, which by Eq. (D2) has unit determinant:

$$\mathbf{X} \equiv \begin{pmatrix} \mathbf{I}_N & z\mathbf{R} \\ \mathbf{0} & \mathbf{I}_M \end{pmatrix}, \tag{D11}$$

where $z = (e-f)/v$. **XYEZ** results in the desired form of Eq. (4.45):

$$\mathbf{XYEZ} = \begin{pmatrix} \frac{t}{v}\mathbf{I}_N + \frac{u}{v}\mathbf{J}_N & \mathbf{0} \\ l\mathbf{R}^T + m\mathbf{J}_{NM}^T & v\mathbf{I}_M \end{pmatrix}, \tag{D12}$$

where

$$t = (\lambda - a + b)v + (N-2)(\iota - h)(\lambda - a + b) + (N-2)(d-c)(e-f) \tag{D13}$$

$$\begin{aligned} u = {} & -kv - (h-\iota)(\lambda - a + b) + (d-c)(e-f) \\ & + \frac{N-1}{2}\left[f(2(d-c) - Nd) - \iota(\lambda - a - (N-1)b) + 4b(h-\iota) - 2d(e-f)\right]. \end{aligned} \tag{D14}$$

As the determinants of **Z**, **Y**, and **X** are unity, the determinant of **XYEZ** and, hence, the characteristic determinant $\det(\mathbf{E})$ may be calculated using Eq. (4.49), which was derived in the previous appendix.

Appendix E

Gramian determinants

The Gramian determinant[112] is defined as:

$$\Gamma \equiv \det(\gamma_{ij}), \tag{E1}$$

where $\gamma_{ij} = \mathbf{r}_i \cdot \mathbf{r}_j / r_i r_j$, the angle cosines between the particle radii $\mathbf{r}_i$ and $\mathbf{r}_j$, represents the elements of an $N \times N$ matrix. A related quantity used in the main text is the principle minor of the Gramian, $\Gamma^{(\alpha)}$, defined as the determinant of the γ_{ij} matrix with the α^{th} row and column removed.

A most challenging part of calculating the large-D minimum and the $\mathbf{F}$ matrix elements in the systems discussed in this paper is handling the Gramian determinants and their derivatives. What makes these calculations feasible is the very high symmetry of the infinite-dimension, symmetric minimum. We make use of Eq. (C30) to obtain the Gramian determinant and its derivatives at the infinite-dimension, symmetric minimum. We will now demonstrate how this is done and summarize the results.

In general $\gamma_{ii} = 1$ and at the infinite-D symmetric minimum all of the remaining direction cosines are equal, $\gamma_{ij} = \gamma_\infty$. Hence, the Gramian determinant is an $(N \times N)$ matrix of the form

$$\Gamma\Big|_\infty = \det \begin{pmatrix} 1 & \gamma_\infty & \cdots & \gamma_\infty \\ \gamma_\infty & 1 & \ddots & \vdots \\ \vdots & \ddots & \ddots & \gamma_\infty \\ \gamma_\infty & \cdots & \gamma_\infty & 1 \end{pmatrix}, \tag{E2}$$

which can be written in the same form as $P_{K_n}(\lambda)$ (Eq. C31 of Appendix B):

$$\Gamma\Big|_{\infty} = (-\gamma_{\infty})^N \det \begin{pmatrix} -1/\gamma_{\infty} & -1 & \cdots & -1 \\ -1 & -1/\gamma_{\infty} & \ddots & \vdots \\ \vdots & \ddots & \ddots & -1 \\ -1 & \cdots & -1 & -1/\gamma_{\infty} \end{pmatrix}. \tag{E3}$$

Setting $\lambda = -1/\gamma_{\infty}$ and $n = N$ in Eq. (C30) gives

$$\Gamma\Big|_{\infty} = [1 + (N-1)\gamma_{\infty}](1-\gamma_{\infty})^{N-1}. \tag{E4}$$

The principle minor evaluated at the infinite-D symmetric minimum $\Gamma^{(\alpha)}\Big|_{\infty}$ is simply related to the corresponding Gramian determinant (E4) by $N \rightarrow N-1$.

To calculate the infinite-D symmetric minimum of the Gramian derivatives, we expand Γ in terms of its cofactors. The cofactor, denoted by C_{ij}, of the element γ_{ij} in Γ is $(-1)^{i+j}$ multiplied by the determinant of the matrix obtained by deleting the i^{th} row and j^{th} column of Γ. We may then write Γ as

$$\Gamma = \sum_{j=1}^{N} \gamma_{ij} C_{ij}. \tag{E5}$$

Then the partial derivative of Γ in terms of the cofactor is

$$\frac{\partial \Gamma}{\partial \gamma_{ij}} = 2C_{ij}. \tag{E6}$$

From this equation, the partial derivative of Γ evaluated at the infinite-D symmetric minimum is

$$\frac{\partial \Gamma}{\partial \gamma_{ij}}\bigg|_{\infty} = -2C_{\infty}^{(N-1)}, \tag{E7}$$

where we have defined the following determinant of an $(N-1) \times (N-1)$ matrix:

$$C_{\infty}^{(N-1)} = \det \begin{pmatrix} \gamma_{\infty} & \gamma_{\infty} & \gamma_{\infty} & \cdots & \gamma_{\infty} \\ \gamma_{\infty} & 1 & \gamma_{\infty} & & \vdots \\ \gamma_{\infty} & \gamma_{\infty} & 1 & \ddots & \vdots \\ \vdots & \ddots & \ddots & \ddots & \gamma_{\infty} \\ \gamma_{\infty} & \cdots & \cdots & \gamma_{\infty} & 1 \end{pmatrix}, \tag{E8}$$

and the superscript $(N-1)$ simply indicates the size of the matrix. From this matrix one can show that the following recursion relation holds:

$$C_\infty^{(N-1)} = \gamma_\infty \left(\Gamma\Big|_\infty^{(N-2)} - (N-2) C_\infty^{(N-2)} \right), \tag{E9}$$

or equivalently

$$C_\infty^{(N)} = \gamma_\infty \left(\Gamma\Big|_\infty^{(N-1)} - (N-1) C_\infty^{(N-1)} \right), \tag{E10}$$

where the (N) superscript in the notation $\Gamma\Big|_\infty^{(N)}$ again refers to the size of the matrix $\Gamma\Big|_\infty$. From the recursion relation (E10), one can easily prove by induction the conjecture that $C_\infty^{(N)} = \gamma_\infty (1-\gamma_\infty)^{N-2}$ and, hence,

$$\left. \frac{\partial \Gamma}{\partial \gamma_{ij}} \right|_\infty = -2\gamma_\infty (1-\gamma_\infty)^{N-2}. \tag{E11}$$

The derivative of the principle minor evaluated at the infinite-D symmetric minimum is simply related to the corresponding Gramian determinant derivative (E11) by $N \to N-1$.

To summarize the above results, the following expressions are needed when calculating the minimum of the effective potential (4.20 and 4.21):

$$\begin{aligned}
\left. \frac{\partial \Gamma}{\partial \gamma_{ij}} \right|_\infty &= -2\gamma_\infty (1-\gamma_\infty)^{N-2} & \left. \frac{\partial \Gamma^{(\alpha)}}{\partial \gamma_{ij}} \right|_\infty &= -2\gamma_\infty (1-\gamma_\infty)^{N-3} \\
\Gamma|_\infty &= [1+(N-1)\gamma_\infty](1-\gamma_\infty)^{N-1} & \Gamma^{(\alpha)}\Big|_\infty &= [1+(N-2)\gamma_\infty](1-\gamma_\infty)^{N-2}.
\end{aligned} \tag{E12}$$

And when evaluating the $\mathbf{F}$ matrix elements at the infinite-D symmetric minimum, the following six second-order derivatives of the Gramian determinants are needed:

$$\begin{aligned}
\left. \frac{\partial^2 \Gamma}{\partial \gamma_{ij} \partial \gamma_{kl}} \right|_\infty &= 0 & \left. \frac{\partial^2 \Gamma^{(\alpha)}}{\partial \gamma_{ij} \partial \gamma_{kl}} \right|_\infty &= 0 \\
\left. \frac{\partial^2 \Gamma}{\partial \gamma_{ij}^2} \right|_\infty &= -2(1-\gamma_\infty)^{N-3}(1+(N-3)\gamma_\infty) & \left. \frac{\partial^2 \Gamma^{(\alpha)}}{\partial \gamma_{ij}^2} \right|_\infty &= -2(1-\gamma_\infty)^{N-4}(1+(N-4)\gamma_\infty) \\
\left. \frac{\partial^2 \Gamma}{\partial \gamma_{ij} \partial \gamma_{jk}} \right|_\infty &= 2\gamma_\infty (1-\gamma_\infty)^{N-3} & \left. \frac{\partial^2 \Gamma^{(\alpha)}}{\partial \gamma_{ij} \partial \gamma_{jk}} \right|_\infty &= 2\gamma_\infty (1-\gamma_\infty)^{N-4}.
\end{aligned} \tag{E13}$$

Appendix F

Regularized Fermi pseudopotential and the low density expansion

The type of BEC discussed in this thesis is of the trapped or inhomogeneous variety. However, it proves useful to call attention to some properties of the homogeneous system because the two systems share similar features when the inhomogeneous density is slowly varying. The low density expansion for a homogeneous (untrapped) bose gas of hard spheres is a perturbation expansion of the energy in terms of the gas parameter na^3, where n is the uniform number density of the gas[14, 95, 96]. The lowest order for the ground-state energy is equivalent to the Bogoliubov mean-field term in the GP equation: $E/N = 2\pi\hbar^2 na/m$. The first-order energy for a homogeneous gas can be calculated by summing over the momentum states with $\vec{k} \neq \vec{0}$, but using the contact potential leads to a divergent ground-state energy (and recall that the contact potential (2.14) is the underlying interaction of the mean-field GP equation (2.23)). One needs to use a pseudopotential or a regularized contact potential that, like the contact potential, replaces the hard-sphere boundary condition, but also removes singularities in the wavefunction of the form $1/r$ by including the operator $(\partial/\partial r)r$.

The goal of the regularized Fermi pseudopotential, which we now derive, is to obtain a Schrödinger equation with an inhomogeneous term that reproduces the effect of the hard-sphere boundary condition on the scattered wavefunction. Stated more simply, we want to derive a pseudopotential that places a node in the wavefunction at $r = a$. The relative-motion Schrödinger equation for two atoms interacting via a hard sphere of radius a is

$$\begin{aligned} \left(\tfrac{1}{r^2}\tfrac{\partial}{\partial r}r^2\tfrac{\partial}{\partial r} + k^2\right)\psi(\mathbf{r}) = 0 \quad &, \quad r > a \\ \psi(\mathbf{r}) = 0 \quad &, \quad r \leq a, \end{aligned} \tag{F1}$$

where k is the relative wavevector defined by $E = \hbar^2 k^2/2\mu$ where E is the relative-motion energy and $\mu = m/2$ is the reduced mass of the system. In the low energy limit ($k \to 0$), the extended wave function,

$$\psi_{ex}(r) \overset{r\to 0}{\to} \left(1 - \frac{a}{r}\right)\chi, \tag{F2}$$

satisfies Eq. (F1) everywhere except at the point $r = 0$. The quantity χ is a constant that depends on the boundary condition at $r = \infty$. Integrating the Laplacian we see that

$$\int d\mathbf{r}\nabla^2\psi_{\mathbf{ex}} = 4\pi r^2 \frac{\partial\psi_{\mathbf{ex}}}{\partial r}, \tag{F3}$$

and using the wave function in Eq. (F2),

$$\int d\mathbf{r}\nabla^2\psi_{\mathbf{ex}}(r) \stackrel{r\to 0}{\to} 4\pi a\chi. \tag{F4}$$

Since we would like the pseudopotential to be an operator acting on $\psi_{\mathbf{ex}}$ (at the origin so that we can interpose a delta function into the pseudopotential), we want to express χ in terms of $\psi_{\mathbf{ex}}$ as $r \to 0$; using Eq. (F2) it is easy to show that

$$\chi = \left[\frac{1}{r}\frac{\partial}{\partial r}(r\psi)\right]_{r=0}. \tag{F5}$$

Substituting this into Eq. (F4) we see that as $k \to 0$ and for $r \geq a$, the hard-sphere boundary conditions and the wave function in Eq. (F1) with the same eigenvalue can be approximately reproduced by the pseudopotential

$$V_{\mathbf{reg-pseudo}}(\mathbf{r}) = 4\pi a\delta(\mathbf{r})\frac{\partial}{\partial r}r. \tag{F6}$$

In a future publication we plan to give the derivation of the generalized pseudopotential for arbitrary dimension. For arbitrary D, one must proceed more carefully than in the above $D = 3$ derivation; otherwise, one finds a pseudopotential for larger D that removes the $1/r^{D-2}$ singularity from the origin, but does not remove the less singular functions. For $D = 7$ for example, this naive pseudopotential removes $1/r^5$ terms from the wavefunction but not $1/r^3$ and $1/r$ terms. The generalized pseudopotential is

$$V^D_{\mathbf{reg-pseudo}} = \Omega(D)\frac{a^{D-2}\Gamma(1/2)}{2^{\frac{D-3}{2}}\Gamma\left(\frac{D-2}{2}\right)}\delta^D(r)\left(\frac{\partial}{\partial r}\frac{1}{r}\right)^{\frac{D-1}{2}} r^{D-1}, \tag{F7}$$

where $\Omega(D) = 2\pi^{D/2}/\Gamma(D/2)$ is the volume of D-dimensional unit sphere. Busch *et al.*[113] derive the following relationship for the energy of two atoms interacting via the three-dimensional regularized pseudopotential of Eq. (F6) in an isotropic, harmonic trap of frequency ω:

$$2a/a_{\mathbf{ho}} = \frac{\Gamma(1/4 - E/2)}{\Gamma(3/4 - E/2)} \tag{F8}$$

where $a/a_{\rm ho}$ is the scattering length in oscillator units ($a_{\rm ho} = \sqrt{\hbar/m\omega}$). The generalization of this result for the regularized pseudopotential of Eq. (F7) is

$$-\frac{\Gamma(1-D/2)}{\Gamma(D/2-1)}(2a/a_{\rm ho})^{D-2} = \frac{\Gamma((4-D)/4-E/2)}{\Gamma(3/4-E/2)}, \tag{F9}$$

where derivation, like that of Eq. (F7), will be given in a future publication.

The low-density expansion of a homogeneous bose gas of hard spheres is well known[14, 95, 96]. As mentioned above, to obtain the correct result one must use the regularized contact potential (F6) rather Eq. (2.14), which would lead to a divergent ground state. The ground-state energy per particle, expanded in terms of the gas parameter $\sqrt{na^3}$, is

$$\begin{aligned}\frac{E}{N} &= \frac{2\pi\hbar^2 na}{m} \times \\ &\left[1 + \frac{128}{15\sqrt{\pi}}(na^3)^{1/2} + \frac{8(4\pi - 3\sqrt{3})}{3}(na^3)\ln(na^3) + O(na^3)\right]. \end{aligned} \tag{F10}$$

In this approximation, it is assumed that the average interatomic spacing is much larger than the s-wave scattering length: stated mathematically as $na^3 \ll 1$.

Appendix G

Homogeneous limit of the GP and MGP equations

Provided the density of the nonuniform gas is slowly varying, the uniform low-density expansion of Eq. (5.3) can be a useful tool for understanding the qualitative features of the inhomogeneous gas theory. We now show that one recovers the first two terms of the uniform bose gas expansion of Eq. (5.3) from the GP and MGP energy functionals (Eqs. (5.4) and (5.6)) in the homogeneous limit. We first rewrite the GP energy functional (5.4) in terms of the ground-state density $n = N\psi^2$:

$$E_{\rm GP}[n] = \int d\mathbf{r} \left[\frac{\hbar^2}{2m} |\nabla \sqrt{n}|^2 + \frac{1}{2} m\omega_{\rm ho}^2 r^2 n + \frac{2\pi\hbar^2 a}{m} n^2 \right], \tag{G1}$$

where we have assumed a large number of atoms so that $N - 1 \approx N$. In the limit of a homogeneous gas in a box of volume V, the quantum pressure and the harmonic trap (the first and second terms in Eq. (G1)) become zero and the nodeless GP wavefunction becomes $\psi = \sqrt{1/V}$. The inhomogeneous energy functional (G1) then reduces to the leading-order term of the homogeneous energy density expansion (5.3), where $n = N/V$:

$$\frac{E_{\rm GP}}{N} \to \frac{2\pi\hbar^2 n a}{m}. \tag{G2}$$

In the homogeneous limit, the mean-field term of the GP equation is equivalent to the leading order (Bogoliubov) term of the low-density expansion (5.3).

Similarly, rewriting the MGP energy functional in terms of the ground-state density,

$$E_{\rm MGP}[n] = \int d\mathbf{r} \left[\frac{\hbar^2}{2m} |\nabla \sqrt{n}|^2 + \frac{1}{2} m\omega_{\rm ho}^2 r^2 n + \frac{2\pi\hbar^2 a}{m} n^2 \times \left(1 + \frac{128}{15\sqrt{\pi}} a^{\frac{3}{2}} \sqrt{n} \right) \right], \tag{G3}$$

and, as above, taking the homogeneous limit, one finds that the nonlinear terms in the MGP energy functional (5.6) are equivalent to the energy per particle for a homogeneous gas in Eq. (5.3) with the logarithmic term neglected:

$$\frac{E_{\rm MGP}}{N} \to \frac{2\pi\hbar^2 n a}{m} \left[1 + \frac{128}{15\sqrt{\pi}} (n a^3)^{1/2} \right]. \tag{G4}$$